DISSERTATION

Titel der Dissertation:

Adsorption of small molecules on metal surfaces

angestrebter akademischer Grad:

Doktor der Naturwissenschaften (Dr. rer. nat.)

Verfasser:	Mag. Konstantinos Termentzidis
Matrikelnummer:	0300410
Dissertationsgebiet:	Physik
Betreuer:	O. Univ. Prof. Dr. Jürgen Hafner

Wien, am 16. März 2007.

" $H\vartheta o\varsigma$ $\alpha\nu\vartheta\rho\omega\pi\omega\iota$ $\delta\alpha\iota\mu\omega\nu$", $H\rho\alpha\kappa\lambda\epsilon\iota\tau o\varsigma$

"The character of man is his guardian spirit.", Heraclitus

(Stoveos, Anthology IV 40,23)

Publications

The help of co-authors in preparing the following publications is gratefully acknowledged:

- A Density-functional theory study of the adsorption of CO molecule on Au/Ni(111), <u>K. Termentzidis</u>, J. Hafner and F. Mitteldorfer, *J. Phys.: Cond. Mat.* **18** p10825, (2006).

- CO adsorption on Au Ni(111) surface alloy - a DFT study, <u>K. Termentzidis</u>, and J. Hafner, *submitted at J. Phys.: Cond. Mat.* (2007).

- CO adsorption on metal surfaces: a hybrid density functional study with plane wave basis set, A. Stroppa, <u>K. Termentzidis</u>, J. Paier, G. Kresse and J. Hafner, *in preparation* (2007)

Abstract

The adsorption of CO in the vicinity of an isolated Au ad-atom on a Ni(111) surface has been studied using ab initio DFT and PBE functionals. Detailed investigations of the potential-energy surface for the binding of CO show that for bonding sites in which the molecule binds at least to one Ni nearest neighbor of the Au ad-atom, the adsorption energy is reduced by up to 1.2 eV. At larger distances from the impurity, the adsorption energies are almost unchanged. On the other hand, binding to the Au ad-atom is much stronger than on a flat Au surface. These results are discussed in relation to the electronic structure of the Au-doped Ni surface.

Furthermore, the adsorption of CO on a Au/Ni(111) surface alloy has been investigated, again with PBE functionals. In contrast to a Au adatom on a Ni(111) surface, a Au impurity binds CO only very weakly. In addition, the impurity induces a reduction of the adsorption energies which is strictly localized to its immediate neighborhood.

Finally the study of the adsorption of CO on the Pt(111) surface, and also on Cu and Rh for comparison, has been performed with the PBE functional, and the hybrid Hartree-Fock density functionals PBE0 and HSE03. The PBE functional tends to favor adsorption in the hollow sites, in contrast with experimental reports which give as the most stable adsorption site the top site on these three metals. The hybrid functionals reduce this tendency, and they predict the correct adsorption site for Cu and Rh, while failing for Pt. On the other hand for Pt the hybrid functionals destabilize the hollow sites by 50 meV compared to the PBE functional. This suggests that hybrid functionals give a better description of the chemisorption of CO molecules on Pt, Cu and Rh, but there are still some contradictions with experiment. The results of the total energy calculations are presented along with an analysis of the electronic structure by means of the density of states.

Acknowledgments

I would like to sincerely thank my advisor, Professor Jürgen Hafner for his guidance, advice, direction and endless source of knowledge in the subject of my thesis.

Best regards to all members of Prof. Dr. Hafner's research group for their friendship. I gratefully acknowledge Dr. Doris Vogtenhuber for many valuable discussions. I thank also Dr. Florian Mittendorfer who guided my first steps through VASP and Mathematica, and Dr. Thomas Bucko and Dr. Maxim Shishkin who were both always there to answer my questions. Last but not least, Michael Pöltl, who guided me in the secure and sophisticated world of LINUX and advised me with his wisdom, on several personal issues.

Furthermore, I would like to thank Prof. Georgio Kanelli and Prof. Eleni Paloura at Aristotle University of Thessaloniki in Greece, who were the first to show me how fascinating and interesting solid state physics can be.

Finally an ex-member of the CMS institute at Vienna, Dr. Melissa Petersen for her friendship and her advice for the English accent.

Contents

List of Abbreviations/Acronyms

AIMD	Ab initio Molecular Dynamics
BO	Born Oppenheimer
CI	Configuration Interaction
CMS	Computational Material Science
DFT	Density Functional Theory
DOS	Density of States
GGA	General Gradient Approximation
HF	Hartree Fock
HOMO	Highest Occupied Molecular Orbital
HSE03	Heyd Scuseria Ernzerhof 2003
KS	Kohn Sham
LDA	Local Density Approximation
LDOS	Local Density of States
LEED	Low Energy Electron Diffraction
LR	Long Range
LUMO	Lowest Unoccupied Molecular Orbital
MGGA	Meta General Gradient Approximation
MEP	Minimum Energy Path
MO	Molecular Orbital
MP	Monkhorst Pack
MP2	Møller Plesset 2
MR	Missing Row
NEB	Nudged Elastic Band
PAW	Projector Augmented Wave
PBE	Perdew Burke Ernzerhof
PES	Potential Energy Surface
PW91	Perdew Wang 1991
RPBE	Revised Perdew Burke Ernzerhof
SR	Short Range
STM	Scanning Tunneling Microscopy
STS	Scanning Tunneling Spectroscopy

TF	Thomas Fermi
TPD	Temperature programmed desorption
VASP	Vienna Ab initio Simulation Package
XC	Exchange Correlation

List of Figures

4

List of Tables

Chapter 1

Dissertation Outline

Surface alloys (e.g. Ag/Cu, Ag/Co and Au/Ni) exhibit a rich phase structure and offer interesting features for several electronic and magnetic nanoscale device applications as well as for catalysis. Au-Ni system displays a large misfit in lattice parameters of the order of 16%. Elemental Au-Ni is immiscible in the bulk and exhibits a positive enthalpy of mixing. Au atoms alloyed into the topmost layer of Ni(111) significantly modify the reactivity of the neighboring nickel atoms, thereby rendering the AuNi alloy an interesting candidate for catalytic applications. In this thesis I investigate, by means of ab-initio DFT calculations, the changes induced by the Au adatom and substitutional Au atom on Ni(111) surfaces. This is done by studying the adsorption of CO molecules on Au adatoms and substitutional Au atoms in a Ni(111) surface.

The thesis will be organized as follows. The first part, presenting the theory, is divided into two chapters. Chapter-2 gives an overview of Computational Material Science and an introduction to Density Functional Theory. Various approximations to the Exchange-Correlation functional are discussed in detail: the local density approximation (LDA), the generalized gradient approximation (GGA) and hybrid functionals mixing GGA and exact (Hartree Fock) exchange energies. Chapter-3 is an introduction to the physics of surfaces, focused on metal surfaces and the adsorption of small molecules on them, subjects that are related to the phenomena that I was involved with in the study of CO adsorption on the Au doped Ni(111) surface.

The second part with the results, is divided into four chapters. In Chapter-

4 the NEB method is applied to the investigation of the substitution of one Ni surface atom by a Au adatom, and the influence of Au like adatom or substitutional on the Density of States of Ni(111) surface, while in Chapters-5 and 6, I present the results on CO adsorption on Au-doped Ni(111) and on a Au/Ni(111) surface alloy. In Chapter-7 adsorption results of CO on Pt(111) surface are given for PBE, PBE0 and HSE03 functionals for the exchange-correlation energy.

Part I
General Theory

Chapter 2

Computational Material Science, Density Functional Theory and Exchange Correlation-functionals

2.1 Computational Material Science

2.1.1 Introduction

Computational Materials Science (CMS) is a young discipline of Condensed Matter Physics, and it is considered as a bridge connecting theory and experiment. CMS often is referred as applied theory or computer experiment[134]. The computer experiments in material science allow theory to examine and to predict experiments[73] and sometimes even to substitute them, when experiment is not practicable. CMS is an interdisciplinary subject, implying the synergy of quantum, classical and statistical mechanical physics, of chemistry and even biochemistry.

CMS investigates for several properties of materials, both existing and new, and their applications, with the use and analysis of numerical models on high performance computers. It provides qualitative and quantitative informations for phenomena that may be too complex to be dealt with analytical methods,

like:

- the atomic structure of the material[1], like bond lengths and angles, crystal lattice parameters, surface reconstructions, structural phase transitions,
  - its electronic and transport properties,
  - elasticity and other mechanical properties (bulk modulus, elastic constants),
    - reactivity of surfaces,
    - chemical reactions (on a microscopic scale),
    - catalytic behavior,
    - magnetic properties and
    - novel materials with predetermined properties.

One should acknowledge the computer performance that has been increased dramatically over the last few decades[219], making possible the investigation of bigger systems. However, the cases for which analytical solutions are possible are limited. Therefore, most calculations done in computational physics involve some degree of approximation.[219]. The challenge of CMS is to find the method with the most appropriate approximations to solve the investigated system.

A computational model is an approximate, but well-defined mathematical procedure of simulation. Generally, there are five different stages in the development and use of such a model: a required **accuracy** must be selected, qualitatively, a model should be able to provide clear distinction between possible differences of the behavior of the system under investigation. The quantitative aim is the reproduction of the data and the prediction of the calculated quantities within experimental accuracy. For energies, an accuracy of at least 10meV/particle (1kJ/mol) would be appropriate. **Formulation**: the mathematical procedure must be precisely formulated and should be general and continuous as far as possible. **Implementation**: the method has to be implemented in a form which permits its application in reasonable time and cost. This stage involves the development of efficient and easy-to-be used computer programs. **Verification**: then one should compare the results of the model with experimental data, to determine whether the expected quantitative accu-

racy is reached. **Prediction** is the final step: an application of the model to problems to which the answer is unknown or in dispute[186], should be possible for a reliable package.

Models which utilize only the fundamental constants of physics are generally termed "ab initio"; if some parameters have to be introduced, which are determined by fitting to some experimental data, the methods are "semi-empirical"[186], like classical Monte Carlo, Brownian motion, Lattice Dynamics, and classical Molecular Dynamics. There is also a third category the hybrid methods, which use both empirical and ab-initio approaches, like ab-initio molecular dynamics (AIMD) simulations[12].

Apart from the ab-initio and semi-empirical methods, one can divide the methods, according to the time and length scale of the systems to be calculated, in: Atomistic Simulations, Mesoscale Methods and Continuum Methods.

2.1.2 Ab-initio, or first principle methods

Ab-initio, or first principle methods, based on quantum mechanics, do not require any other input quantities but the atomic species, their coordinates[123] and some basic constants, like Planck constant over 2π: $\hbar$, the mass and the charge of electron: m_e, e, etc. These methods are particularly useful in predicting the properties of novel materials and trends for a wide range of materials which cannot be done with empirical or semi-empirical methods. Comparing them with the empirical methods, one can notice that the level of sophistication for these methods is higher, but one can study smaller systems, and fast processes only, as computationally they are more expensive[134].

In almost all ab-initio methods several specific approximations have to be done:

• The Born-Oppenheimer approximation: nuclear and electronic motions are decoupled and treated separetly.

• Electronic Schrödinger equation cannot be solved exactly, except for very simple systems like the hydrogen atom. Therefore, the electronic wavefunction is expanded in certain finite basis sets (e.g. Gaussian functions or plane wave

basis sets). The N-electron functions are expanded as a linear combination of antisymmetrized products (Slater determinants) of the molecular orbitals. However, the number of Slater determinants which can be constructed may become enormous, and very quickly increase with the number of electrons and orbitals. Therefore, approximations have to be made also at this point, like the expansion of the wavefunction into a subset of all possible Slater determinants.

A very successful method for many body systems is the density functional theory (DFT)[59]. DFT considers the many-electron problem as a single-electron problem, by using the exchange-correlation potential, which gathers all the many-body quantum phenomena like electron correlation and Pauli's exclusion principle. The exchange-correlation potential is a functional of the charge density and whether it is exact for the ground state, approximations are used, as the exact functional is unknown[134].

2.2 The Quantum Many-Body Problem

2.2.1 Introduction

The exact determination of the electronic structure of atoms, molecules and solids is a difficult problem, as the electrons must be treated using the laws of quantum mechanics and not these of classical physics[1]. Another difficulty is the number of electrons that are involved - the coupling of the electron interactions makes an analytic solution impossible for systems with more than one electron, and the complexity grows dramatically with increasing the electron number.

The properties of any time-independent quantum system can be determined by solving the Schrödinger equation[197]:

$$\hat{H}\Psi(\mathbf{r}_1, \mathbf{r}_2 \ldots \mathbf{r}_N) = E\Psi(\mathbf{r}_1, \mathbf{r}_2 \ldots \mathbf{r}_N), \tag{2.1}$$

where $\hat{H}$ is the Hamiltonian, $\Psi(\mathbf{r}_1, \mathbf{r}_2 \ldots \mathbf{r}_N)$ is the many-body wavefunction

---

[1]The de Broglie wavelengths of the electrons overlap and the interactions between the electrons become correlated quantum-mechanically.

and E is the total energy of the system. Electrons and nuclei interact with each other with Coulomb forces, consequently the Hamiltonian in atomic units[2] is given by:

$$\hat{H} = -\frac{1}{2m_{Z_i}} \sum_{i=1}^{M} \nabla_{\mathbf{R}_i}^2 - \frac{1}{2} \sum_{i=1}^{N} \nabla_{\mathbf{r}_i}^2 + \sum_{i}^{M} \sum_{j>i}^{M} \frac{Z_i Z_j}{|\mathbf{R}_i - \mathbf{R}_j|} \\ - \sum_{i=1}^{N} \sum_{j=1}^{M} \frac{Z_j}{|\mathbf{r}_i - \mathbf{R}_j|} + \sum_{i=1}^{N} \sum_{j>i}^{N} \frac{1}{|\mathbf{r}_i - \mathbf{r}_j|}, \tag{2.2}$$

where M and N are the number of nuclei and electrons in the system, m_Z, Z and $\mathbf{R}$ are the mass, charge and position of the nuclei, and $\mathbf{r}$ represents the position of the electrons. The first two terms in Eq. 2.2 are the kinetic energy contributions from the nuclei and the electrons respectively, and the rest three are Coulombic potential energy terms, representing the ion-ion repulsion, the ion-electron attraction and the electron-electron repulsion respectively. The Schrödinger equation (Eq. 2.1) with this Hamiltonian is too difficult to be solved analytically. Approximations to the Hamiltonian (Eq. 2.2) and the many body wavefunction Ψ, have to be made.

The first simplification of this problem is done by Born and Oppenheimer[30] (BO), as mentioned at the introduction, in which the nuclear and electronic degrees of freedom are decoupled, since the nuclei are $\sim 10^3$ times heavier than the electrons and can be considered to be stationary compared to them, while electrons are moving within a fixed external potential due to the nuclei. With the BO approximation the full many-body Hamiltonian (Eq 2.2) becomes simpler to that of an electronic Hamiltonian:

$$\hat{H} = -\frac{1}{2} \sum_{i=1}^{N} \nabla_{\mathbf{r}_i}^2 - \sum_{i=1}^{N} \sum_{j=1}^{M} \frac{Z_j}{|\mathbf{r}_i - \mathbf{R}_j|} + \sum_{i=1}^{N} \sum_{j>i}^{N} \frac{1}{|\mathbf{r}_i - \mathbf{r}_j|}. \tag{2.3}$$

But, solving the Schrödinger equation with the above Hamiltonian (Eq. 2.3) is still too complex for most cases, since the many-electron wavefunction contains $3N$ variables, (a solid containing $N \sim 10^{26}$ electrons). Therefore, for

---

[2](Hartree) Atomic Units from now on: $\hbar, \frac{1}{4\pi\epsilon_0}, e, m_e = 1$

solids calculations are performed for a small part of a crystal, the computational cell. To take periodicity into account periodic boundary conditions are imposed on super-cell. This is the way to transform the task of calculation of a system of large number of electrons into a task of calculation of much smaller super-cell.

Several approaches have been made for finding approximations for the many-electron problem. An early one and very important made by Thomas-Fermi theory[52, 220] with the presumption to have for an unknown variable the electron density, $n(\mathbf{r})$, instead of the many-electron wavefunction. This approach simplified the problem, as the density contains just three degrees of freedom, the x, y, z coordinates of the system. Hartree-Fock theory [57] was developed based upon the single-particle approximation proposed by Hartree[85, 199], but with additional exchange interactions between electrons, by antisymmetrising the single-particle functions $\psi_i(\mathbf{r}_i s_i)$:

$$\Psi(\mathbf{r}_1 s_1, \mathbf{r}_2 s_2 \ldots \mathbf{r}_N s_N) \approx \frac{1}{\sqrt{N}} \mathcal{A}\big[\psi_1(\mathbf{r}_1 s_2)\psi_2(\mathbf{r}_2 s_2) \ldots \psi_N(\mathbf{r}_N s_N)\big], \qquad (2.4)$$

where $\mathcal{A}$ is the antisymmetric linear combination upon exchange, and s_i gives the spin dependence. Now it is included the decoupling of the $3N$ degrees of freedom in the many-electron wavefunction, by writing the total electronic wavefunction as a product of single electronic wavefunctions, and thus each degree of freedom can be solved independently. At the following sections there is a short review of Thomas-Fermi and Hartree-Fock theory, and after them a more detailed for DFT.

2.2.2   Thomas-Fermi Theory

Thomas and Fermi[52, 220] (TF) proposed one model for solving the many-electron problem, by introducing the electron density $n(\mathbf{r})$ as the central variable, while the total energy of the system is a functional of the density: $E_{TF}[n(\mathbf{r})]^3$. The energy functional has three terms[74]:

---

[3]Square brackets are used to express functionals, which in this case is the density.

$$E_{TF}[n(\mathbf{r})] = C_F \int n(\mathbf{r})^{5/3} d^3\mathbf{r} + \int n(\mathbf{r}) v_{ext}(\mathbf{r}) d^3\mathbf{r}$$
$$+ \frac{1}{2} \iint \frac{n(\mathbf{r})n(\mathbf{r}')}{|\mathbf{r} - \mathbf{r}'|} d^3\mathbf{r} d^3\mathbf{r}', \qquad (2.5)$$

the kinetic energy of the non-interacting electrons in a homogeneous electron gas with density n is the first term ($C_F a constant$). The second term is the electrostatic energy between nuclei and electrons, where $v_{ext}(\mathbf{r})$ is the static Coulomb potential from the nuclei:

$$v_{ext}(\mathbf{r}) = -\sum_{j=1}^{M} \frac{Z_j}{|\mathbf{r} - \mathbf{R}_j|}, \qquad (2.6)$$

while the third term (Eq. 2.5) is the classical Coulomb repulsion between electrons, known as the Hartree energy.

The TF-method has been used frequently in the past and has been found to give a rough description of the charge density and the electrostatic potential. The TF scheme is exact in the limit of infinite nuclear charge. However, there are severe deficiencies in the model. The charge density is infinite at the nucleus, and it does not decay exponentially far from the nucleus of an atom, but as r^{-6}. Furthermore, TF theory does not result in atoms binding to form molecules or solids[11, 135, 217]. As TF atom is characterized by the lack of shell structure, the periodic variation of many observed properties with changing atomic number cannot be reproduced. The main source of error for this model comes from the approximation of the kinetic energy. Another problem is the over-simplified description of the electron-electron interactions, which are treated classically and hence do not take account of quantum phenomena such as the exchange interaction[102, 194].

2.2.3 Hartree-Fock Theory

Hartree simplified the problem of electron-electron interactions, expanding the many electrons wavefunction into a product of single electron wavefunction (simple plane waves in a uniform system). With this ansatz for the wavefunc-

tion and the use of the **variational principle**[4], N equations have to be solved for an N single electrons system, with wavefunctions, $\psi_i(\mathbf{r}_i s_i)$:

$$\Psi(\mathbf{r}_1 s_1, \mathbf{r}_2 s_2, \ldots, \mathbf{r}_N s_N) = \frac{1}{\sqrt{N}} \psi_1(\mathbf{r}_1 s_1) \psi_2(\mathbf{r}_2 s_2) \ldots \psi_N(\mathbf{r}_N s_N), \qquad (2.7)$$

where $\psi_i(\mathbf{r}_i s_i)$ is composed of a spatial function $\phi_i(\mathbf{r}_i)$, and an electron spin function $\sigma(s_i)$ such that:

$$\psi_i(\mathbf{r}_i, s_i) = \phi_i(\mathbf{r}_i)\sigma(s_i) \qquad (2.8)$$

and $\sigma = \alpha, \beta$ represent up-spin and down-spin electrons respectively.

However, as mentioned previously, the Hartree approximation does not account for exchange interactions since Eq. 2.7 does not satisfy:

$$\begin{aligned}
\Psi(\mathbf{r}_1 s_1, \ldots, \mathbf{r}_i s_i, \ldots, \mathbf{r}_j s_j, \ldots \mathbf{r}_N s_N) = \\
= -\Psi(\mathbf{r}_1 s_1, \ldots, \mathbf{r}_i s_i, \ldots, \mathbf{r}_j s_j, \ldots \mathbf{r}_N s_N),
\end{aligned} \qquad (2.9)$$

under the interchange of particle coordinates required by the Pauli principle.

Hartree approximation fails because the Hartree product wavefunction is symmetric and not antisymmetric, imposed by the **Pauli exclusion principle**[5]. Any wavefunction that characterized by the Pauli's principle will vanish, when a pair of fermions with the same quantum numbers approach each other.

The problem of exclusion principle was solved by the Hartree-Fock (HF) approximation[57], writing the wavefunction as an antisymmetrised product of orbitals:

$$\begin{aligned}
\Psi_{HF} = \frac{1}{\sqrt{N!}} \Big[& \psi_1(\mathbf{r}_1 s_1) \psi_2(\mathbf{r}_2 s_2) \ldots \psi_N(\mathbf{r}_N s_N) \\
& -\psi_1(\mathbf{r}_2 s_2) \psi_2(\mathbf{r}_1 s_1) \ldots \psi_N(\mathbf{r}_N s_N) + \ldots \Big].
\end{aligned} \qquad (2.10)$$

---

[4]for a system set of unknown parameters, the set of parameter values which describes the ground state of the system most correctly is the set of values which minimises the total energy.

[5]Two fermions cannot have the same set of quantum numbers and be coinstantaneously at the same space. The Pauli exclusion principle can be expressed mathematically by an antisymmetric wavefunction for a set of identical fermions under exchange (see eq. 2.9).

This ansatz fulfills eq. 2.9. Slater[199] realized that the Hartree-Fock wavefunction can be represented as an $N \times N$ determinant, (Slater determinant):

$$\Psi_{HF} = \frac{1}{\sqrt{N!}} \begin{vmatrix} \psi_1(\mathbf{r}_1 s_1) & \psi_2(\mathbf{r}_1 s_1) & \dots & \psi_N(\mathbf{r}_1 s_1) \\ \psi_1(\mathbf{r}_2 s_2) & \psi_2(\mathbf{r}_2 s_2) & \dots & \psi_N(\mathbf{r}_2 s_2) \\ \vdots & \vdots & & \vdots \\ \psi_1(\mathbf{r}_N s_N) & \psi_2(\mathbf{r}_N s_N) & \dots & \psi_N(\mathbf{r}_N s_N) \end{vmatrix}, \tag{2.11}$$

or shortly:

$$\Psi_{HF} = \frac{1}{\sqrt{N!}} det\big[\psi_1(\mathbf{r}_1 s_1)\psi_2(\mathbf{r}_2 s_2)\dots\psi_N(\mathbf{r}_N s_N)\big], \tag{2.12}$$

where the orbitals are subject to the orthonormal constraint:

$$\int \psi_i^*(\mathbf{r})\psi_j(\mathbf{r}) \, d\mathbf{r} = \langle \psi_i | \psi_j \rangle = \delta_{ij}. \tag{2.13}$$

The HF energy can be evaluated by taking the expectation value of the Hamiltonian, with the above Slater determinant. This yields[74]:

$$E_{HF} = \langle \Psi_{HF} | \hat{H} | \Psi_{HF} \rangle$$

$$= \sum_i^N \int \left(\frac{1}{2}|\nabla\psi_i(\mathbf{r})|^2 - \frac{Z}{\mathbf{r}}|\psi_i(\mathbf{r})|^2 \right) d^3\mathbf{r}$$

$$+ \frac{1}{2}\sum_{i,j,i\neq j}^N \iint |\psi_i(\mathbf{r})|^2 \frac{1}{|\mathbf{r}-\mathbf{r}'|}|\psi_i(\mathbf{r}')|^2 d^3\mathbf{r} d^3\mathbf{r}' \tag{2.14}$$

$$- \frac{1}{2}\sum_{i,j,i\neq j}^N \delta_{s_{zi}s_{zj}} \iint \psi_i^*(\mathbf{r})\psi_j^*(\mathbf{r}') \frac{1}{|\mathbf{r}-\mathbf{r}'|}\psi_j(\mathbf{r})\psi_i(\mathbf{r}') d^3\mathbf{r} d^3\mathbf{r}'$$

The first term is the kinetic energy of electrons, the second the interaction between electron-ion and the third between electrons. The last term arises from the antisymmetric nature of the HF wavefunction and it vanishes when $s_i \neq s_j$, and is the so-called **exchange energy** E_x.

Assume an electron with spin-up, then the Pauli exclusion principle means that other nearby spin-up electrons will be repelled. Spin-down electrons will not be affected since they have a different spin quantum number. Thus spin-up

electron is surrounded by a region which has been depleted of other spin-up electrons (similarly, for a spin-down electron there is a region depleted of other spin-down electrons). This region is the **exchange hole**.

The motions of electrons in real systems are more correlated than in HF description. The interaction energy missed by HF is termed the **correlation energy** E_c[54]:

$$E_c = E_0 - E_{HF}, \tag{2.15}$$

where E_0 is the exact groundstate energy[153].

A way to introduce the correlation effects is to mix a linear combination of Slater determinants corresponding to excited state configurations. These methods are the post Hartree-Fock methods, such as the Configuration Interaction (CI)[6], the coupled-cluster and Møller-Plesset[7]. Unfortunately these methods are computationally very expensive and can apply only in small systems[194].

There is a second type of hole in the region surrounding any electron, due to the lack of electrons as a consequence of electrostatic repulsion. This leads to a slightly positively electron-depleted region that surrounds each electron, known as the **Coulomb hole** or the **correlation hole**. This effect has a double meaning: a binding force exist between the negatively charged electron and its positively charged hole (electrostatics), and a third particle interacts with both the electron and the correlation hole. Consequently, exchange effects will be screened by the correlation hole[100].

The HF approach is an improvement over the Hartree theory. The many-electron wavefunction is now constructed by antisymmetric single-electron wavefunctions. As in HF methods the correlations between electrons are neglected, they produce too large band gaps, too small band widths and higher

---

[6]CI is a very good approach, but very slow of a linear combination of Slater determinants as basis-set

[7]A perturbation series is made out of the error in the correlation energy. The most popular approach is MP2, which takes into account the lowest-order correction.

energies. The HF approach is particularly suited for oxides and crystals of small organic molecules, which have small number of localized electrons. For high electron density materials such as transition metals is less appropriate. The theory fails for the "perfect metal", as it ignores the collective Coulomb screening in a completely delocalized electron system[182].

2.2.4 Density Functional Theory

DFT methods have become the most widely-spread ab-initio methods in CMS and solid state physics, due to their high computational efficiency and very good accuracy, for the structure of molecules, crystals, surfaces and their interactions[8]. DFT is based on the electronic charge density distribution $n(\mathbf{r})$, instead of the many-electron wave function $\Psi(\mathbf{r}_1, \mathbf{r}_2, \mathbf{r}_3, ...)$[112]. Both Thomas-Fermi and Hartree-Fock-Slater methods (for clarifying the concepts of exchange and correlation), can be regarded as predecessors of modern DFT, but although those theories are approximate, modern DFT is in principle exact for the ground state[112].

DFT deals with inhomogeneous systems of identical particles[51], providing a simple method for describing the effects of exchange and correlation in an electron gas. The minimum of the total-energy as a functional of $n(\mathbf{r})$ is the **ground state energy** of the system, and the density that yields this minimum value is the **exact single-particle ground-state density**. Kohn and Sham[110] showed how to replace the many-electron problem by an exactly equivalent set of self-consistent one-electron equations. Furthermore, they showed that all other ground state properties of the system (e.g. lattice constant, cohesive energy, etc) are functionals of the ground state electron density[100]. Kohn and Sham in 1965[110] showed that the Hamiltonian equations derived from this variational approach take a very simple form. The so-called Kohn-Sham equations are similar in form to the time-independent Schrödinger equation. In addition to the contribution from the electron-ion interaction, the electron-electron interaction potential is split for convenience into two parts: the Hartree potential, and an exchange-correlation potential, whose form is, in general, unknown[100, 112].

The computing time in DFT, for a system of many atoms with no structural symmetries, grows like N_{at}^2 - N_{at}^3[112]. The accuracy of DFT with respect to bond length calculations, for a great number of solids, molecules and surfaces, interatomic equilibrium distances are predicted to within about 0.02 Å of experiment; bond angles are found within a few degrees of their experimental values.

There are state-of-the-art applications of DFT in many areas, like catalysis and surface science, nanomaterials, biomaterials and geophysics[75]. DFT has been applied to degenerate ground states[111], spin-polarized ground states[112], paramagnetism, magnetism[111], magnetic and electric susceptibilities, orbital magnetism, diamagnetism, quantum Hall effect[87], relativistic corrections, free energy for finite temperature ensembles, plasmas, excited states, superconductors, time-dependent phenomena, multicomponent systems, nuclei, electron-hole droplets in semiconductors, soft condensed matter, where the collective interaction and correlation effects are known to play an important role[64, 111, 114]. Superconductivity, atoms in the focus of strong laser pulses, relativistic effects in heavy elements and in atomic nuclei, classical liquids, and magnetic properties of alloys have all been studied with DFT.[35]

DFT cannot be used to provide information about some excited states of the system, in particular, in semiconductors band gaps are 50-100% smaller than the experimental[100]. A list of the failures of DFT with functionals used today are: larger binding energies in LDA, van der Waals forces are not included, the Kohn-Sham potential decays exponentially for large distances instead of $\propto 1/r$, band gaps are underestimated in both LDA and GGA and strongly correlated solids such as NiO and FeO are predicted as metals and not as antiferromagnetic insulators.[68]

The Hohenberg-Kohn Theorems

For a N-electron system, the external potential $V_{ext}(\mathbf{r})$ completely fixes the Hamiltonian; thus N and $V_{ext}(\mathbf{r})$ determine all properies for the ground state. Instead of them, the first Hohenberg-Kohn theorem[94] legitimizes the use of electron density $n(\mathbf{r})$ as basic variable[114]. It states:

Theorem I: *For any given set of electrons in an external potential V_{ext}, this potential is determined uniquely, within a trivial additive constant, by the electron density $n(r)$.*

Notice that this additive constant does not change anything, since the Schrödinger equation with Hamiltonians H and $H + const$ will yield exactly the same eigenfunctions and all the eigenenergies will be simply shifted by the value of this constant[114].

An alternative formulation of the theorem is: every observable of a stationary quantum mechanical system can be calculated exactly from only the ground-state density, i.e., every observable can be written as a functional of the ground-state density.

Thus, $n(\mathbf{r})$ determines N and $V_{ext}(\mathbf{r})$ and hence all properties of the ground state, for example the kinetic electron energy $T[n(\mathbf{r})]$, the potential energy $V[n(\mathbf{r})] = U_{ee}[n(\mathbf{r})] + V_{ext}[n(\mathbf{r})]$, where U_{ee} stands for electron-electron interactions, and the total energy $E[n(\mathbf{r})]$[114]:

$$E[n(\mathbf{r})] = V_{ext}[n] + T[n] + U_{ee}[n]. \tag{2.16}$$

We can group together all functionals which are secondary to $V_{ext}(\mathbf{r})$

$$E[n(\mathbf{r})] = V_{ext}[n] + F_{HK}[n] = \int n(\mathbf{r})V_{ext}(\mathbf{r})d\mathbf{r} + F_{HK}[n]. \tag{2.17}$$

The Hohenberg-Kohn functional F_{HK} operates only on density and is universal[114].

Theorem II: *It is possible to define a universal functional for the energy $E[n]$ depending on the electron density $n(r)$. The true ground state energy is the global minimum of the energy functional, and the density $n(r)$ which minimizes the functional is the exact ground state density.*

In other words, if some density represents the correct number of electrons N, the total energy calculated from this density cannot be lower than the true

energy of the ground state and the ground state density can be calculated, in principle exactly, using the variational method involving only density[114].

The Kohn-Sham Formulation

In 1965, Kohn and Sham[110] (KS) introduced an orbital method for the quantitative modeling of electronic structure. In order to evaluate the kinetic energy of N noninteracting particles given only their density distribution $n(\mathbf{r})$, they simply found the corresponding potential $v_{eff}(\mathbf{r})$, and used the Schrödinger equation[8]:

$$\left(-\frac{1}{2}\nabla^2 + v_{eff}(\mathbf{r}) \right)\psi_i(\mathbf{r}) = \varepsilon_i \psi_i(\mathbf{r}), \qquad (2.18)$$

such that:

$$n(\mathbf{r}) = \sum_i^N |\psi_i(\mathbf{r})|^2. \qquad (2.19)$$

As $v_{eff}(\mathbf{r})$ potential is "local" and as it is functional of the density, eqs 2.18 and 2.19 have to be solved self-consistently.

The KS total-energy functional for a set of doubly occupied electronic states ψ_i can be written:

$$E[\{n(\mathbf{r})\}] = -\sum_i \int \psi_i \nabla^2 \psi_i d^3\mathbf{r} + \int V_{ion}(\mathbf{r})n(\mathbf{r})d^3\mathbf{r}$$
$$+\frac{1}{2}\int \frac{n(\mathbf{r})n(\mathbf{r}')}{|\mathbf{r}-\mathbf{r}'|}d^3\mathbf{r}d^3\mathbf{r}' + E_{xc}[n(\mathbf{r})] + E_{ion}(\{\mathbf{R}_I\}), \qquad (2.20)$$

with E_{ion} representing the Coulomb energy associated with interactions between the nuclei (or ions) at positions $\mathbf{R}_I$, V_{ion} is the static total electron-ion potential, $n(\mathbf{r})$ is the electronic density, and $E_{xc}[n(\mathbf{r})]$ is the exchange-correlation energy.

Only the minimum of the KS energy functional has physical meaning, corresponding to the ground-state energy of the system of electrons with the ions in positions $\mathbf{R}_I$[168].

It is necessary to determine the set of wave functions ψ_i that minimize the KS energy functional. These are given by the self-consistent solutions to the KS equations[110], which are a set of eigenequations:

$$\left\{ -\frac{1}{2}\nabla^2 + V_{ion}(\mathbf{r}) + V_H(\mathbf{r}) + V_{xc}(\mathbf{r}) \right\}\psi_i(\mathbf{r}) = \varepsilon_i\psi_i(\mathbf{r}), \qquad (2.21)$$

where ψ_i is the wave function of electronic state i, ε_i is the KS eigenvalue and the terms within the brackets in eq. 2.21 can be regarded as a Hamiltonian, and V_H is the Hartree potential of the electrons given by:

$$V_H(\mathbf{r}) = \int \frac{n(\mathbf{r}')}{|\mathbf{r} - \mathbf{r}'|} d^3\mathbf{r}'. \qquad (2.22)$$

The exchange-correlation potential, V_{xc}, is given by the functional derivative

$$V_{xc}(\mathbf{r}) = \frac{\delta E_{xc}[n(\mathbf{r})]}{\delta n(\mathbf{r})}. \qquad (2.23)$$

The KS equations represent a mapping of the interacting many-electron system onto a system of noninteracting electrons moving in an effective potential due to all the other electrons. They must be solved self-consistently so that the occupied electronic states generate a charge density that produces the electronic potential that is used to construct the equations. The sum of the single-particle KS eigenvalues does not give the total electronic energy because this overcounts the effects of the electron-electron interaction in the Hartree energy and in the exchange-correlation energy[171].

2.3 Exchange-correlation energy

2.3.1 Introduction

The exchange-correlation potential V_{xc} is a functional derivative of the exchange correlation energy with respect to the local density (see eq 2.23). For a homogeneous electron gas, this will only depend on the value of the electron density. For a nonhomogeneous system, the value of the exchange correlation potential at the point $\mathbf{r}$ depends not only on the value of the density at $\mathbf{r}$, but also on its variation close to $\mathbf{r}$, where "close" is a microscopic distance

of comparable magnitude as the local Fermi wavelength or the TF screening length[113]. It can therefore be written as an expansion over the gradients of the density:

$$V_{xc}[n(\mathbf{r})] = V_{xc}[n(\mathbf{r}), \nabla n(\mathbf{r}), \nabla(\nabla n(\mathbf{r})), ...]. \tag{2.24}$$

The exact form of the energy functional is unknown, as the inclusion of density gradients makes the solution of the DFT equations difficult. The simplest way to obtain this contribution is to assume that the exchange correlation energy leads to an exchange correlation potential depending on the value of the density in $\mathbf{r}$ only (not on its gradients).

J.Perdew presented the five generations of functionals in the DFT 2000 symposium[36] in a following manner:

• first the LDAs which describe only the local density,

• second, the GGAs in which further the dependence on the gradients of the density is added,

• third, the MGGAs, including the dependence on the kinetic energy density,

• fourth, the Hybrid functionals, in which is added further the dependence on the occupied orbitals, exact exchange,...

• and fifth, the fully non-local functionals, in which the dependence on the unoccupied orbitals is further added.

2.3.2   Local Density Approximation (LDA)

The simplest method of describing the exchange-correlation energy of an electronic system is to use the LDA[110]. In this approximation the exchange-correlation energy of an electronic system is constructed by assuming that the exchange-correlation energy per electron at a point $\mathbf{r}$ in the electron gas, $\varepsilon_{xc}(\mathbf{r})$, is equal to the exchange-correlation energy per electron on a homogeneous electron gas that has the same density as the electron gas at point $\mathbf{r}$. Thus:

$$E_{xc}^{LDA}[n(\mathbf{r})] \equiv \int \varepsilon_{xc}(n(\mathbf{r}))n(\mathbf{r})d\mathbf{r}, \tag{2.25}$$

and

$$\frac{\delta E_{xc}[n(\mathbf{r})]}{\delta n(\mathbf{r})} = \frac{\delta[n(\mathbf{r})\varepsilon_{xc}(\mathbf{r})]}{\delta n(\mathbf{r})}, \tag{2.26}$$

with

$$\varepsilon_{xc}(\mathbf{r}) = \varepsilon_{xc}^{hom}[n(\mathbf{r})],$$

where $\varepsilon_{xc}(n)$ is the exchange-correlation energy per particle of a uniform interacting electron gas of density n and is known to a very high accuracy. The LDA becomes exact when the length scale over which $n(\mathbf{r})$ varies is large[112].

In the LDA at each point there exists a well defined density; it is assumed that an electron at such a point experiences the same many-body response by the surrounding electrons, as if the density of these surrounding electrons had the same value through the entire space as at the point of the reference electron. The exchange-correlation energy is then the integral over the contributions from each volume element. The LDA works very well for systems with slowly varying valence charge density and becomes less accurate for systems with directed chemical bonds.

The LDA assumes that the exchange-correlation energy functional is purely local. Several parameterizations exists for the exchange-correlation energy of a homogeneous electron gas[110, 170, 227], all of which lead to similar total-energy results. Considering the inexact nature of the approximation, it is remarkable that LDA has been so successful[168]. The LDA appears to give a single well-defined global minimum for the energy of a non-spin-polarized system of electrons in a fixed ionic potential. For magnetic materials, however, one would expect to have more than one local minimum in the electronic energy[168].

The LDA often permits useful predictions of electron densities, atomic positions, and vibration frequencies (to within 10-50 cm^{-1}[114]), etc. However, the LDA also makes some errors: total energies for atoms are less realistic than those of the HF approximation[72, 170], and binding energies are typically over-estimated, sometimes even by a factor of two[114]. LDA also systematically underestimates the band gap, and it fails totally in some cases, like Ge in

which the calculated band gap is negative, meaning that Ge should be metal, and not a semiconductor. Finally, LDA systematically overestimates the band width of alkali metals.

2.3.3 General Gradient Approximation (GGA) and Meta-GGA

The next level of approximations beyond LDA is a number of non-local approximations, with a spatial variation of density, and they are usually termed as Generalized Gradient Approximations (GGAs):

$$E_{xc}^{GGA} = \int f\big(n(\mathbf{r}), |\nabla n(\mathbf{r})|\big)d\mathbf{r}, \tag{2.27}$$

in which $f(n, |\nabla n|)$ is a suitably chosen function of its two variables[112].

By imposing the conditions for the correct exchange hole on the approximate hole given by the gradient expansion, Perdew[172] proposed a model which leaves only a 1% error in exchange energy. This model has also been further simplified[173][167] to:

$$E_x^{GGA}[n] = -C_1 \int d\mathbf{r} n^{4/3} F(s), \tag{2.28}$$

with

$$s = \frac{|\nabla n(\mathbf{r})|}{2k_F n}, \tag{2.29}$$

$$k_F = C_2 n^{1/3}, \tag{2.30}$$

and

$$F(s) = \big(1 + 1.29s^2 + 14s^4 + 0.2s^6\big)^{1/15}. \tag{2.31}$$

C_1 and C_2 are constants, including π. The LDA corresponds to $F(s) = 1$, but several other forms for $F(s)$ have been suggested[16].

Details for the proposed GGA of Perdew, Burke, and Ernzerhof (PBE), which satisfies energetically significant conditions on the exact xc energy functional can be found in [176, 177, 179].

The driving force for the suggestion of non-local approximations was the high density gradient in some materials, like Cu. The GGA due to Perdew and Wang[172–175] is widely used[114]. Finally, a useful collection of explicit expressions for some GGAs can be found in the appendix of Ref.[56], and more detailed discussion of some selected GGAs and their performances is given in Ref.[239].

The GGA functionals lead to good qualitative results for many purposes, but often have difficulties in describing systems with long range correlations. Functionals which take more semi-local information into account than GGA, are called **meta-GGA (MGGA)**[17, 25, 63]. MGGAs include additional semi-local information beyond the first-order density gradient, such as higher order density gradients, or the inclusion of the kinetic energy density $\tau(\mathbf{r})$[127, 180, 215, 216] which involves derivatives of the occupied Kohn-Sham orbitals. The MGGA may be written with the general form:

$$E_{xc}^{MGGA}[n(\mathbf{r})] = \int f[n(\mathbf{r}), \nabla n(\mathbf{r}), \nabla^2 n(\mathbf{r}), \tau(\mathbf{r}), \sigma_1(\mathbf{r}), \ldots \sigma_k(\mathbf{r})]d\mathbf{r} \qquad (2.32)$$

where $\sigma_1(\mathbf{r}), \ldots \sigma_k(\mathbf{r})$ are other possible semi-local quantities that could be used in the construction of MGGAs.

There are several MGGA forms[5, 20, 48, 49, 55, 180, 187, 226] and some improvement has been obtained over the GGA[127]. MGGA calculations for solids are performed non-selfconsistently, as they use GGA orbitals and densities to evaluate $E_{xc}^{MGGA}[n(\mathbf{r})]$[194]. In several tests[127, 215, 216] MGGAs have given favorable results, even when compared to the best GGAs. For molecules, MGGA functionals have been shown to yield accuracy comparable to hybrid functionals[207]. In addition, MGGAs yield significant improvements in solids[208].

2.3.4   Hybrid Functionals

Hybrid functionals, such as PBE0, HSE03 and B3LYP, include a fixed combination of conventional DFT and exact HF exchange[99] giving a significant improvement over the LDA and GGA description of molecular properties and for structural calculations[166]. Traditionally, 20-25% of exact HF exchange

is included in hybrid methods[2, 19]. Hybrid-functional methods represent a good compromise between the DFT and the HF method[165]. The hybrid methods success partially because of the reduction of self-interaction error by the use of a fixed portion of HF exchange in the functional[99], in which part of the exchange energy cancels out the self-coulomb energy. The formation energies of small molecules are in better agreement with experiment comparing with local functionals, and band gaps and band structures often have a good agreement with experiment[48, 49, 150].

The general form of Hybrid functionals[18] is:

$$E_{xc}^{hybrid} = \mu\left(E_x^{HF} - E_x^{GGA}\right) + E_{xc}^{GGA}, \qquad (2.33)$$

in which E_x^{HF} is the HF exchange term, and the coefficient μ determines the amount of exact-exchange mixing and is fitted semi-empirically.

Hybrid methods are based on the adiabatic formula:

$$E_{xc} = \int_0^1 d\mu E_{xc,\mu}, \qquad (2.34)$$

where:

$$E_{xc,\mu} = \langle \Psi_\mu | V_{ee} | \Psi_\mu \rangle - \frac{1}{2} \iint \frac{n(\mathbf{r}_1) - n(\mathbf{r}_2)}{|\mathbf{r}_1 - \mathbf{r}_2|} d^3\mathbf{r}_1 d^3\mathbf{r}_2, \qquad (2.35)$$

which connects the non-interacting KS system where $\mu = 0$, to the fully interacting real systems[71]. Several hybrid schemes were suggested based on formula 2.34[3, 4].

Jaramillo et. al[99] defined a local hybrid functional, where the amount of exact HF and DFT exchange varies according to the local function, $f(\mathbf{r})$:

$$E_{xc} = \int d^3\mathbf{r} n(\mathbf{r}) \left[f(\mathbf{r})\varepsilon_x^{DFT}(\mathbf{r}) + \left(1 - f(\mathbf{r})\right)\varepsilon_x^{exact}(\mathbf{r}) + \varepsilon_c^{DFT} \right], \qquad (2.36)$$

in which with DFT is declared a regular DFT exchange and correlation like LDA or GGA. The exact exchange energy density is derived from the definition of the non-local exact exchange energy expression:

$$E_x = \int \varepsilon_x^{exact}(\mathbf{r}_1) n(\mathbf{r}_1) d^3\mathbf{r}_1 = \frac{1}{2} \iint \frac{|n_1(\mathbf{r}_1, \mathbf{r}_2)|^2}{\mathbf{r}_{12}} d^3\mathbf{r}_1 d^3\mathbf{r}_2. \qquad (2.37)$$

PBE0 and HSE03 functionals

One very promising group of hybrid functionals that have been implemented recently in VASP are the PBE0 and HSE03 functionals. The computational model **PBE0** is obtained by combining the Perdew-Burke-Ernzerhof (PBE) generalized gradient functional with 25 % amount of exact exchange self-consistently, which overcomes many problems arising from the standard functionals (LDA, GGA)[3, 5]. PBE0[4, 176–179] functional is one of the few "parameter-free" hybrid functionals that are widely applicable. The effects of electronic correlation are represented by the corresponding part of the PBE density functional. The resulting expression for the exchange-correlation energy then takes the following simple form[8]:

$$E_{xc}^{PBE0} = \frac{1}{4}E_x + \frac{3}{4}E_x^{PBE} + E_c^{PBE}, \tag{2.38}$$

where the non-local Fock exchange energy, E_x, can be written as:

$$E_x = -\frac{1}{2}\sum_{\mathbf{k}n,\mathbf{q}m} f_{\mathbf{k}n}f_{\mathbf{q}m} \times 2w_{\mathbf{k}}2w_{\mathbf{q}}\times$$
$$\times \iint \frac{\phi_{\mathbf{k}n}^*(\mathbf{r}_1)\phi_{\mathbf{q}m}(\mathbf{r}_1)\phi_{\mathbf{q}m}^*(\mathbf{r}_2)\phi_{\mathbf{k}n}(\mathbf{r}_2)}{|\mathbf{r}_1 - \mathbf{r}_2|}d^3\mathbf{r}_1 d^3\mathbf{r}_2, \tag{2.39}$$

$\phi_{\mathbf{k}n}^*(\mathbf{r}_1)$ is a set of one-electron Bloch states of the system, while $f_{\mathbf{k}n}$ is the corresponding set of occupational numbers. The sums over $\mathbf{k}$ and $\mathbf{q}$ run over all k-points that are chosen to sample the Brillouin zone (BZ), and the sums over m and n run over all occupied bands at these k-points[166]. $w_{\mathbf{k}}$ $w_{\mathbf{q}}$ are the the k-point weights, and the factor of two is a consequence of the time symmetry.

Another hybrid functional, proposed by Heyd et al[92] the so-called **HSE03**, helps to decrease the large computational effort because of the Fock exchange. This is done, by separating the exchange interaction into a short and long range part (SR and LR respectively). It is characterized as screened exchange hybrid functional, as it makes use of a screened Coulomb potential in order

---

[8]$E_{xc}^{PBE0} = \mu E_x^{HF} + (1 - \mu)E_x^{PBE} + E_c^{PBE}$ the general equation

to reduce the spatial extent of the exact exchange interaction. It provides results similar to traditional hybrid functionals but with great reduction of the computational effort[14]. The mix of Fock and DFT exchange is made now, only in the SR part. The LR part of the Fock exchange interactions the corresponding part of the DFT functional[166]. The exchange-correlation energy for the HSE03 functional is written as[9]:

$$
\begin{aligned}
E_{xc}^{HSE03} = \frac{1}{4}E_x^{SR}(\xi) + \frac{3}{4}E_x^{PBE,SR}(\xi) \\
+ E_x^{PBE,LR}(\xi) + E_c^{PBE}.
\end{aligned}
\tag{2.40}
$$

The separation of the electron-electron interaction into a SR and LR part is done only in the exchange interactions. Electronic correlation is represented by the corresponding part of the PBE density functional. The parameter ξ defines the range-separation, and is related to a characteristic distance $2/\xi$, at which the SR interactions distinguish[166]. For $\xi = 0$, the LR equals to zero and the SR equals to the full Coulomb operator, becoming pure PBE0 functionals, while for $\xi \to \infty$, it is the other way around, becoming a pure PBE calculation[222].

---

[9]$E_{xc}^{HSE03} = \mu E_x^{HF,SR}(\xi) + (1-\mu)E_x^{PBE,SR}(\xi) + E_x^{PBE,LR}(\xi) + E_c^{PBE}$ the general equation

Chapter 3

Adsorption of small molecules on Metal Surfaces

3.1 Clean Surfaces

3.1.1 Introduction

One of the main aims of surface science is to explain chemisorption, and surface chemical reactions. For this, knowledge of the nature of the chemisorption bond, the energetics of adsorption, the adsorbate geometries and the bond lengths are very important. The theory of adsorption has been developed at a level to calculate adsorption energies, as well electronic and atomic structures with a good predictive accuracy, but it remains the need to find explanations and develop simple concepts[196]. DFT is an important tool for analyzing surface geometries, and is capable to discover the underlying mechanisms. DFT calculations describe well the geometry, but absolute adsorption energies are not more accurate than 0.2 eV/atom. However, energy differences of chemically similar bound adsorbates are described with very good accuracy[196].

3.1.2 Structure of Clean Surfaces

The structure of an ideal surface can be defined by taking the positions of bulk crystals and eliminating atoms to expose the desired plane. Generally two kind

of surfaces can be differentiated: low index (close packed) and higher indexed, stepped surfaces. In a fcc crystal, the atoms in the (111) facet are arranged to form close packed hexagons, while the atoms in the (100) facet are arranged to form a square, and in the (110) facet have an up and down, arrangement. In a bcc crystal, the atoms in the (110) facet have a hexagonal arrangement, but in contrast to the (111) facet of a fcc metal the hexagon is elongated and there are gaps between the atoms. The atoms in the (100) face of a bcc material show a square atomic arrangement. The (111) facet of a bcc material shows a more complex atomic arrangement with three layers of exposed atoms, each of which forms a centered rectangle. Surface structures in hcp materials are more complex than surface structures in fcc or bcc, as hcp is not a primitive Bravais lattice[139, 225].

3.1.3 Metal Surfaces - Relaxation and Reconstruction

There are basically two kinds of rearrangements that occur when surfaces are created: reconstructions and relaxations. Both are driven by the energetics of the system like the tendency to reduce the surface free energy, but there may be kinetic limitations (preventing or hindering) at low temperatures. Both may occur with clean surfaces, and in addition the adsorption of species at the surface may enhance, alter or even reverse the process. Experimentally, most surfaces relax. Reconstructions are less common, but they happen in some important materials, like metals. For example, some of the facets of platinum, iridium, gold, tungsten and molybdenum also reconstruct.[139]

Relaxation is a small rearrangement of the surface layers which may be significant energetically. It involves adjustments in the layer spacings perpendicular to the surface, but no changes in the periodicity parallel to the surface and in the symmetry of the surface. Relaxation occurs often for metal surfaces.

The reconstruction of surfaces on the other hand is a much more pronounced effect, with larger displacements of the surface atoms, but still in an atomic scale. There is a variety of reconstructive phase transitions for solid surfaces, as a function of temperature[237]. Reconstruction occurs with many of the less stable high index metal surfaces, but is much stronger on semi-

conductor surfaces. Reconstructions involve a change in the periodicity of the surface structure and even a change in surface symmetry. The driving force for the reconstruction is again the minimization of the surface energy - at the atomic level[189]. Low index metal surfaces usually do not reconstruct[69], with an exception of the fcc(110) surfaces, that are well known for their strong tendency to missing-row (MR) type reconstructions either in the clean state (Au, Pt) or driven by adsorbates (Ni, Cu, Pd, Ag)[108].

Important reconstructions occur with platinum, iridium and gold. The so-called "(2x1)" reconstruction of Au(110)[38] has a missing row structure, with every other row of atoms missing. At Pt(110)[136] and Ir(110)[38, 107] there is a similar surface reconstruction. There are two other important reconstructions in transition metal surfaces; the so-called "hex" or "(5x1)" reconstruction of Au(100)[41, 47], Ir(100)[106, 203, 204] and Pt(100)[40], where the top layer of atoms rearranges to form a hexagonal array, and finally the c(2x2) reconstruction of W(100)[205], that produces a zig-zag chain of atoms in the [011] direction.

One can understand how metal surfaces relax or reconstruct by examining how the electron density around the metal atoms changes when a surface is formed. The topmost atoms have densities much smaller than the bulk atoms, and this results a driving force for the atom to increase its overlap with other atoms by moving toward the second layer. In general atoms would like to have an electron overlap similar to that, which they experience in the bulk[201]. When the top layer of atoms moves in, the inward motion increases the electron density at the second layer of atoms. In the third layer, the electron density is above that in the bulk, so the third layer moves out. That leaves the fourth layer with a lowered electron density, so the fourth layer moves in. The displacement is negligible at the fifth layer[139].

3.1.4 Surface States

At the surfaces the three dimensional Brillouin zone is projected on two dimensions. The electronic structure of a metal surface is closely related to this of the bulk, with some additional states because of perturbations due to the surface[139]. As the three-dimensional periodicity of the potential is lost at

the surface, the solutions of the Schrödinger equation can be found within the band gap of the bulk solid. These special solutions are waves which can travel parallel to the surface, but not into the solid, they are localized at the surface and they are known as **surface states**. If charge (electrons or holes) is situated in these surface states it will result in electronic fields entering into the solid. Surface states can be associated with the termination of a three-dimensional potential, with changes in the potential due to relaxation, reconstruction, structural imperfections or adsorbed impurities. The surface states affect on one hand the electrical properties of a surface, as they are a source (or a sink) of electrons and on another the chemical reactivity, as they modify the affinity of the surface for electrons.[188]

3.1.5   Technical aspects

Let us assume a specific surface plane cleaved out, frozen in geometry, from the bulk. That solid is periodic in two dimensions, and aperiodic in the direction perpedicular to the surface, where the translational symmetry is lost. To enable calculations, the semi-infinite solid must be replaced by a slab of finite structure. The slab should be thick enough so that its inner layers approach the electronic properties of the bulk. In practice, it is more often the typical choice of three or four layers. The plane wave approach require the use of periodic boundary conditions[144], and this leads to the use of the slab model, to model extended surfaces. This basis works well for periodic systems, although convergence can be slow (e.g sharp electronic gradients)[66]. The slab models represent the materials properly, but they are problematic to describe the electronic correlation and the excited states[96].

3.2 Adsorption on Surfaces

3.2.1 Substitutional adsorption and formation of surface alloys

Adsorbed adatoms may replace a substrate atom and adsorb substitutionally. Substitutional adsorption is the result of an irreversible phase transition, from an "on surface" site, without changes in the periodicity of the surface unit cell or of the coverage. The process of substitution may be kinetically hindered, but this can be overcome even at rather low temperatures by the heat of adsorption. Steric restrictions for a substitutional adsorption can be overcome much easier on surface than in the bulk.

Alloying effects have been shown experimentally to change the reactivity of single crystal surfaces[21, 33, 137, 156] and it is used extensively in the development of catalysts[84]. Generally, one can tailor the strength of the bonding between a surface and an intermediate, by changing the composition of the surface (e.g. by combining two transition metals). Alloying changes the electronic structure of the surface, which leads to changes in reactivity.

The elemental chemical composition at the surface of an alloy often differs from the composition in the bulk. One of the components is often enriched in the surface region, due to differences in surface segregation energies between the alloy components, resulting changes on the reactivity of the surface. Ruban et al.[192] have performed an extensive analysis of the electronic properties of pseudomorphic metal overlayers and of surface metal impurities. It is shown that when metals with small lattice constants are overlayed or alloyed on metals with larger lattice constants, the d-band center shifts up, and vice-versa. Trends appear to result from a combination of d-band bandwidth changes upon overlaying or alloying, followed by d-band shifts to preserve a local d-band filling that is constant. Finally, Ruban et.al.[193] have created an extensive database of surface segregation energies for bimetallic systems (Fig. 3.1). There are two important periodic trends in surface segregation energies: in agreement with observations[6, 7], a substantial portion of the surface segregation energy is determined by the difference in surface energies of

the host and the impurity. No impurities in the middle of a transition series are excepted to segregate to the surface of early or late transition metals. Secondly, crystal structure differences between the host and the impurity can have a significant effect on segregation energies. Such differences change the local d-state character around the impurities and also the surface segregation energy even up to 1eV. The changes are more pronounced when the host or the impurity, comes from the beginning of a transition metal series[66].

3.2.2 The nature of surface chemical bond

A classification of adsorption distinguishes two classes, a weak interaction between adsorbate and substrate, the so-called **physisorption**, where the adsorption energy is typically less than 0.3 eV per adsorbate particle (6.9 Kcal/mol) and there is no covalent bond and secondly **chemisorption**, where the adsorption energy is larger and there is a chemical bond between the adsorbate and the surface[196] and the adsorbate's electronic structure is significantly modified. In contrast to chemisorption, physisorption is governed by polarization and dispersion (Van der Waals) forces, and as a result, the electronic structure of the adsorbate is perturbed to a much lesser extent[139]. DFT calculations using the LDA or the GGA functionals, lacking a description of the Van der Waals interaction, as non-local, but seems to give a reasonable description of adsorption of noble-gas atoms at surfaces[32].

For chemisorption systems there is a further classification of the nature of bonding, based on electronic, electrical, vibrational and thermal properties. Altogether there are four different types of bonding:
- Van der Waals,
- Covalent
- Metallic
- Ionic

3.2.3 Potential Energy Surfaces, Adsorption Energy

The DFT total energy, $E^{total}(V, N_A^{nuc.}, N_B^{nuc.}, ..., \mathbf{R}_I)$, at volume V, and composition $N_A^{nuc.}, N_B^{nuc.},...$ when studied as a function of the atomic coordinates, is
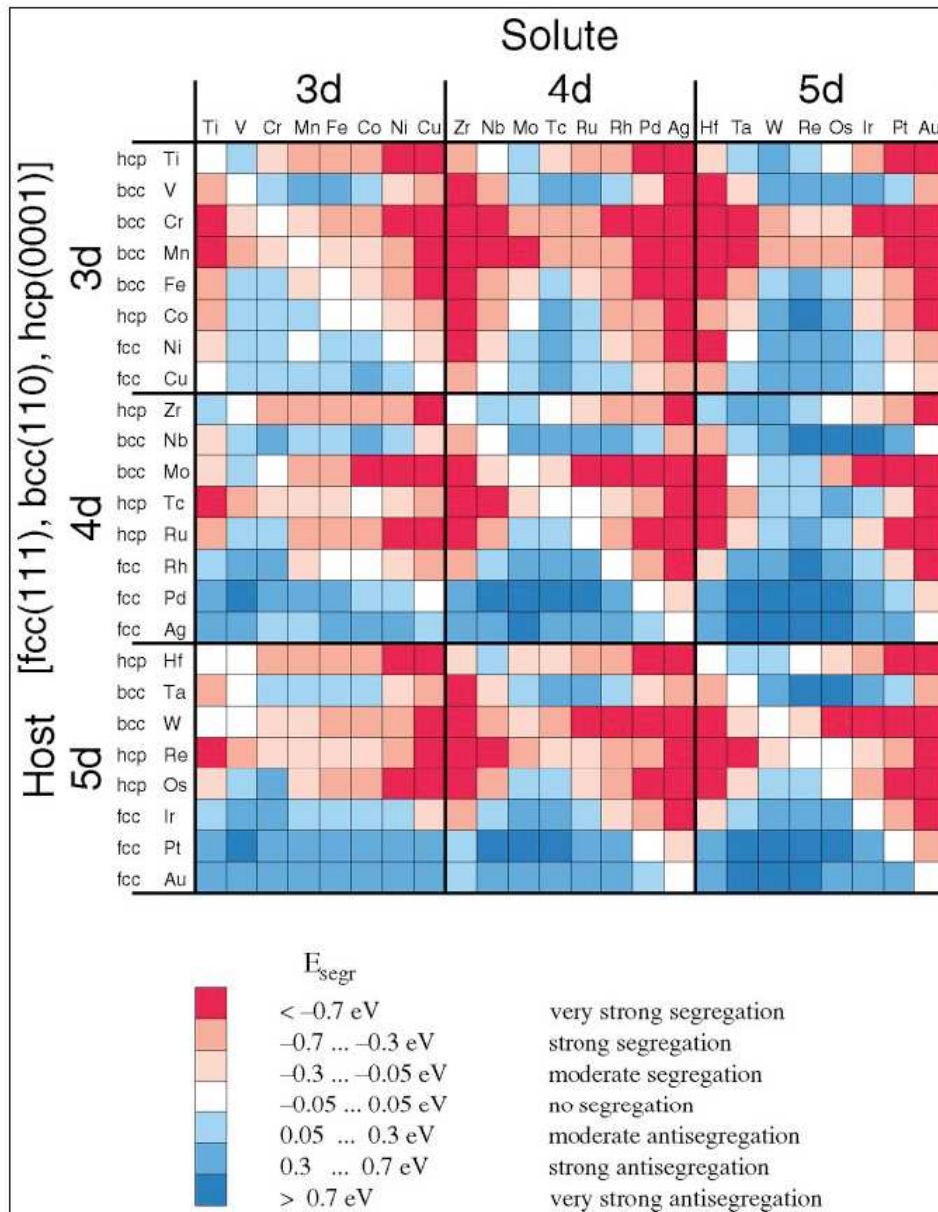
Figure 3.1: Surface segregation energies of transition metal impurities (solutes) for the close-packed surfaces of transition metal hosts. Reprinted from[193]

often called the potential-energy surface (PES)[196]. It is a hypersurface which can help find the global minimum for the energy that corresponds to the most stable configuration. PES is related to the Born-Oppenheimer approximation, and it is an experimentally accessible quantity only when the self-consistent calculations are performed at constant volume, then the DFT total energy corresponds to the Helmholtz free energy at zero temperature and neglecting zero-point vibrations.

The adsorption energy per atom is the difference of the total energy of the adsorbate system and the total energy of the clean substrate together with a corresponding number of free, neutral atoms. For on-surface adsorption this reads

$$E_{ads} = -\Big(E_{total} - E_{clean-surface} - NE_{adatom}\Big)/N \qquad (3.1)$$

where E_{total} is the total energy per adatom of the adsorbate system, $E_{clean-surface}$ is the total energy of the clean substrate, and NE^{adatom} is the total energy of N free adsorbates that take part in the adsorption of on a clean surface.

3.2.4 Adsorption on Transition Metal Surfaces

Adsorption is a process where atoms or molecules from the gas phase or from solution bind in a condensed layer on a solid or liquid surface. The molecules that bind to the surface are called the **adsorbates** while the substance that holds the adsorbate is called the **absorbent or substrate**. Removal of the molecules from the surface is called desorption. Kayser[104], proposed a distinction between **adsorption**, where the gas binds directly to the surface of a solid, and **absorption**, where the gas dissolves directly into the bulk of a fluid or solid. Adsorption of a gas onto a solid is quite different from absorption of a gas into a solid or liquid in that in adsorption, the quantity of gas that adsorbs scales with the surface area rather than the volume of the adsorbent.

The nature of the adsorbate-surface bond varies significantly with the substrate. On metals, the largest contribution to bonding comes from an interaction with the conduction band[97]. The conduction band shares electrons with the adsorbate. The electron density changes only in the neighborhood of

the adsorbate[139]. A surface has three effects: stabilizes intermediates, acts as a source of radicals or ions, and interacts with antibonding orbitals. The stabilization of intermediates allows surfaces to catalyze reactions and also low defect films to grow.

When the adsorbate and the substrate brought together, they start to interact. The adsorbate wave functions are hybridized and the s-band states of the substrate give rise to a broadening of the adsorbate levels. Secondly, the electron chemical potential of the atom become aligned, as the atomic levels will shift to the substrate Fermi level. The broadening (and shifting) of electronic levels is the first modification occurring as an atom is brought close to a surface, due to the spill out of the substrate s-electrons mostly into the vacuum[196]. Broadening implies a coupling of the electrons of the adatom, which are localized, to the substrate, leading to a delocalization. When the adsorbate is closer to the surface, the atomic levels interact with the more localized d-states. As the d-band is rather narrow, the interaction will result in a splitting into bonding and antibonding states. The low-energy peak is due to states, which have an increased electron density between the adsorbate and the substrate, while the high-energy peak is due to states, which have a node between the adsorbate and the substrate. The first is called bonding, while the second antibonding states, and both of them are referred as a splitting. At the final adsorbate-induced DOS, the peaks are close to the lower and upper edge of the d-band, and inside the d-band the density is reduced. That means that these states are shifted from inside the d-band to higher and lower energy due to the hybridization with the adsorbate states. The bonding is strongest when bonding states are occupied and antibonding states remain empty. Finally, when the adatoms approach the surface, the substrate Fermi level acts as an electron reservoir[196].

Hammer and Nørskov[77, 82, 84, 157] have developed a simplified theory of covalent adsorbate bonding on transition metal surfaces. The main assumption of the theory is that the interaction of adsorbate orbitals with surface sp- and d-bands will determine periodic trends in the chemisorption energy of the system. For atomic adsorbates, the model is:

$$E_{d-hyb} = -2(1-f)\frac{V^2}{|\varepsilon_d - \varepsilon_a|} + 2(1+f)\alpha V^2 \qquad (3.2)$$

where E_{d-hyb} is the energy gained from hybridization of the adsorbate orbital with the metal d-bands, f is the fractional metal d-band filling, V is a Hamiltonian matrix element (describing the coupling between the metal d-band states and the adsorbate orbital), ε_d is the the d-band center, ε_a is the adsorbate orbital energy (renormalized by the metal sp-bands), and α is a constant independent of the metal, but depending weakly on the adsorbate[82]. Adsorbates-metal sp-bands interactions depend only on the nature of the adsorbate, and so ε_a is essentially constant for all metals. The changes in E_{d-hyb} for adsorbates on metals are equal to the corresponding changes in their chemisorption energies. This leads to the major conclusion of the Hammer-Nørskov model, that changes in chemisorption energies over different metals are related to changes in the metal d-band centers. This model is useful for describing trends in atomic chemisorption energies on transition metals[66] and one proof is the empirical Bronsted-Evans-Polanyi principle, where there is a linear correlation between energy of activation and enthalpy of reaction. Furthermore, it gives periodic trends for dissociation barriers, with an example the changes in the energy of dissociative adsorption of dihydrogen on several metals[77].

Adsorption of isolated atoms

The theoretical surface science is on a state that can investigate adsorbate structures on an atomic scale. Some important correlation for the adsorption of isolated atoms on metallic surfaces is that stronger bonding, go together with shorter bondlengths. For sites with lower coordination than hollow adsorption site, the strength per bond will typically increase, because the same number of adsorbate electrons have to be distributed over fewer bonds, resulting to a decrease of the bond length on top and bridge sites. This correlation between local coordination and bond strength, and the correlation between bond strength and bond length is well known. Analysis of the adsorbate-induced change in the density of states offers important informations[84].

The binding energy has two components, one from the coupling to the metal s states, and one due to the extra coupling to the d states[77, 80]. Comparing several calculated densities of states we can arrive at two conclusions: (i) the coupling to the d-states is essentially a two level problem giving rise to a bonding and an anti-bonding state, and (ii) the d-bands can be characterized by the band center, ε_d, only. The general trends for the transition metals are that the further to the left in the Periodic Table, the d-band is filled less, and the bond becomes stronger, and that there is a tendency that the further down in the Periodic Table, the weaker the interaction; the 5d metals are more noble than the 4d metals and the 3d metals[84].

Adsorption of CO

The adsorption of a diatomic molecule on a surface is the next degree of complexity and is a link to understanding the behavior of more complex molecular adsorbates, as several of orbitals are now important for the interaction with a surface. The adsorption of the diatomic molecules CO, N_2 and NO is a group often discussed together, as a result of similar binding to transition metal surfaces and as it can be explained within the Blyholder model[162]. For CO, N_2 and NO, as we move to the left from the noble metals, the bond strength increases, as the d states are located at higher energies. Adsorption is molecular on the noble metals and transition metals with a mostly filled d-bands. As the adsorption strength increases, dissociative adsorption becomes more favorable. For all simple molecular adsorbates there is a crossover between molecular and dissociative (atomic) adsorption. The crossover point depends somewhat on the transition metal row - the 5d's tend to favor molecular dissociation less than the 4d's and 3d's. The origin of this effect is the increase in nobleness from the 3d's to the 4d's and 5d's. The exact point of the crossover depends also on the molecule[84].

CO adsorption has been extensively studied both experimentally and theoretically [34, 58, 79, 90, 91, 93, 206]. CO molecules adsorb mostly in an upright position with the oxygen atom pointing outwards. The metal atoms in the immediate surrounding of CO move outwards, but this effect is quite localized. The height of the CO molecule above the metal surface, is determined

by the extention of the d-states of the metal. The C-O bond is generally elongated when it is adsorbed on metals. Higher reactivity of the surface leads to the stronger bonding and population of $2\pi^*$-derived orbitals, resulting a more elongated C-O bond length and lower stretching frequency. DFT calculations indicate that absolute binding energies for CO increase as one moves from right to left across the periodic table[66].

Much effort has been devoted to study CO chemisorption and dissociation on transition metals. There is a rich bibliography of investigations of several aspects like electronic, structural, and vibrational properties of these systems[9, 28, 32, 60, 79, 163, 206, 214].

The three outer valence orbitals of a free CO molecule are sketched in Fig. 3.2. These are the 5σ orbital, the doubly degenerate 1π orbital and the 4σ orbital, with increasing binding energies. The first unoccupied state is the antiboding $2\pi^*$ orbital. For the following discusion, the two most important orbitals are the 5σ and the $2\pi^*$ (HOMO and LUMO) orbitals.

When CO is adsorbed on a metal surface the CO 5σ is significantly hybridizing with the substrate d-electrons, see Fig. 3.2. This gives rise to a charge transfer from the CO 5σ orbital to the metal, but the metal also donates charge back into the antibonding $2\pi^* - CO$ orbital. This donor-acceptor model for CO bonding [28, 29] is known from the metal carbonyls. The back donation from the substrate into the $2\pi^* - CO$ orbital weakens the bonding within the CO molecule and strengthens the bond to the substrate. At close distances the ordering of the 1π and the 5σ-derived levels is reversed compared with the gas phase. In the Blyholder model the lower lying 4σ and 1π MOs (as well as the 3σ and of course the core states) are assumed not to play an important role in the CO-metal bond formation.

With the Blyholder donor-acceptor model we have depletion from the σ orbitals of CO and an increase in electron density into the $2\pi^*$ orbitals[10, 229]. An extensive DFT study of the adsorption of CO on the close-packed surfaces of Co, Ni, Cu, Ru, Rh, Pd, Ag, Ir, Pt and Au is given in the paper of M.Gajdos et al (2005) [60]

As mentioned above, the process of σ donation is partially counterbalanced
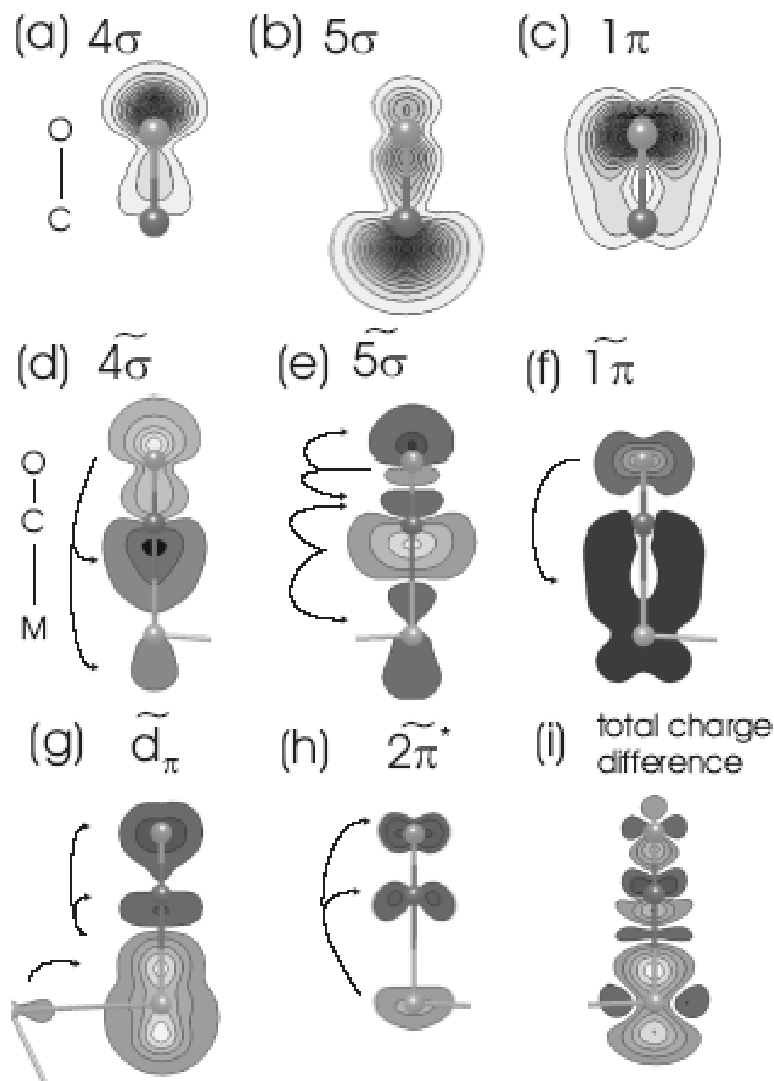
Figure 3.2: Charge density of (a)4σ, (b)5σ, (c)1π CO orbitals for the free molecule and the difference ($\Delta\rho = \rho_{CO+Au(111)} - \rho_{Au(111)} - \rho_{CO}$) after the adsorption in the top site of the Au(111) surface (d,e,f). Figures (g) and (h) show the change in the metal charge density due to CO adsorption in the energy interval $(-5.9, -1.0)$ and just below the Fermi energy $(-0.2, E_F)$. The total charge density difference due to adsorption is shown in Fig. (i). Dark regions: charge accumulation, light regions charge depletion. Reprinted[60]

by back donation of charge from the metal to the $2\pi^*$ MO of the CO[28]. The predominant contribution to the CO-metal bond comes from the back bonding. If the back donation is suppressed by missing d-charge density near the $2\pi^*$MO level (as encountered with the quasi s-p metals, Cu, Ag, and Au), then the CO-metal bond is always weak. From simple symmetry arguments, the overlap of CO $2\pi^*$ orbitals with metal d_π orbitals works best in high-coordinated adsorption sites, while the overlap between CO-5σ orbitals is maximized for on-top adsortpion. Another trend for the CO adsorption on metals is that with increasing CO coverage the C-O bond length decreases. This happens because as we increase the coverage, the CO back bonding is weakened due to competition for electronic density.

Coadsorption systems, adsorbate-adsorbate interactions

The surface coverage of reactants, intermediates and products on a catalyst can vary significantly depending on reaction conditions, and often the coverages are so high that adsorbate-adsorbate interactions give an important contribution to the chemistry of the surface. These interactions can be both attractive and repulsive. The first case is the reason for the island formation. Repulsive interactions lead to dispersed overlayers and a strongly coverage dependent heat of adsorption. While attractive interactions are often quite weak and depend on the details of the system, repulsive interactions are very common, in particular at high coverages. The attractive interactions are usually dependent on details in the electronic structure[84].

There are four common interactions between adsorbates:

• Direct interactions due to overlap of wave functions. They may lead to attraction if there are states close enough to the Fermi level.

• Indirect interactions. One adsorbate may change the electronic structure of the surface, by effecting the adsorption energy of a second adsorbate. One observed effect is that adsorption leads to a shift of the d states to lower energies of the neighboring transition metal atoms[81, 147], and this leads to a weaker interaction with an adsorbate. This implies that a second adsorbate may be bound less strongly, comparing to the first one at the same transition metal atom.

- Elastic interactions. Adsorption usually leads to local distortions of the surface lattice, which will be experiences by other adsorbates as a repulsion[131].
- Non-local electrostatic effects. These can be described as dipole-dipole interactions[84], and they are important at self assembly processes.

The strong coverage dependence of adsorption energies affects the reactivity of a surface. A weaker bound adsorbate may be more reactive and changing the reaction conditions (temperature and/or partial pressures) can therefore change the reactivity considerable[84].

3.2.5   Importance of Ni, Pt, Au in catalysis

Platinum and nickel are used extensively as hydrogenation/dehydrogenation catalysts, and also are useful for oxidation. Oxygen dissociates at temperatures between 50 and 300 K on them. The adsorbed oxygen is a strong nucleophile that reacts with hydrocarbons, alcohols, etc., to yield partially oxygenated species on the surface. However, partially oxidized species usually do not desorb from the surfaces of platinum or nickel. Instead partially oxygenated species further react (and decompose) to eventually yield CO, CO_2 and water[139].

The surfaces of gold are fairly inert. Hydrocarbons, alcohols, amines or H_2 only interact weakly with them. Generally, one does not observe any reactions of these species on clean gold surfaces[139]. On the other hand small clusters of this metal have different properties than the clean surfaces[76, 126, 140], exhibiting stronger interaction with molecules.

3.3   Reactions on Surfaces

3.3.1   Introduction

Reactions on metal surfaces are important in heterogeneous catalysis[93, 139]. In general surfaces stabilize reaction intermediates, and that is part of why a catalyst works. However, it may occur that, the surface binds the intermediates so much that the intermediates become unreactive. For example, tungsten is

not a good catalyst for hydrogen oxidation, although it dissociates hydrogen and oxygen. However, the resultant species are so strongly bound that they are fairly unreactive. The hydrogen/oxygen reaction forming water occurs rapidly at 300 K on platinum. However, on tungsten one needs to go to temperatures over 1100 K to get a reasonable rate[139].

It is possible to add the so-called poison or promoter to modify the reactivity of a surface. Generally **poisons** are species (e.g. sulphur) that bind to surfaces strongly and thereby inhibit desirable reactions. **Promoters** are generally species such as alkalis that can donate electrons to the metal and thereby modify the metals properties. Finally, there are some species called structural promoters. **Structural promoters** are thought to modify the distribution of sites in a supported metal catalyst so that there is a higher proportion of active sites. For example, iron catalysts are used for ammonia synthesis, promoted by potassium (chemical promoter) or alumina (structural promoter).[139].

There are three generic types of surface reactions: those that follow Langmuir-Hinshelwood mechanisms, in which the reaction occurs between species that are adsorbed on the surface, those that follow Eley-Rideal, in which the reaction occurs between a reactant molecule in the gas phase and one that is adsorbed on the surface[130] and finally those that follow precursor mechanisms, where the reactants are weakly bound to the surface. One can find a very good and detailed description at the book of Masel[139].

3.3.2 Chemical Reactions/Catalysis on Metal Surfaces

An important contribution of reactivity comes from the surfaces' ability to break the bonds of an approaching molecule and to adsorb the fragments. On the other hand, too strong adsorption of the fragments lowers the reactivity. For example, in the ammonia synthesis the role of limiting has the dissociation of N_2, and in oxidation catalysis (e.g. the catalytic oxidation of CO) the dissociation of O_2.

Any chemical reaction can be described as a transition between two local minima on the potential energy surface of the system as a function of the coordinates of all the involved atoms. The reaction path is defined as the minimum energy path leading from the reactant minimum to the product minimum. The saddle point on this path defines the transition state and the

energy difference between the saddle point and the reactant minimum is the activation energy of an elementary process[84].

A general rule is that the higher d-band center is correlated with a lower activation energy[43, 44, 77, 78, 80]. Moving to the left in the transition metal series, gives a lower activation energy, but also stronger bonding of the reactants and thus less free surface area. The "Sabatier principle"[195] type behavior, usually leads to "Volcano curves"[31] describing the relation between catalytic activity and position in the periodic table[202]. The chemisorption and the reactivity of a metal surface will depend on the electronic as well as the geometric structure of the surface. It can be changed substantially by changing the surface structure, by alloying or by introducing impurities or coadsorbates on the surface, by defects, and by the coverage of the surface. The structure sensitivity can vary by the strain, the facets, the steps and the defects.

Finally, the activity of realistic catalysts is often assumed to be dominated by so-called active sites, i.e., sites with a specific geometric configuration that modifies their electronic and chemical properties. In fact, many adsorbates bind much stronger to step sites than to sites on a flat terrace[69].

Part II
Applications

Chapter 4

Au - Ni(111) system, NEB and DOS

4.1 Introduction

The modification of the chemical reactivity of a metal by surface-alloying with a second element, is a timely and challenging field of research. Bulk immiscible metals (e.g. Ag/Cu, Ag/Co and Au/Ni) can form binary alloys on certain surfaces, where the substrate mediates the elastic misfits between the two components, thus relieving the elastic strain in the ovelayer. These novel surface alloys exhibit a rich phase structure and offer amenable features for several electronic and magnetic nanoscale device applications as well as for catalysis[39].

Au/Ni is a type of alloy, which was investigated by Kratzer et al.[116] for its ability to crack methane and gold-doped Ni surfaces have received much attention since the development of a novel steam-reforming catalyst[1] with improved resistance against carbidization of the surface[22]. However, the material continues to be of timely interest, as demonstrated by the recent work of Lahr and Ceyer[129] on CO oxidation on Au/Ni surface alloys, and the studies of

---

[1]Steam reforming is very widely used method for the production of syngas, with the use of Ni catalysts. The CH_4 reacts with H_2O and forms H_2 and CO. The CO reacts further with the steam to form CO_2 and again H_2. There is also the so-called secondary steam reforming for the production of ammonia.

Vestergaard et al.[224] and Zhdanov et al.[238] on CO-mediated removal of Ni atoms from the topmost layer of a Au/Ni(111) surface alloy.

Gold and nickel are immiscible in the bulk, due to a substantial size-mismatch of about 16 % (the nearest-neighbor distances in face-centred cubic Au and Ni are 2.88 Å and 2.49 Å, respectively[221]), while elemental Au-Ni is immiscible in the bulk[98] and have positive enthalpy of mixing[128]. However, a two dimensions surface alloy exists, in which gold alloys into the outermost surface layer of a Ni(111)[154] (the segregation energy at the close-packed Ni(111) surface is $\Delta E_{seg} = -0.69$ eV[193]). The alloy is interesting also from a synthesis point of view; as the gold does not dissolve into the Ni bulk[142], only small traces of Au is required to create the alloy.

The central questions are under which conditions surface alloying can occur and how the presence of Au adatoms on the surface (chapter-4)[218] or of Au atoms in substitutional sites in the surface layer (chapter-5) modifies the adsorption properties. Equilibrium segregation experiments performed on dilute alloys indicate that Au segregates on top of Au-Ni alloys[210, 233]. Surface alloy of Au on Ni(110) is also detailed investigated with STM studies and computationally[154, 155]. The Au itself is inert for methane decomposition and because the Au causes a down shift of the Ni d-bands at neighboring sites, the ability of the alloy to catalyze the C-H bond activation is slightly inferior to that of the clean Ni(111).

At this chapter, is examined how the Au adatom can substitute a Ni atom from the surface and create an alloy, using the NEB method. It is found that alloying Au into a Ni(111) surface (exchanging a Au adatom against a Ni atom from the surface layer) is an activated endothermic process with an activation energy of 1.7 eV and a heat of reaction[2] of 0.44 eV. If surface alloying takes place, it is driven by entropic effects. A number of experimental studies suggest the simultaneous presence of adatoms and substitutional impurities on a Au-doped Ni surface [98, 117, 183, 184]. This phenomenon is closely related to the competition between short-range order and phase-separation in bulk Au-Ni alloys[39, 190, 230]: chemical interactions favor ordering based

---

[2]The amount of heat absorbed or released or else the change in the enthalpy of the system that occurs in a reaction, at constant pressure. For exothermic reactions the convention is that the enthalpy change (heat of reaction) is negative

on heterocoordination of Au by Ni, strain-induced interactions drive phase-separation. Furthermore, there is a extend study of the Density of States of the Au/Ni(111) for the both cases: meaning when Au is an adatom and when an alloy is formed.

4.2 Methodology

To locate transition states and for the determination of reaction barriers, the nudged-elastic-band method[151] has been used. The calculations have been performed using VASP [120, 228]. For the NEB calculations a less intense k-mesh has been used. For the Density of States "high precision" was used. A simulation of STM picture and a contour plot of the iso-density is presented for the Au doped Ni(111) surface, using the PARCHG output file. In both cases, Au adatom and substitutional, the coverage is 0.11ML, as it has been used one Au atom for a p(3x3) surface cell.

For both cases, spin polarized and paramagnetic calculations have been performed for the system Au/Ni. The plane-wave basis-set contained component with a kinetic energy of up to E_{cut}=270 eV.

4.3 Nudged Elastic Band Method (NEB)

4.3.1 Theory of NEB Method

In surface kinetics it is often desirable to know the energy needed to overcome an energy barrier in a surface reaction[103]. Hence, it is necessary to know the reaction path, the saddle points and minimum energy path (MEP) between known reactants and products. The Nudged Elastic Band (NEB) method[88, 89] provides a way to determine them. The method works by optimizing a number of intermediate images along the reaction path. Each image converges to the lowest energy possible, while maintaining equal spacing to neighboring images. This is done by adding spring forces along the "band" connecting the images and by projecting out the component of the force perpendicular to the band ("nudging").

A path connecting the initial and the final states that typically has the
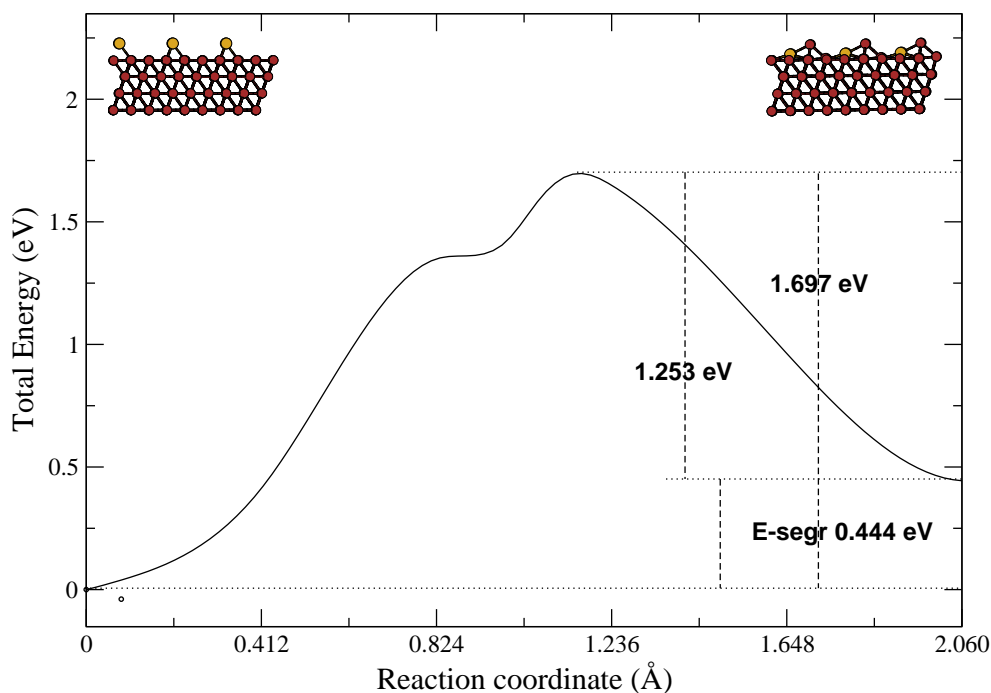
Figure 4.1: Potential-energy profile for the exchange between a Au adatom and a Ni-surface atom on Ni(111). The inset shows the initial and final configurations.

highest probability is the MEP. At any step along the path, the force acting on the atoms is only pointing along the path. The energy is stationary for any perpendicular degree of freedom. The maxima along the MEP are saddle points on the energy surface. The relative distance along the MEP is a natural choice for a reaction coordinate and at the saddle point the direction of the reaction coordinate is given by the normal mode eigenvector corresponding to negative curvature. Many different methods have been presented for finding MEPs and saddle points[88], but NEB method is an efficient one. An essential feature of the NEB method, which distinguishes it from other elastic band methods is the force projection, mentioned above.

4.3.2   Application of NEB Method to Au/Ni(111) system

Although gold does not form bulk alloys with nickel at ordinary temperatures [142] and surface segregation is favored by an exothermic segregation energy [193] of $\Delta E_{seg} = -0.69$ eV, at elevated temperatures the formation of surface alloys on Ni(111) [155] and Ni(110) [98, 154] surfaces has been reported. Photoelectron spectroscopy [235, 236] of ultrathin bimetalllic Au/Ni films vapor-deposited on Y-doped ZrO_2 revealed a pronounced tendency of the Au atoms to segregate to the surface. Temperature-programmed desorption (TPD)[3] studies of adsorbed CO showed a strong shift of the TPD peaks to lower temperatures even at the lowest Au/Ni ratios.

Using the Nudged Elastic Band method[151] is calculated the potential-energy profile for the exchange-reaction between a Au ad-atom and a Ni atom from the top layer. The initial configurations had a Au atom in a fcc hollow of a clean Ni(111) surface, in the final configuration, Au occupied a substitutional site in the Ni(111), while one of the Ni atoms was expelled to an ad-atom position in a threefold hollow next to the Au impurity. The reaction coordinate measures the distance between these two configurations, all coordinates perpendicular to the reaction path are allowed to relax. The resulting potential-energy profile is shown in Fig. 4.1. It is found that surface alloying is an activated and endothermic process. The energy cost for the exchange process is 0.44 eV - this is substantially lower than the bulk segregation energy of 0.69 eV calculated by Ruban et al.[193]. The activation energy for the exchange process is 1.70 eV. In the final configuration, the Au atom protrudes from the Ni surface. The center of the Au atom is located at about 0.65 Å above the Ni surface. The six nearest neighbor Ni atoms in the surface relax by about 0.14 Å away from the Au atom and they are pushed slightly deeper into the surface by 0.015 Å. This distortion of the Ni surface accounts for a substantial part of the endothermic energy of formation of a Au surface impurity.

Results suggest that the surface alloying observed at elevated temperatu-

---

[3]A process of characterization for catalysts. A gas (e.g. Xe) at various temperatures is passing through a sample and after through a detector, e.g. a mass spectrometer. With TPD one can determine at what rate a sample is adsorbed or desorbed.

res[154] is entropy-driven. This conclusion agrees with the findings of Ozolins et al.[164], which show that Ni-Au alloys have a large configurational and nonconfigurational (vibrational) entropy of formation. As a Au impurity is only loosely anchored in the Ni surface layer, we can expect the vibrational contribution to the entropy to be even larger for a surface impurity than in the bulk.

4.4 Au adatom on Ni(111)

An isolated Au atom in a $p(3 \times 3)$ surface cell of Ni(111) is adsorbed in an fcc hollow, which is favored by 10 meV/atom over the hcp hollow. The adsorption of Au is determined by hybridization of the d_{xz} and d_{yz} orbitals of Ni with the d_{xz}, d_{yz} and d_{z^2} states of Au. Adsorption on an on-top site is locally stable, but disfavored by about 0.8 eV/atom, whereas the bridge-site represents only a saddle-point. Details of the calculated adsorption geometries are compiled in Table 4.1, together with adsorption energies with respect to gas-phase Au ($E_{ads} > 0$ meaning exothermic adsorption). The presence of the Au ad-atom induces a slight outward relaxation of the top Ni-layer, in contrast to the clean Ni(111) surface[146], which shows a very modest inward-relaxation by -0.9%. The Au-induced outward relaxation of the top layer is modest for the stable location of Au in the threefold hollows, where it is accompanied by a contraction of the distance between the Ni sub-surface layers. The presence of the Au ad-atom induces only a very modest change in the structure of the surface layer: nearest-neighbor Ni atoms relax lateral by about 0.01 Å, the buckling of the surface layer is ≤ 0.01 Å. For the metastable location of the Au-atom in an on-top position, a more pronounced outward relaxation and a stronger surface buckling is found.

The presence of a Au impurity induces a change in the d-band position of the neighboring Ni atoms (see Fig. 4.2). For Ni-atoms that are nearest neighbors to the Au ad-atom, the peak in the density of states (DOS) immediately below the Fermi-energy is reduced, and due to the hybridization with the Au-d states, the DOS is enhanced at a binding energy of about -3 eV. Hence the center of gravity of the d-band is locally shifted to higher binding energies. The changes are the same for the spin-polarized and the paramagnetic DOS.
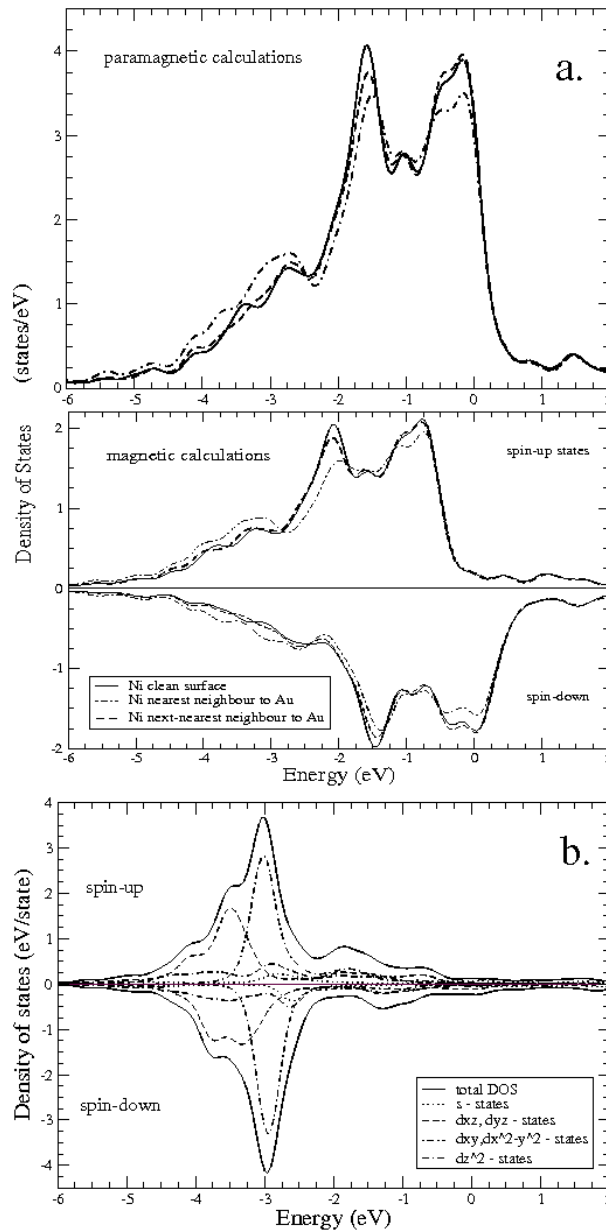
Figure 4.2: (a) Spin-polarized and paramagnetic electronic density of states (DOS) of the d-band for a Ni-atom on a clean Ni(111) surface and for Ni atoms in nearest and next-nearest neighbor positions to a Au adatom on Ni(111). (b) Local electronic DOS of a Au ad-atom.

Table 4.1: Adsorption energies (E_{ads}, in eV/atom) and geometries (relaxation of Ni-Ni interlayers distances and shortest Ni-Au distance) for Au ad-atoms on Ni(111) at a coverage of 0.11 ML.

Au/Ni(111)	top	hcp	fcc	bridge
E_{ads} (eV)	2.04	2.83	2.84	2.31
d_{1-2} (%)	5.7	2.4	1.9	-1.0
d_{2-3} (%)	-0.3	-1.1	-1.4	-0.2
d_{NiAu} (Å)	2.3	2.6	2.4	2.5

Both effects - the reduction of the DOS near E_F and the shift of the d-band-center lead to a reduced chemical reactivity of the Ni atom. However, already for next-nearest neighbors to the ad-atom, the local DOS is almost unchanged with respect to the clean surface. The center of gravity of the d-band DOS of the Au ad-atom is located at ~ -3 eV, compared to a clean Au(111) it is shifted by ~ 0.4 eV to higher binding energies (see Fig. 4.6). The d-band of the adatom is rather narrow, but due to the hybridization with the Ni-d states, a significant d-band DOS is also found between -2 eV and the Fermi energy.

Experimental STM studies, for the adsorption of Au on Ni(111), held by Prof.Dr. Karl-Heinz Rieder at Freie Universität Berlin, Institute for Experimental Physics, display a broken symmetry in the pictures taken in the dI/dV mode[4]. That was the driving force to simulate STM pictures for the system. The STM simulation has been done using the Tersoff-Hamann approach[5]. Therefore, the STM calculations do not include the modulation of the tip. The bright spots are located at the position of Au adatoms Fig.- 4.3. No broken symmetry is observed for the simulated STM picture in dI/dV mode. It might be necessary to include the influence of the tip to reproduce the experimental perturbations.

For the further study, of the experimental STM studies with the broken

---

[4]There are three operation modes of STM: constant height scanning, constant current scanning and I-V mode, which is spectroscopic. The dI/dV measurement, using the STS technique, is a direct probe of the DOS at the location of the tip.

[5]$I(x,y) = A \int_{E_F}^{E_F + eV_{bias}} dE \sum_m |\psi(x,y)|^2 \delta(E - E_m)$, which is work well for flat surfaces. At low bias voltages, one can measure Local DOS at the E_F. Fixing the position of the STM tip, then dI/dV_{bias} is proportional to LDOS[115]
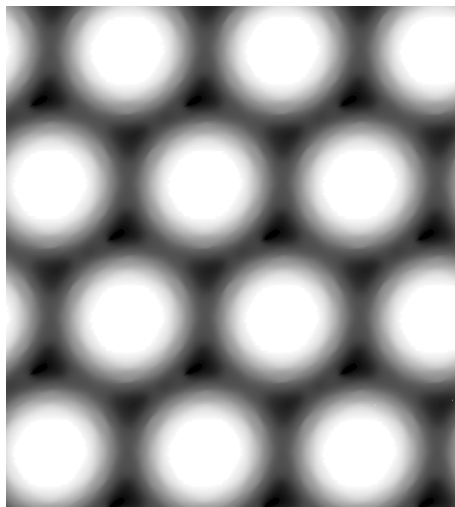
Figure 4.3: Simulated Constant Current STM image, using a bias-voltage of -0.2 eV.

symmetry, an iso-density surface was created (Fig.- 4.4). Here one can see that from the right side of Au adatom (atom above the surface) there is a small gap of charge-distribution between Au adatom and the Ni surface atoms, inwards the substrate (see the arrow at the fig. 4.4). That might related with the broken symmetry observed by Prof. Rieder, but further analysis is necessary to be done.

4.5   Au substitutional atom on Ni(111)

The presence of Au substitutional atom induces changes in the d-band position of the nearest, but also to the next nearest neighboring Ni atoms (Fig. 4.5). The picks in the DOS for Ni-atoms first neighbors to Au substitutional, immediately below the Fermi-energy, but also at energy -1.6 eV are reduced, while the pick at energy -3 eV is enhanced. The center of gravity of the d-band is shifted again to higher binding energies, due to the hybridization with the Au-d states. This effect is observed in both the magnetic and the paramagnetic calculations. This leads to a reduction of the chemical reactivity of the Ni nearest-neighbor to Au. For the next-nearest neighbor, there is a reduction of DOS at energies -1.6 eV and in the region -2.5 to -3.5 eV and an increase
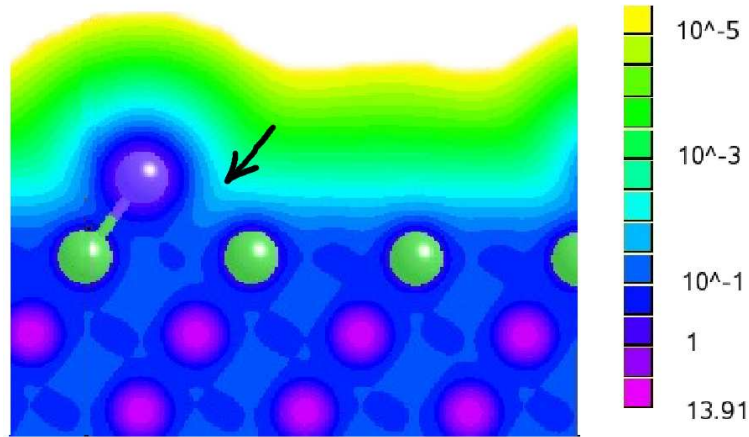
Figure 4.4: Calculated charge density iso-surfaces around a Au adatom on Ni(111).

at -5 eV, where is observed the highest pick of Au. For this Au/Ni system, the effect of Au impurity is more extend concerning changes on the Densities of States, but on the other hand there is no total shift of the center of the d-bands for the second Ni neighbor to Au. This and the preservation of the DOS below the Fermi Energy makes the adsorption on the second-neighboring Ni atoms from Au to bind CO molecule equally strong like a clean Ni(111) surface.

Furthermore, the total DOS is more narrow compared to a clean Au(111) surface, so the states are more localized, but in the other hand, the DOS of the Au substitutional has more extended width compared to this of the Au adatom on Ni(111).

In the Table 4.2 is shown the magnetic moment of Ni, the nearest neighbors to the Au substitutional is reduced due the Au atom, but the Ni, the next-neareast neighbor exhibits a behavior very similar to that of a clean Ni surface atom. The Au substitutional-atom, from zero at the case of clean Au(111) surface atom, appears a small amount of magnetic moment (0.02), smaller than that of Au adatom on Ni(111). For the charge we can notice that the total charge of Ni is increased for all the atoms by a small amount (0.02). The same phenomenon like the enhance of the charge of Au adatom is observed for the Au substitutional atom, but here the increase is more pronounced (0.2).

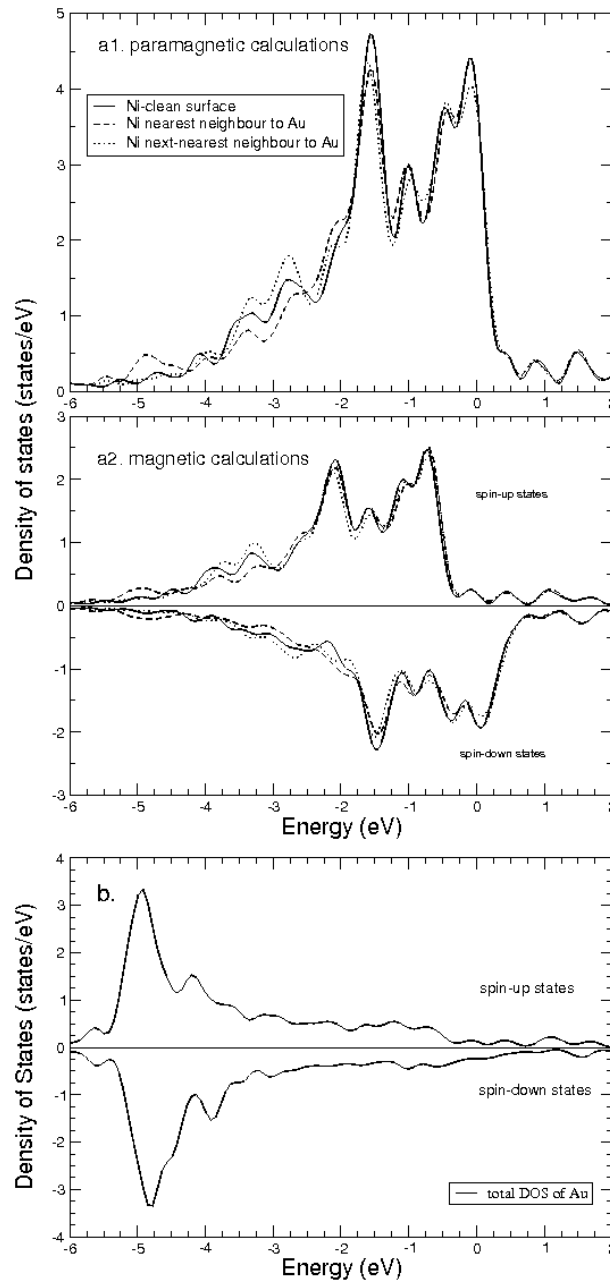Figure 4.5: (a) Spin-polarized and paramagnetic electronic density of states (DOS) of the d-band for a Ni-atom on a clean Ni(111) surface and for Ni atoms in nearest and next-nearest neighbor positions to a Au substitutional atom on Ni(111). (b) Local electronic DOS of a Au substitutional-atom.

Table 4.2: The magnetic moments and the charges for the s, p, d and total amounts for both of them for a clean Ni atom, for a Ni nearest and the next-neighbor from Au substitutional, as well for the Au substitutional atom, the Au adatom on a Ni(111) surface and finally for a Au atom on clean Au(111) for comparison.

atom	s-mm	p-mm	d-mm	tot. mm	s-c	p-c	d-c	tot. c
Ni-clean	−0.01	−0.02	0.73	0.70	0.49	0.39	8.30	9.18
Ni-1st	−0.01	−0.02	0.70	0.68	0.49	0.40	8.32	9.20
Ni-2nd	−0.01	−0.02	0.72	0.69	0.50	0.40	8.31	9.21
Au-substit.	−0.01	−0.03	0.06	0.02	0.69	0.37	8.66	9.72
Au-adatom	0.01	0.00	0.03	0.04	0.67	0.11	8.82	9.60
Au-clean	0.00	0.00	0.00	0.00	0.54	0.24	8.73	9.50

Note that there is a small overlap of the radii of the Au and Ni of about 0.22 Å. But this is not the reason for such a change of the total charge of Au.

4.6 Comparing the Density of States

It is also interesting to explore the electronic origin of the striking differences of the adsorption behavior of a Au atom in adatom and impurity sites. Fig. 4.6 shows the total electronic density of states (DOS) of a Au(111) surface, of a Au adatom and of a Au impurity on Ni(111), while at Fig 4.7 it is displayed a more detailed description of them. For the adatom the change relative to the Au clean surface consists mainly in a pronounced band-narrowing, the center of gravity of the d-band DOS is located at lower binding energy of about 3 eV. For the surface impurity the much stronger hybridization with the Ni-substrate leads to a strong repulsion between the d-bands, the peak in the d-DOS of the Au impurity is shifted to a binding energy of 5 eV, while the center of gravity is shifted to higher binding energies by 0.5 eV compared to the clean Au. Hence, while for the adatom the presence of a hybridization-induced d-DOS close to the Fermi energy leads to an at least partially covalent character of the Au-CO binding, due to the d-band shift of the impurity the binding mechanism consist only of a weak polarization-induced interaction.

Figure 4.6: Electronic density of states of a Au(111) surface and local density of states of a Au adatom and of a Au impurity on a Ni(111) surface. The center of gravity for the occupied states are at -2.96 eV for the Au-adatom on Ni(111), at -3.37 eV for the Au-clean surface, and further at -3.86 eV for the Au substitutional atom.

Some additional informations can be obtained by the Fig. 4.7. The d_{xz} and d_{yz} states in both cases of Au impurity on Ni(111) are shifted to higher binding energies. This change is more pronounced for the Au substitutional atom. In contrast with these states, the changes for d_{xy}, $d_{x^2-y^2}$ and d_{z^2} are modest. The s-states for Au in both cases are shifted to lower binding energies.

The most important conclusions from the comparison of the Au adatom and Au substitutional on Ni(111) with the clean Au(111) surface are:

• the DOS is much more narrow for both cases.

• the center of gravity of the d-band occupied-states for the Au(111) clean surface that is located at energy -3.37 eV is shifted to lower binding energy by 0.4 eV for the Au-adatom and to higher binding energy by 0.5 eV for the Au-substitutional atom.
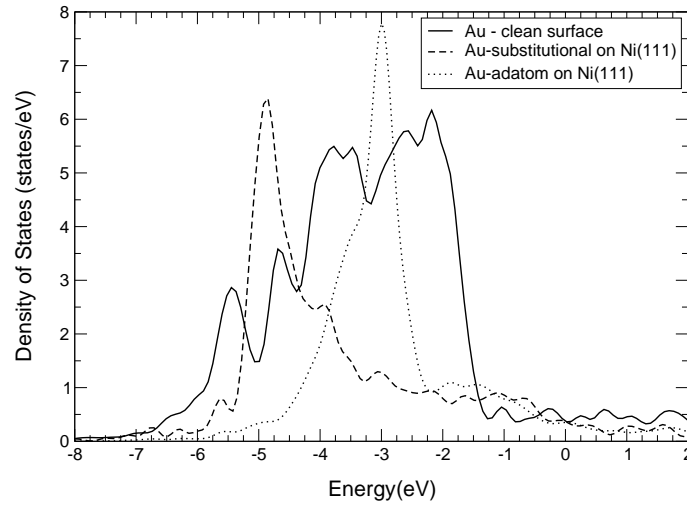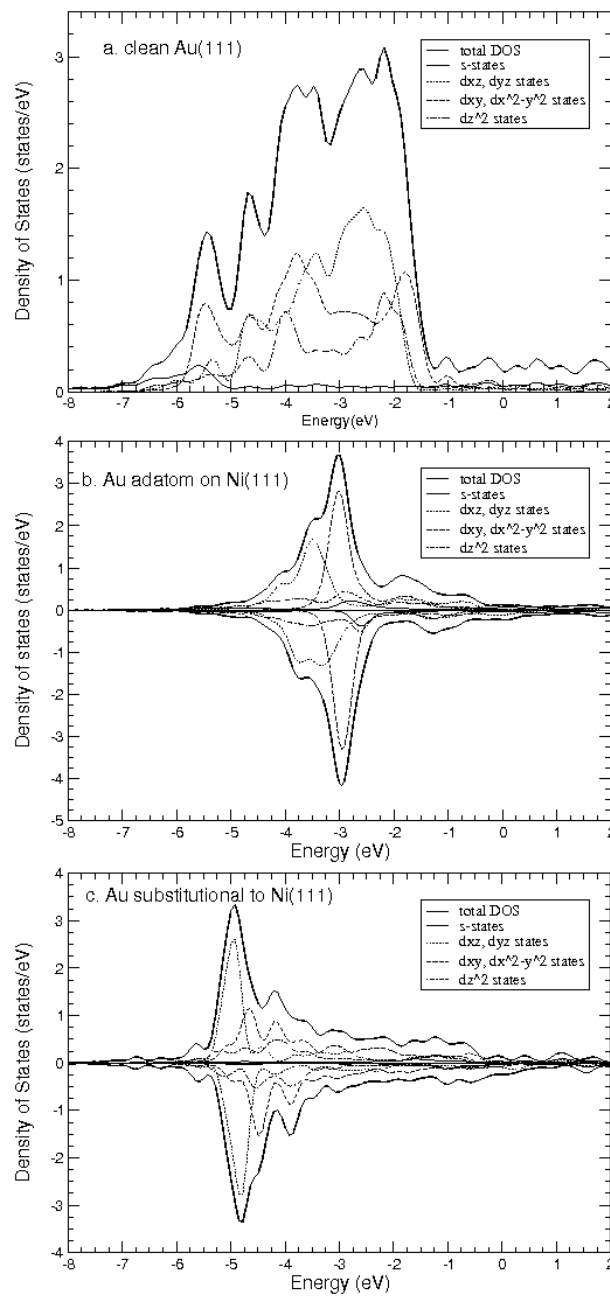
Figure 4.7: Detailed electronic density of states of a Au(111) surface and local density of states of a Au adatom and of a Au impurity on a Ni(111) surface.

4.7   Conclusions

Using the NEB method is found that the surface alloying for the Au/Ni(111) system is an activated and endothermic process. The activation energy for the exchange process of Au adatom on a substitutional position is 1.70 eV, while the energy cost is 0.44 eV.

An isolated Au atom is adsorbed on an fcc hollow site on the Ni(111) surface, with adsorption energy of 2.84 eV, and induces modest changes in the structure of the surface layer. The center of gravity of d-band for Ni next neighbor to Au is shifted to higher binding energies and there is a significant reduction of the DOS below the Fermi energy, due to the hybridization with Au. This leads to a reduction of the reactivity of Ni, as it will be shown at next chapters. Less pronounced changes occurs with the DOS of Ni atom next neighbor to Au substitutional.

For the DOS of Au atoms for both cases is observed a narrowing of the bands compared to clean Au surface. For the Au adatom the center of gravity of occupied states is shifted to lower binding energies by 0.4 eV, while for the Au substitutional the shift is to higher binding energies by 0.5 eV compared again with a clean Au(111) surface.

Finally, the results are also relevant for the interpretation of catalytic reactions on Au/Ni(111) surface. In their recent report on CO oxidation catalyzed by Au-doped Ni(111), Lahr and Ceyer[129] tentatively attribute the production of CO_2 to the reaction between CO and O bound to Au impurities in the Ni surface. This interpretation is probably too simplistic, and our results suggest a modified mechanism. Recent investigations of catalytic reactions of diatomic molecules have established a universal linear Brønsted-Evans-Polanyi relationship between the adsorbate binding energies and the activation energies[61, 158]. Kinetic modeling studies have shown that the optimum catalysts have intermediate binding energies of -1.1 ± 0.3 eV. Hence pure Ni(111) surfaces bind CO too strongly for an efficient activation of the molecule, while binding to Au atoms in a Au/Ni(111) surface alloy is much too weak. Binding to Au adatoms and to sites in the vicinity of a Au impurity on the other hand occurs at energies within the range for an optimal reactivity.

Chapter 5

CO adsorption on clean Ni(111) and Au doped Ni(111) surfaces

5.1 Introduction

The design of surfaces with tailor-made properties is one of the goals of surface science, e.g. a capability to bind a molecule strongly enough to initiate a catalytic reaction without dissociation of it, that would poison the catalyst. Alloying can modify the catalytic activity and selectivity of a metal significantly and alloy catalysts represent a successful route towards novel catalysts with superior properties compared with elementary metals[185, 198]. During the recent years, DFT studies of alloy surfaces[70] have been developed to a point, where realistic predictions of the reactivity governed by the interplay of electronic and geometric effects become possible.

One of the first examples of the design of a novel alloy catalyst inspired by theoretical concepts and ab-initio calculations was the development of a novel steam-reforming catalyst[22] based on gold-doped Ni. Clean Ni surfaces have a good performance as a steam-reforming catalyst, because of the ability to easily dissociate CH_4. However, the activity of Ni-catalysts rapidly deteriorates because Ni binds C atoms too strongly, resulting in carbide-formation and graphitization of the surface. Various attempts have been made to reduce the Ni-C bond-strength, like the selective poisoning of the surface with sulphur[191]. Doping the surface with a sub-monolayer amount of Au turned out

to be much more successful. Only a small fraction of Au atoms incorporated into the outermost Ni layer induces a substantial modification of the surface reactivity:

• DFT calculations show that the chemisorption energy of C on Ni(111) is reduced by almost 2 eV/atom if the C atom binds to a site next to a Au impurity, and even next-nearest neighbor sites are still significantly destabilized[22].

• Again according to DFT calculations[116], the dissociation barrier for CH_4 is increased by 0.17 eV/molecule and 0.39 eV/molecule for a Ni atom with one or two Au neighbors, respectively.

• TPD[46] studies[95] have shown that the binding energies of CO and D_2 decrease by approximately 0.26 to 0.31 eV/molecule as the Au concentration in the surface layer increases from 0 to 0.7 monolayers.

• Scanning-tunneling microscopy (STM) studies combined with DFT calculations have demonstrated that CO binding is excluded at the threefold hollows next to a Au atom.

These results show that the doping of the Ni surface will strongly reduce the tendency to carbide formation and graphitization, while the barrier for methane dissociation is only modestly increased.[132]

There are, however, certain aspects that are still incompletely understood. For example, it has been reported that at high pressure CO induces a tendency to reverse surface alloying[224]. Au is the noblest of all metals, and its low-index surfaces show a very low reactivity. On the other hand, nanoparticles of gold, deposited on inert substrates have been found to be very reactive and to show catalytic activity at or even below room temperature[138].

In this chapter is presented a study of the chemical reactivity at a Au ad-atom adsorbed on a Ni(111) surface and its influence on the surrounding Ni atoms via the simulated adsorption of CO molecules. The adsorption of carbon monoxide on clean-Ni(111) and in the vicinity of an isolated Au ad-atom on a Ni(111) surface has been studied using ab-initio DFT. Detailed investigations of the potential-energy surface for the binding of CO atoms show that for bonding sites in which the molecule binds at least to one Ni nearest neighbor of the Au ad-atom, the adsorption energy is reduced by up to 1.2 eV compared to the adsortpion energy on a clean Ni(111). At larger distances from the

impurity, the adsorption energies are almost unchanged. On the other hand, binding of CO molecule to the Au ad-atom is much stronger than on a flat Au surface.

5.2 Methodology

The adsorption of CO on clean Ni(111) and on the system Au/Ni(111) has been studied using DFT. The calculations have been performed using the Vienna ab initio simulation package VASP [118, 120, 121, 228], which performs a variational solution of the Kohn-Sham equations in a plane-wave basis set[1]. The electron-ion interaction is described using ultrasoft pseudopotentials[2][119, 223], atomic pseudo-charge densities are transformed to all-electron charge densities according to the projector-augmented-wave (PAW) method[3] introduced by Blöchl[26] as modified by Kresse and Joubert[122]. Electronic exchange and correlation are described in the GGA, using the functional proposed by Perdew, Burke and Ernzerhof (PBE)[169]. The plane-wave basis-set contained component with a kinetic energy of up to E_{cut}=400 eV for studying CO adsorption. Convergence with respect to the basis set has been checked very carefully in an extended study of CO adsorption on transition-metal surfaces.[60]

The substrate was modeled by slabs consisting of four nickel layers with a periodicity of $p(3 \times 3)$ in the surface-lane, separated by about 20Å of vacuum. The upper two layers of the surface have been allowed to relax, while the

---

[1]A convenient way to approximate the one particle wavefunctions within periodic boundary conditions. The wavefunction can be written: $\psi_i, k(\mathbf{r}) = \sum_G c_{i,G} e^{[i(\mathbf{G+k})\cdot\mathbf{r}]}$, with sum over all the reciprocal lattice vectors $\mathbf{G}$ defined by $\mathbf{G}\mathbf{l} = 2\pi n$, where n is integer. They form a complete and orthonormal set, that is independent from the atomic positions.

[2]The pseudopotential theory[86, 181] provide us a way to replace the strong electron-ion potential with a weaker potential- a pseudopotential, describing all the features of an electron moving through the solid. With the pseudopotentials, a solid can be modelled by pseudo valence electrons and pseudo-ion cores. These pseudoelectrons experience the same potential outside the core region as the original electrons, but have a much weaker potential inside the core region.

[3]PAW is a combination and extention of the augmented wave methods and the pseudopotential approach. It is an all electron method, which is advanced compared to the pseudopotential approach for high spin atoms and more rapid convergence[27].

remaining layers were fixed at their bulk-like positions. A single Au atom and a single CO molecule were adsorbed per surface cell, this yields a coverage of 0.11 ML of Au atoms and of CO molecules. For the Brillouin zone integrations a $5x5x1$ Monkhorst-Pack grid[4][148] has been used. With this computational setup, differences in adsorption energies are converged at the level of a few meV/molecule.

For the mapping the potential energy surface of CO on Au/Ni(111), the in-plane coordinates of the carbon atom were fixed at positions corresponding to on-top, bridge, and hollow sites. Only non-magnetic calculations have been used for studying CO adsorption on Au/Ni. A recent extended DFT study of CO adsorption on close-packed metal surfaces[60] has demonstrated that spin-polarization has only a minimal influence on the adsorption properties.

5.3 CO adsorption on clean Ni(111)

To obtain detailed information about the reference system, the adsorption of CO on a clean Ni(111) surface at a coverage of $\Theta = 0.11$ ML has been studied, complementing earlier investigations at higher coverages ($\Theta \geq 0.25$ ML)[45, 60]. The results are compiled in Table-5.1, while in Fig. 5.1 is displayed a contour plot of the adsorption energies of a CO molecule on a Ni(111) surface, where one can see that the hollow sites exhibit higher adsorption energies for CO molecule.

The most favorable adsorption site for CO is the fcc hollow with an adsorption energy of 2.13 eV/molecule, which is only 2 meV larger than for adsorption in a hcp hollow. Adsorption in bridge and on-top sites is less favorable by 0.15 eV/molecule and 0.52 eV/molecule, respectively. The adsorption energies calculated in this low-coverage limit are substantially higher than those reported for 0.25 ML coverage. The difference is largest ($\Delta E_{ads} = 0.18$ eV/molecule) for adsorption in a threefold hollow, and only very modest ($\Delta E_{ads} = 0.04$ eV/molecule) for on-top adsorption. The results of Gajdos et al.[60] have been

---

[4]The k-grid expressed in terms of a Monkhorst-Pack (MP) grid, is a division in equally distant in the Brillouin zone points, in the directions: k_x, k_y, and k_z. These points are unique, and not related by any symmetry operation. Large k-point grids for metals are often necessary for convergence.

Table 5.1: Adsorption energies (E_{ads}), length of the CO bond (d_{CO}), Ni-C distance (d_{Ni-C}), and vertical distance of the C atom in the CO molecule from the surface (z_{Ni-C}),for all adsorption sites.

site	E_{ads} (eV)	d_{CO} (Å)	d_{Ni-C} (Å)	z_{Ni-C} (Å)
fcc	2.13	1.20	1.94	1.30
hcp	2.13	1.20	1.94	1.30
bridge	1.97	1.19	1.87	1.39
top	1.61	1.16	1.74	1.74

calculated with a different exchange-correlation functional(PW91) proposed by Perdew et al.[175], which produces, however, very similar results as the PBE functional. A revised variant of the PBE functional (RPBE) has been designed by Hammer et al.[83], with the aim of improving the prediction of molecular adsorption energies. While the RPBE functional indeed reduces the adsorption energy of CO on Ni(111) by 0.46 eV/molecule compared to the results achieved with the PW91 functional and hence largely improves agreement with experiment (E_{ads} = 1.44 eV/molecule (theor.), 1.32 eV/molecule (exp.)), the results for adsorption on noble metal surfaces are disappointing. For the Au(111) surface one finds using the PW91 functional E_{ads} = 0.32 eV/molecule (theor.), 0.40 eV/molecule (exp.), while the RPBE functional predicts CO adsorption to be endothermic by −0.12 eV/molecule (for details see Gajdos et al.[60]). Hence, for the transition metal surfaces the difference in the adsorption energies predicted by the PW91(or PBE) and the RPBE functionals consists in an almost constant shift to lower (and hence more realistic) values. For the noble metals PW91 and PBE correctly predict exothermic adsorption, where as using RPBE the CO molecule does not bind at all, the prediction is qualitatively wrong. For this reason, the present study has been performed using the unmodified PBE functional[169].

The stronger adsorbate-surface interaction at reduced coverage leads also to a slightly more pronounced stretching of the C-O bond length compared to its value in the gas-phase molecule (d_{CO} = 1.14 Å), whereas the surface-adsorbate distances were found to be hardly coverage-dependent.
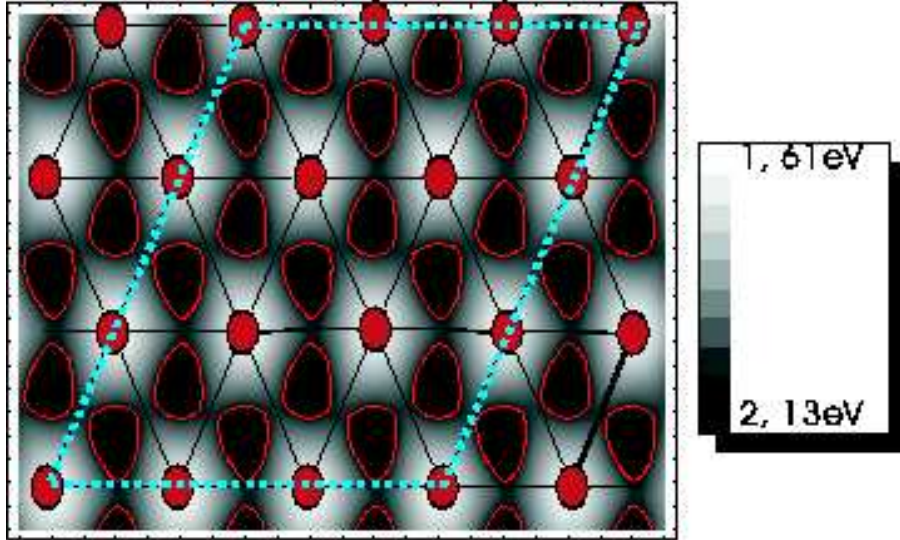
Figure 5.1: Contour plot of the adsorption energies of a CO molecule on a clean Ni(111) surface. The doted line indicates the p(3x3) cell used for the calculations. The bright lines enclose the spots with $E_{ads} \geqslant 2eV$/molecule.

5.4   CO adsorption on Au-doped Ni(111)

For the investigation of CO adsorption in the vicinity of a Au adatom adsorbed in a threefold (fcc) hollow site of the Ni(111) surface, we used the $p(3 \times 3)$ surface cell shown in Fig. 5.2. For the mapping of the potential-energy surface of CO on the Au/Ni(111) surface, the lateral coordinates of the C atom were fixed at the high-symmetry sites (hollow, bridge, on-top) defined in Fig. 5.2, while the height of the CO molecule, its angles relative to the surface normal, and the coordinates of the Ni atoms in the two top layers were allowed to relax. As the interaction between the CO molecule and the Au-atom is repulsive, in addition the lateral coordinates of the adatom were frozen- this must be considered in an analysis of the potential-energy surface. The calculations have demonstrated that mobility of the adatom is restricted by a diffusion barrier of ∼0.53 eV.

Details on the adsorption energies and adsorption geometries are compiled in Table 5.2. To facilitate the interpretation of the data, contour plots of the adsorption energies and of the difference in the adsorption energies on a clean Ni(111), induced by the presence of the Au-adatom, are given in Figs. 5.3 and
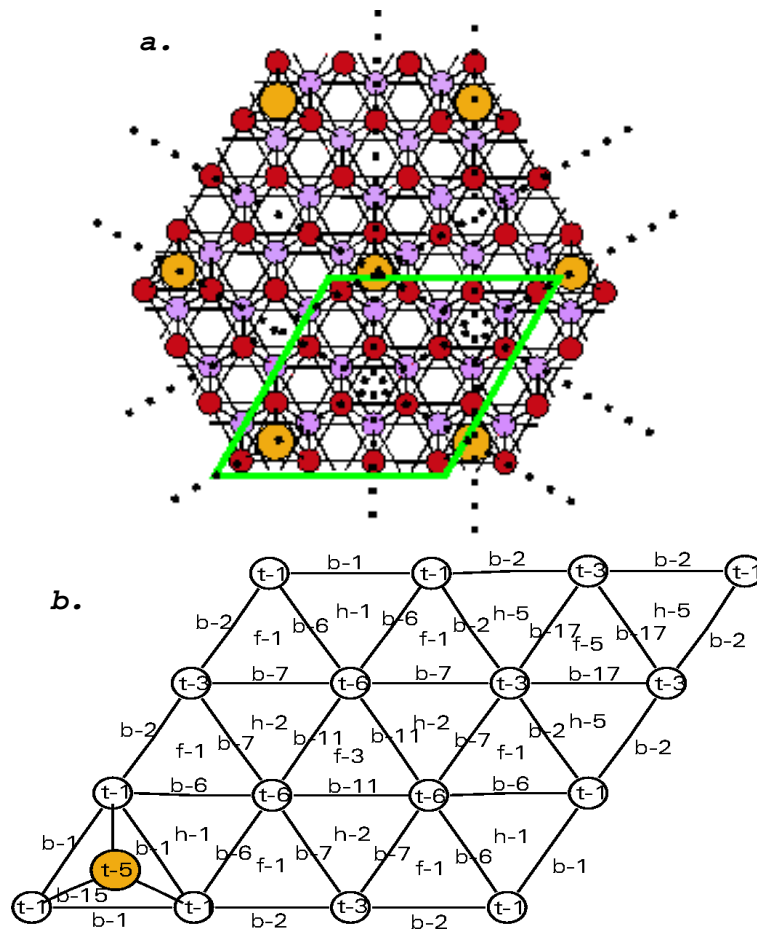
Figure 5.2: (a). The Au/Ni(111) surface for a coverage of 0.11ML. Dark circles represent Ni atoms in the surface layer, light circles subsurface Ni atoms. The large dots represent the Au adatoms. Dotted lines mark mirror symmetries in the p(3x3) surface cell, which is marked by the parallelogram. (b).The $p(3 \times 3)$ surface cell used for studying the adsorption of CO in the vicinity of a Au adatom on Ni(111). The Au-atom is placed into a threefold hollow next to the corner of the surface-cell (position t5). The figure serves to define the nomenclature for the sites for which the adsorption energy and geometry of CO has been calculated.
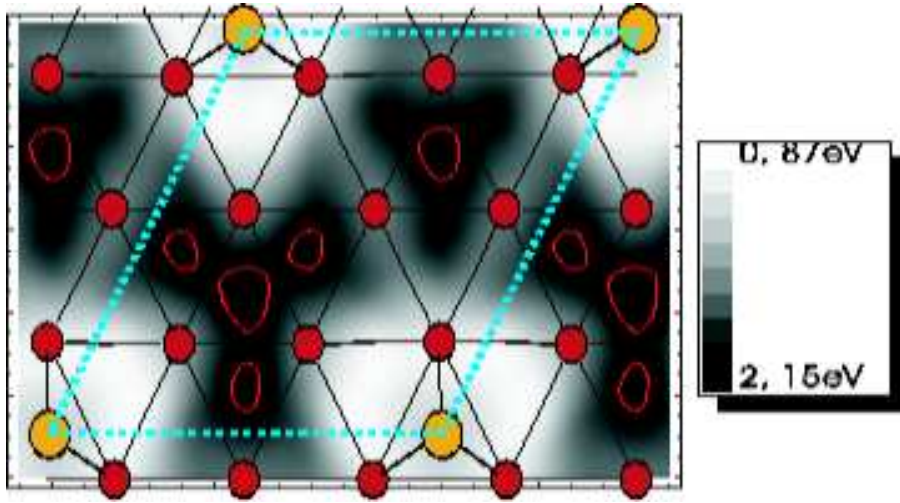
Figure 5.3: Contour plot of the adsorption energies of a CO molecule in the vicinity of a Au adatom on a Ni(111) surface (located in the lower left corner of the $p(3 \times 3)$ surface cell). The bright line encloses the spots with $E_{ads} \geq$ 2eV/molecule.

5.4.

Due to the presence of the Au adatom the adsorption energies of CO are reduced by up to about -1.25 eV/molecule. As expected, the sites in the center of the cell, at the largest distance from the Au atom are the least affected. On the fcc site f3 located in the center of the cell, the adsorption energy is even slightly increased by 0.03 eV, and on the surrounding bridge (b11) and hexagonal hollow (h2) sites, the adsorption energy is decreased only by -0.02 eV and -0.04 eV, respectively. At these sites, the adsorption geometries (CO bond length, adsorbate-surface distance) are also almost unchanged with respect to the clean Ni(111) surface. A rather modest change in the adsorption properties is also found for the group of adsorption sites around the f5 center of symmetry (hollow f5, bridge b17, hollow h5). The reduction of the CO binding is strongest (-0.2 eV) in the vicinity of the Au atom (hollow h5), where the Ni substrate atoms share bonds with CO as well as Au. On the f5 and b17 sites, the change in the adsorption energy is only -0.04 eV/molecule, and the adsorption geometry is also almost unchanged.

The other extreme is found at the site of the Au atom and in its immediate

Table 5.2: CO-adsorption in the vicinity of a Au adatom on a Ni(111) surface: adsorption energy (E_{ads}), change of adsorption energy relative to a clean Ni surface (ΔE_{ads}), C-O bond-length (d_{CO}), height of the C-atom above the Ni-surface (z_{Ni-C}), and tilt angle relative the surface-normal (θ).

site	E_{ads} (eV)	ΔE_{ads} (eV)	d_{CO} (Å)	z_{Ni-CO} (Å)	$\theta(^o)$
f1	1.66	−0.46	1.21	1.34	10
f3	2.15	+0.03	1.20	1.37	0
f5	2.09	−0.04	1.20	1.34	0
h1	0.88	−1.25	1.15	3.47	80
h2	2.08	−0.04	1.20	1.36	0
h5	1.93	−0.20	1.20	1.34	4
b1	1.11	−0.87	1.16	3.96	32
b2	1.58	−0.40	1.20	1.44	8
b6	0.87	−1.10	1.22	1.50	36
b7	1.84	−0.13	1.19	1.45	0
b11	1.96	−0.02	1.19	1.48	0
b15	1.10	−0.87	1.15	3.96	35
b17	1.93	−0.05	1.19	1.44	0
t1	0.88	−0.74	1.15	3.55	87
t3	1.55	−0.06	1.16	1.80	0
t5	1.16	−0.45	1.16	1.95^a	0
t6	1.41	−0.20	1.17	1.86	7

[a] Height of the C-atom above the Au impurity. The hight from the average Ni surface is 4.08 Å.
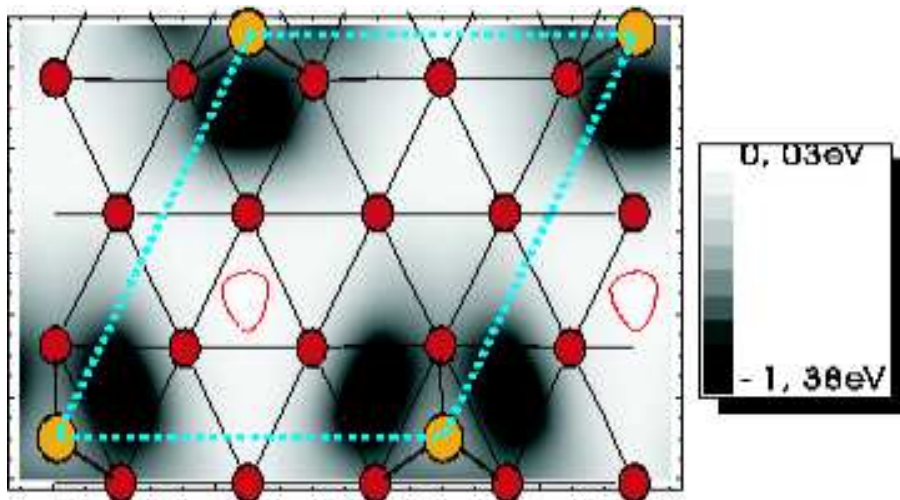
Figure 5.4: Same as Fig. 5.3, but showing the difference in the adsorption energies induced by the presence of the Au-adatom. The line encloses sites with $\Delta Eads \geq 0$eV.

environment. Since the adsorption energies of Au and CO on clean Ni(111) are comparable, a relaxation of the lateral coordinates of the Au atom, with the C atom in a fixed position, would lead to a displacement of Au such that the CO-Ni binding can be optimized. Since this is not the effect we want to study, the Au atom has been fixed in the hollow. On top of the Au atom (position t5), the adsorption energy of CO is 1.16 eV/molecule. CO is adsorbed in an upright configuration, the Au-C distance is about 1.8 Å. This means that CO adsorption on an isolated Au adatom on Ni(111) is much stronger than on a close-packed Au(111) surface (where the adsorption energy is only 0.32 eV/molecule). This confirms the enhanced chemical reactivity of Au nanoparticles, even if they are supported on a metallic surface. Note that binding of CO on-top of the adatom is at least locally stable, with surrounding barriers of nearly 0.3 eV located at the surrounding on-top (t1), hollow (h1) and bridge (b6) sites.

The b15 bridge sites connect the Au adatom and the nearest-neighbor Ni atoms. The CO binding energy on these sites is about 1.1 eV, the axis of the CO molecule is tilted away from the surface normal by about 35°. Some typical bonding geometries in the vicinity of the Au atom are shown in Fig. 5.5. A molecule placed into the b1 bridge sites cannot really bind to the Ni-atoms,
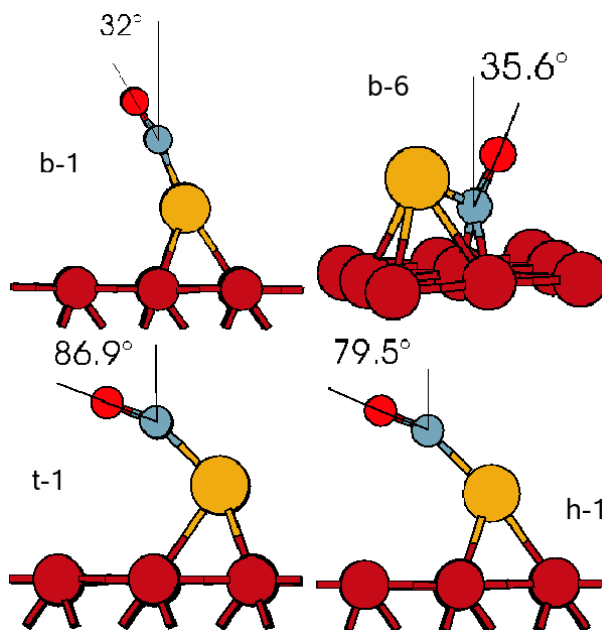
Figure 5.5: Adsorption geometries in the immediate vicinity of the Au adatom on Ni(111).

because they are screened by the extended electron density around the Au. The next sites are CO on-top of one of the Ni atoms binding to the Au adatom (sites t1). In this case the adsorption energy is only about half as large as on-top of a Ni atom on a clean surface, the Ni-C distance is strongly increased and in equilibrium the CO molecule lies almost parallel to the Ni-surface. Again this reflects the fact that the Ni atom is screened by the Au ad-atom.

In Fig. 5.6 there is displayed the contour plots of the carbon-oxygen bond and the vertical distance of the CO molecule from the metal surface. One can see the correlation of the adsorption energies (Fig. 5.3) with the CO bond lengths and the vertical distance of the molecule from the surface. The lower the adsorption energy is (weaker binding), the smaller the C-O bond length and the higher the distance, that the molecule bound to the surface, and vice-versa. There is a different behavior at t6, which might be, due to the fact that this on top site of a Ni is still close enough to Au and furthermore the strong repulsion of O atom from Au.

Bonding in the "threefold", respectively "twofold" sites h1 and b6, is most strongly affected by the impurity - the adsorption energy is decreased by -1.1

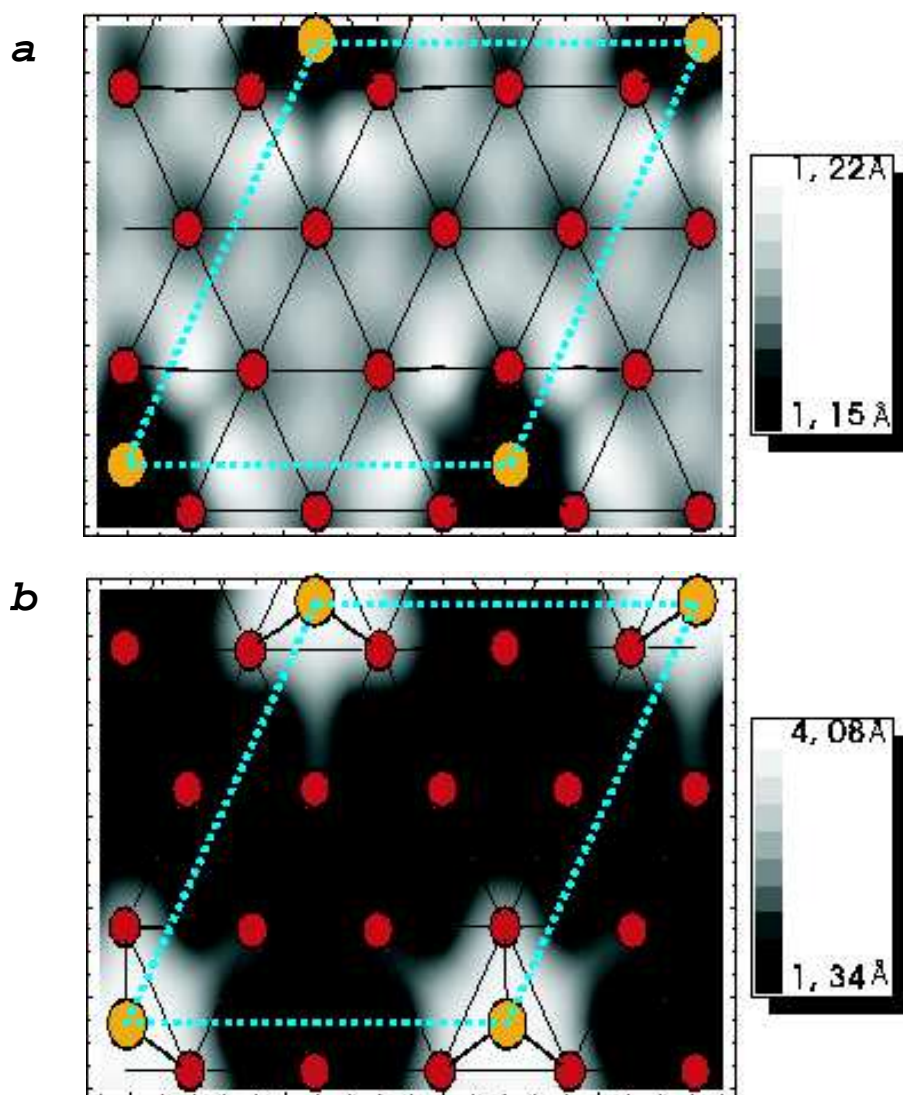Figure 5.6: Contour plots of a. the C-O bond length in the vicinity of a Au adatom on a Ni(111) surface and b. the vertical distance of CO molecule from the metal surface, in the vicinity of a Au adatom on a Ni(111) surface.

to -1.2 eV/molecule. The binding energy in the threefold hollow h1 is strongly reduced, because two of the substrate atoms binding to the adsorbate bind also to the impurity. The molecule drifts to a large distance from the surface and adopts a position almost parallel to the surface (see Fig. 5.5). Binding in the b6 bridge has a rather special character: in this location the CO molecule binds to two substrate atoms (one is a 1st, the other a 2nd nearest neighbor to the Au atom) and to the ad-atom. Hence in this configuration the molecule binds in a pseudothreefold site. The adsorption energy is about as strong as in the h1 site, but the molecule approaches the surface much more closely and undergoes only a moderate tilt with respect to the surface normal. Hence, in configuration h1 the molecule binds rather to the Au adatom screening the neighboring adsorption sites than to the Ni surface. However, the binding to the isolated Au atom is more than twice as strong as on a Au(111) surface. Remarkably, the elongation of the C-O bond is largest for this tilted b6 geometry. The reason is that due to the tilted geometry, interactions forbidden in an upright geometry (e.g. the interaction between the d_{z^2} orbital of Ni and the $2\pi^\star$ antibonding orbital of the CO molecule) can weaken the intramolecular bond. The situation is similar as for the tilted adsorption of CO on Fe(100) surfaces.[212]

Holmbladh et al.[95] have used temperature-programmed desorption spectroscopy to investigate the influence of Au impurities on the desorption energy of CO from Ni(111) surfaces. For coverages up to 0.1 ML, the TPD spectra show a broadening of the peak located at about 315 K, with only a very moderate shift of the peak position. For coverages above 0.15 ML, a side-peak at about 180 K begins to grow, while the main peak gradually fades out. For coverages above about 0.6 ML, no CO is adsorbed. Our results provide an explanation for the bimodal structure of the TPD spectrum, the high- and low-T peaks corresponding to adsorption in Au-free and Au-contaminated parts of the Ni surface.

5.5 Conclusions

The presence of a Au ad-atom leads to a strong local reduction of the adsorption energy of CO. On a clean Ni(111) surface, CO adsorbs in a threefold hollow with an adsorption energy of 2.13 eV/molecule. At an adatom concen-

tration of ~ 0.1 ML, the impurity-induced reduction of the adsorption energy is smaller than 0.2 eV/molecule for 44% of the hollow sites able to accommodate a CO molecule and ≤ 0.5 eV/molecule for 77% of all sites. If the Au ad-atom is placed into a fcc hollow of the surface, the adsorption energy of CO in the neighboring hcp hollows sharing two Ni atoms with the ad-atom (site h1) is reduced by -1.25 eV, in the nearest fcc hollow sharing a single Ni atom with the ad-atom (site f1), the reduction is only -0.46 eV. In the hcp hollow neighboring the Ni-Au bond (site h5), the adsorption energy is reduced only by -0.20 eV. In all other hollow sites in the $p(3{\times}3)$ surface cell, the adsorption energy is almost unchanged. Hence the doping of a Ni surface with Au has a very local influence on the adsorption properties. On the other hand, the Au ad-atom binds a CO molecule much stronger than a Au(111) surface.

On all noble metal surfaces, CO adsorption is very weak, because the low-lying d-band suppresses any formation of covalent adsorbate-substrate bonds through the interaction of the d-states with the 5σ and $2\pi^\star$ molecular orbital of CO (see also the detailed discussion in Gajdos et al. [60]). For the Au ad-atom, the presence of a substantial d-band DOS at energies of -2 to -1 eV below the Fermi energy (see chapter 4) leads to a contribution to the adsorption bonding similar to that on transition-metal surfaces. A CO molecule adsorbed at the Au adatom site is located in a local potential energy minimum surrounded by barriers resulting from the strong reduction of the adsorption energy at the hollow, bridge and on-top sites closest to the ad-atom. Adsorption at these sites is unstable (in accordance with the STM observations) as there is no barrier against diffusion into a more attractive site.

Chapter 6

CO adsorption on a Au/Ni(111) surface alloy

6.1   Introduction

In the past it has been shown that Au atoms alloyed into the topmost layer of Ni(111) significantly modify the reactivity of the neighboring nickel atoms, thereby rendering the AuNi alloy an interesting candidate for catalytic applications[22, 70, 95, 224]. Deposition of up to 0.3 ML of Au does not result in an epitaxial overlayer or islands. Instead, Au atoms randomly replace Ni atoms[98, 221], resulting in a strongly bound surface alloy and preserving the hexagonal, two-dimensional structure of the clean Ni surface. In the work of Lahr[129] it is reported that Au/Ni(111) catalyzes CO oxidation at low temperature.

At the recent works of Vestergaard[224] and Zhdanov[238] it is investigated the phase separation of the Au-Ni surface alloy at high pressures of CO. The atomistic mechanism of the process is shown to be a kink-site carbonyl formation and evaporation which is found to be enhanced by the presence of Au. In the other hand the phase separation of Ni-Au system has been reported in several works[67, 190, 230, 231].

CO adsorption on Au/Ni(111) surface alloys has been studied both theoretically and experimentally. DFT calculations for the adsorption of CO on Au/Ni(111)[224] surface alloys with different Au concentrations showed that

Au atoms bind the CO about 1 eV weaker than the Ni atoms, but stopped short of analyzing the potential-energy surface for CO adsorption. This is the aim of the study.

In this chapter an extention of the investigation of Au impurity in a substitutional site on a Ni(111) surface is presented. In contrast to a Au-adatom on a Ni(111) surface (chapter 5)[218], a Au impurity binds CO only very weakly. In addition, the impurity induces a reduction of the adsorption energies which is strictly localized to its immediate neighborhood. The adsorption of CO was reduced by up to 1.25 eV in the vicinity of Au adatom. At larger distances from the impurity, the adsorption energies were almost unchanged. Here the Au substitutional starts already to act like a clean Au(111) surface, as the adsorption energy on top of Au substitutional is -0.36 eV, similar to that on the clean Au(111). The reduction of the adsorption energy is less localized compared with the Au adatom, and only the 25 % of all sites have a reduction of adsorption energy more than 0.05 eV.

6.2 Methodology

The adsorption of CO on the alloy system Au/Ni(111) has been studied using again DFT and VASP [118, 120, 121, 228]. Electronic exchange and correlation are described in the generalized gradient approximation, using the functional proposed by Perdew, Burke and Ernzerhof (PBE) [169]. The plane-wave basis-set contained component with a kinetic energy of $E_{cut} = 400$ eV. The substrate was modeled by slabs consisting of four nickel layers with a surface periodicity of $p(3 \times 3)$, separated by about 20 Å of vacuum. The upper two layers of the surface have been allowed to relax, while the remaining layers were fixed at their bulk-like positions. A single Au atom substitute one Ni atom from the surface, and a single CO molecule was adsorbed per surface cell, this yields a coverage of 0.11 ML of CO molecules. One can find more details for the used set-up of the calculations at the previous chapter.

6.3 Results and discussion

Due to its much larger size, the center of the substituted Au atom is located about 0.5 Å above the average location of the Ni-atoms in the surface layer and the three nearest-neighbor Ni atoms relax slightly outwards (note that for the adsorption of CO on Au/Ni more intense k-mesh has been used, compared with that for NEB-chapter4). Concerning the relaxation due to CO adsorption on Au-Ni(111) alloy, for the sites f3, h1 and b1 there is an outward relaxation of the first layer of about 1.5% and for the rest of the sites an inwards relaxation up to 2%. For the second layer there is observed a modest inwards relaxation with average of 0.6%. Finally we should notice, that for the Ni atoms bind with CO, is observed an extra outward relaxation of around 0.1 Å compared with the rest Ni atoms of the surface.

For the mapping of the potential-energy surface of CO on the alloy surface, the lateral coordinates of the C atom were fixed at the high-symmetry sites (hollow, bridge, on-top) defined in Fig. 6.1, while the height of the CO molecule, its angles relative to the surface normal, and the coordinates of the Ni atoms in the two top layers were allowed to relax. Table 6.1 compiles the adsorption energies, CO bond-lengths and the height of the C atom of the molecule relative to the Ni atoms, calculated for all hollow (fcc and hcp), bridge, and top sites in the (3×3) surface cell.

The changes in the adsorption energies are accompanied by small changes in the adsorption geometry. In contrast to the situation with a Au adatom (where CO atoms adsorbed close to Au undergo a strongly tilting), on the surface alloy CO is always adsorbed in an nearly upright position, as the axis of the molecule is tilted away from the surface normal by $0 - 3$ degrees. Only at the sites b1 linking the Au atom to its nearest Ni neighbors, the adsorbed CO molecule is tilted 13° from the surface normal towards the Au atom. The extraordinary in this case is that the O atoms tiltes towards the Au substitutional atom and not outwards from it, as in all cases of the Au doped Ni(111) surface. In the threefold hollows surrounding Au (h1,f3) a very weak tilting of 3 to 5° away from the impurity is observed. For adsorption in a threefold hollow, the reduction of the binding energy is accompanied by a change of the height of the C atom above the surrounding Ni atoms by up to 0.1 Å, on the bridge and top site the variation is distinctly smaller. Changes in

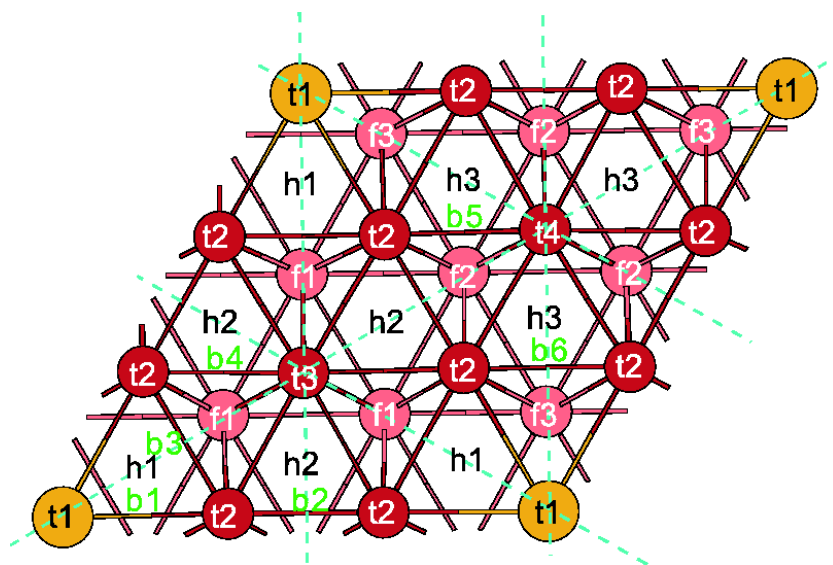Figure 6.1: The p(3 × 3) surface cell used for studying the adsorption of CO in the vicinity of a substitutional Au impurity (located at position t1) in the Ni(111) surface. The figure serves to define the nomenclature for the sites for which the adsorption energy and geometry of CO has been calculated. The doted lines indicate the mirror symmetries of the surface.

Table 6.1: CO-adsorption in the vicinity of a substitutional Au impurity in a Ni(111) surface: adsorption energy (E_{ads}), change of adsorption energy relative to a clean Ni surface (ΔE_{ads}), C-O bond-length (d_{CO}), and height of the C-atom above the Ni-surface (z_{Ni-C}).

site	E_{ads} (eV)	ΔE_{ads} (eV)	d_{CO} (Å)	z_{Ni-CO} (Å)
f1	2.09	-0.04	1.195	1.31
f2	2.16	$+0.03$	1.193	1.32
f3	1.17	-0.96	1.187	1.41
h1	1.18	-0.95	1.187	1.41
h2	2.16	$+0.03$	1.193	1.33
h3	2.10	-0.04	1.194	1.31
b1	0.96	-1.01	1.176	1.45
b2	2.01	$+0.04$	1.184	1.43
b3	1.81	-0.16	1.187	1.42
b4	2.00	$+0.03$	1.186	1.41
b5	2.00	$+0.03$	1.185	1.41
b6	1.82	-0.15	1.187	1.41
t1(Au)	0.36		1.154	2.00^a
t2	1.61	$+0.00$	1.163	1.74
t3	1.70	$+0.09$	1.162	1.73
t4	1.69	$+0.08$	1.162	1.74

[a] Height of the C-atom above the Au impurity. The height of C-atom from the average Ni surface atoms is 2.65 Å.

the CO bond lengths are rather modest, the differences compared to the clean Ni(111) are less than 0.02 Å. The maximum differences are in the vicinity of Au atom, where there is a tendancy of smaller bond lengths, something that it is expected due to the smallest adsorption energies on these sites.

Due to the presence of the Au the adsorption energies of CO are reduced by up to about 1.25 eV/molecule. The maximum reduction occurs at the site of Au (t1). The reference values for the adsorption energy are the binding energies of CO on a clean Ni(111) surface (2.13 eV in fcc or hcp hollows, 1.97 eV in bridge, and 1.61 eV in top sites). The lowest adsorption energy of $E_{ads} = 0.36$ eV is calculated for a CO molecule on top of the Au atom. This is very close to the experimental adsorption energy on a Au(111) surface of $E_{ads} = 0.40$ eV, and to the value of 0.32 eV calculated by Gajdos et al.[60] (note that in this paper a slightly different GGA functional has been used), but much lower than the binding energy of CO on a Au-adatom on Ni(111) ($E_{ads} = 1.16$ eV). The CO molecule adsorbed on the Au atom is located 2.00 Å above the metal atom - this shows that in this position it is only weakly physisorbed. At the bridge-sites connecting the impurity to the nearest Ni neighbors (b1), the adsorption energy is 0.96 eV, i.e. reduced by 1.01 eV compared to a bridge position on a clean Ni(111) surface, on the hollow sites h1 and f3 surrounding the impurity the adsorption energy is 1.18 eV and 1.17 eV, respectively, corresponding to a reduction by 0.96 eV. At the bridge sites next to these hollows (b3, b6) the influence of the impurity is already much weaker (the adsorption energy is reduced by only 0.15 eV), on all other sites the impurity-induced change in the adsorption energy varies only between −0.04 eV and +0.09 eV. On the sites with the largest distance from the impurity, the adsorption energies are even slightly enhanced (as already noted in the presence of a Au-adatom). The impurity-induced changes in the adsorption energies are summarized in Fig. 6.3 in the form of a contour-line plot - this demonstrates that the effect is strongly localized. Energetically the most favorable sites are f2 and h2 with adsorption energy of 2.16 eV, slightly increased (by 30 meV) compared to the adsorption energy on hollow site at clean Ni(111) surface. The Au substitutional atom on Ni(111) surface effects only the adsorption energy of the first neighbors from the Au. After these atoms the adsorption energy is almost the same as on a clean Ni(111) surface and the sites t3 and t4 exhibit
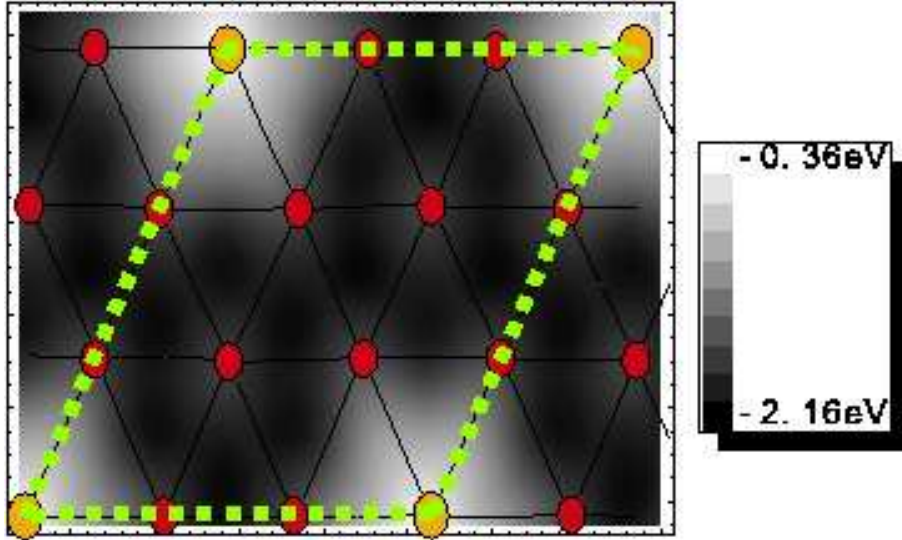
Figure 6.2: Contour plot of the of the adsorption energy of CO in the vicinity of a substitutional Au atom in a Ni(111) surface.

a further enhancement of binding energies for CO molecule of 0.09 and 0.08eV respectively, compared to the adsorption energy on-top site of a clean Ni(111) surface.

A further difference between the potential-energy surface of CO on a Ni(111) surface with a Au adatom and on a Au/Ni(111) surface alloy is that a CO molecule adsorbed on an adatom sits in a local potential-energy minimum, surrounded by barriers of about 0.28 eV located at the top and hollow positions surrounding the adatom (see chapter 5 for details). In contrast, a CO molecule adsorbed on a Au impurity occupies a global maximum on the potential-energy surface and there is no barrier against diffusion to a hollow site where it is strongly adsorbed. This is illustrated in Fig. 6.4 for a diffusion path along the long diagonal of the cell shown in Fig. 6.1. Note that also far from the impurity, the barrier for diffusion between two hollows across a bridge is only 0.16 eV, as on the clean Ni surface. Figure 6.4, also serves an easy way to notice the hints of the adsorption phenomena on Au substitutional Ni(111) surface. We see that there is a correlation among E_{ads}, d_{CO} and z_{M-CO}. The vertical distance of the CO from the Ni surface has the same behavior like the adsorption energy. The reverse happens for the CO bond-length and the two other quantities. ($E_{ads} = f(z_{M-CO}) = g(d_{CO})$)
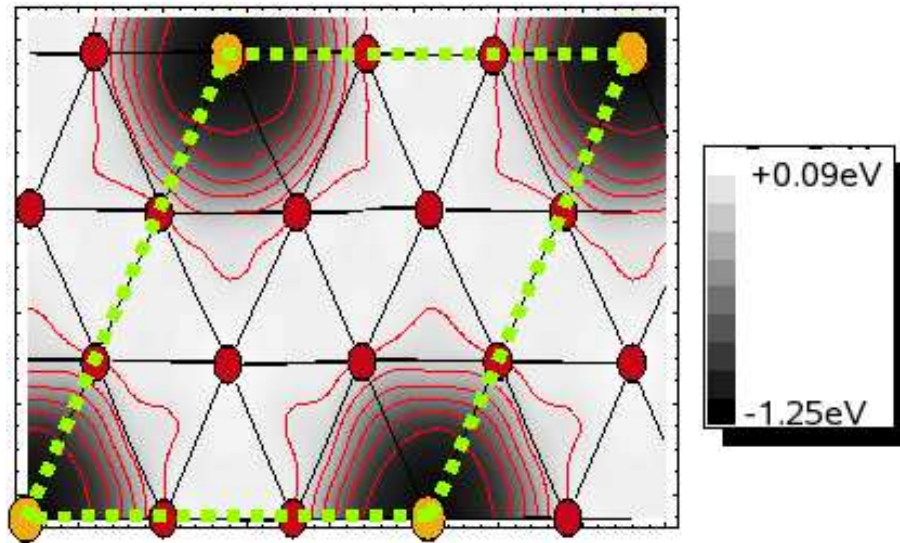
Figure 6.3: Contour plot of the impurity-induced changes of the adsorption energy of CO in the vicinity of a substitutional Au atom in a Ni(111) surface compared with the adsorption energy of CO on clean Ni(111). The contour interval is 0.2 eV, the last contour line around the impurity is drawn for $\Delta E_{ads} = 0$.
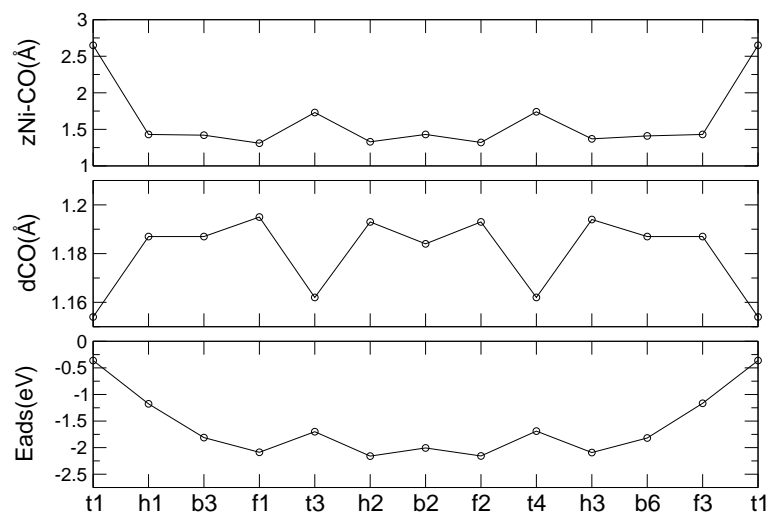
Figure 6.4: Potential-energy profile, CO-bond length and adsorption height of a CO atom adsorbed on a Au/Ni(111) surface alloy, along a path connecting two Au atoms - cf. Fig. 6.1.

Hence, any molecule impinging on the alloy surface close to the impurity will immediately diffuse to the strongly attractive sites far from the impurity. As shown in Fig. 6.3, out of the 18 hollow sites in our surface cell, six will be blocked for CO adsorption by the presence of the Au impurity such that the effective coverage (calculated with respect to the available binding sites in the threefold hollows) is increased from 0.11 ML to 0.166 ML. As analyzed in detail by Eichler[45], at higher coverages CO/Ni(111) forms superstructures based on hollow- and bridge-adsorbed CO. It is also important to emphasize that the difference between the binding energy of CO at adatoms and at impurities leads to a further stabilization of Au adatoms over surface-impurities at higher partial pressures of CO.

Hence, while for the adatom the presence of a hybridization-induced d-DOS close to the Fermi energy leads to an at least partially covalent character of the Au-CO binding, due to the d-band shift of the impurity the binding mechanism consist only of a weak polarization-induced interaction. (see chapter 4)

These results are also relevant for the interpretation of catalytic reactions on Au/Ni(111) surface. In their recent report on CO oxidation catalyzed by Au-doped Ni(111), Lahr and Ceyer[129] tentatively attribute the production of CO_2 to the reaction between CO and O bound to Au impurities in the Ni surface. This interpretation is probably too simplistic, and our results suggest a modified mechanism. Recent investigations of catalytic reactions of diatomic molecules have established a universal linear Brønsted-Evans-Polanyi relationship between the adsorbate binding energies and the activation energies[61, 158]. Kinetic modeling studies have shown that the optimum catalysts have intermediate binding energies of -1.1 ± 0.3 eV. Hence pure Ni(111) surfaces bind CO too strongly for an efficient activation of the molecule, while binding to Au atoms in a Au/Ni(111) surface alloy is much too weak. Binding to Au adatoms and to sites in the vicinity of a Au impurity on the other hand occurs at energies within the range for an optimal reactivity.

6.4 Conclusions

In this chapter it has demonstrated that the presence of a Au substitutional-atom leads to a strong local reduction of the adsorption energy of CO. This

effect is more localized to the nearest-neighbors of Au impurity, compared with the effect on Au adatom on Ni(111). In this case, Au substitutional behave like a clean Au(111) surface, exhibiting similar binding energies for CO.

For the alloy the CO binds almost in an upright position, while for the adsorption of CO on Au adatom/Ni(111) on more than the 1/3 of all sites there is a tilt angle relative to the surface-normal from 32-87°.

The adsorption energy of CO in the neighboring hcp and fcc hollows close to the Au substitutional atom (sites h1, f3) is reduced by 0.95 eV, while at the next-neighboring hollows (sites h3 and f1), the reduction is only 40 meV, and at f2 and h2 there is a small increase of 30 meV. We conclude that the Au substitutional-atom influence the adsorption properties of CO very locally and less extended than the Au adatom on Ni(111).

The Au substitutional-atom binds a CO molecule much weaker than a Au adatom on Ni(111) surface. The effect of Au adatom for the binding of CO molecule is already disappeared when the Au creates a surface-alloy on Ni(111). A CO molecule adsorbed at the Au substitutional-atom site is located in the global potential energy maximum. The surrounding sites exhibit a monotonic increase of the adsorption energies that leads to the global minimum at the hollows sites the most distanced from Au substitutional (f2 and h2), where the binding is even slightly increased compared to the adsorption on clean Ni(111).

The doping of a Ni surface with Au has a very local influence on the adsorption properties. This agrees also with the analysis of the local electronic densities of states: already for next-nearest Ni atoms, Au-induced changes are very small. The reduction of the adsorption energy is a direct consequence of the reduced Ni-DOS and of the shift of the d-band center to higher binding energies, in accordance with the Hammer-Nørskov model [84]. For the Au adatom, the presence of a substantial d-band DOS at energies of -2 to -1 eV below the Fermi energy leads to a contribution to the adsorption bonding similar to that on transition-metal surfaces.

Finally a very important modification of the nature of the bond between Au and CO molecule is observed for the two cases. The adsorption energy of CO on Au adatom is 1.16 eV and it has partially covalent character, while for the Au substitutional the Au impurity exhibit behavior similar of the Au(111) clean surface, the adsorption energy is only 0.36 eV, indication for a weak

polarization-induced interaction.

Chapter 7

CO adsorption on Pt(111) with PBE, PBE0 and HSE03 functionals

7.1 Introduction

Well converged DFT calculations based on local and semilocal functionals do not predict the correct the adsorption site for CO on Pt(111), Cu(111) and Rh(111), whether using all-electron potentials or pseudopotentials[53]. LEED analysis reported[159] that there is half occupancy of top sites and half at bridge sites, while Blackman[24] reported that for 0.33ML of CO there is $88 \pm 5\%$ occupation of top sites and $12 \pm 5\%$ of bridge sites. Despite, experimental evidence (LEED, thermal desorption, vibrational spectroscopy) that at low coverages CO adsorbed on top[13, 24, 62, 209], calculations with DFT predict the hollow site to be the more preferable energetically[53]. The reason for that might be the tendency of LDA and GGA to favor higher coordination sites for the adsorption of CO on metals[53, 124]. This might be related with the use of a plane-wave basis-set, or the incorrect description of the relative positions of HOMO and LUMO of CO molecule with respect to the Fermi energy[65]. Olsen et al[160] claimed that relativistic effects are significant for the correct description of the adsorption of CO on Pt(111). There are a couple of theoretical reports with local basis set, that predict the correct adsorption

sites[141, 160, 161] for Pt, but till now the reason for this discrepancy between the different codes is not understood.

In this chapter I present an extensive DFT study of the adsorption of CO (0.25ML) on Pt(111), using PBE, PBE0 and HSE03 functionals. In addition I report on CO adsorption on Cu(111) and Rh(111)[213], where again there is disagreement of experiment and theoretical calculations. Even if the PBE functional is considered to be the best parameter free functional, as mentioned above they fail for the adsorption of CO on Pt(111). That was the driving force to compare the results of PBE with the hybrids: PBE0 (or PBE1PBE)[3, 4, 48, 49], which exhibit very good performance for the majority of important properties, and HSE03[92], in which there is a separate description of only the exchange interaction into a long-range part, treated with semilocal functionals and short-range part.

For the case of Pt(111) the PBE0 and the HSE03 predict again the wrong adsorption site, even if the HSE03 gives better results comparing with the other functionals, closer to the experimental ones.

7.2 Methodology

The study is done with VASP, in which the PBE0 and HSE03 have been recently implemented. The ion-electron interactions are described within the projector augmented wave method (PAW)[26], implemented in VASP by Kresse and Joubert[122]. The cutoff energy was fixed to 400eV. The Brillouin zone integration is done using the Monkhorst-Pack scheme[148]. For the acceleration of k-point convergence, the Methfessel-Paxton[145] smearing[1] width has been set to 0.1 eV. The k-point convergence was checked carefully using 2x2x1, 4x4x1, 6x6x1, 8x8x1 and even 12x12x1 points. The test showed that a 6x6x1 k-point mesh is sufficient for well converged results for the structural properties, while for the energetics the 8x8x1 k-mesh was used.

The surface has been modeled by four periodic layers of metal atoms with CO molecule adsorbed on all possible high symmetry positions (fcc, hcp, top,

---

[1]It is a sampling method for Brillouin-zone integration for metals, which converges exponentially with the number of sampling points. The band structures of simple and transition metals are significantly improved with this method.[145]

bridge). We have also investigated three, five and six layers for Pt(111), to check the convergence with respect to the slab thickness. The relative stability of the different sites does not change. The slabs are separated by a vacuum of about 10 Å. The two uppermost layers and the CO molecule were allowed to relax. We have used a $c(2x4)$ surface cell, and one molecule of CO, leading to a coverage of 0.25ML. This separation of CO molecules secures that there are no adsorbate-adsorbate interactions, which would effect the adsorption energies and the site preference of CO on Pt(111). The range separation parameter[2] ξ was set to $\xi = 0.3\text{Å}^{-1}$ for both the density functional part and the non-local Fock exchange.

7.3 Bulk Pt and clean Pt(111) surface

7.3.1 Bulk Pt

The structural properties for bulk Pt calculated with the three functionals (PBE, PBE0 and HSE03), but also the B3LYP[3] results[42, 152] are summarized in Table 7.1: the lattice constant (a_0), the Bulk modulus (B_0) obtained by the Murnaghan equation of state[4], the cohesive energy (E_{coh}) is calculated considering the spin-polarized ground state of the atom[165] are given. In the same table, there are also the relative errors with respect to experiment. These informations are also displayed in Fig. 7.1, where a_0, B_0 and E_{coh} for Pt(111) as well for Rh(111) and Cu(111)[213] are shown for comparison.

The PBE functional gives overestimate lattice constants with respect to the experiment (1.2 %). With hybrid functionals this effect is reduced and the

---

[2]see chapter-2, in the HSE03 functional for description.

[3]B3LYP functional was proposed by Stevens et al.[211] and is a generalization of the B3P86 form devised by Becke[19]. B3LYP is a combination of the LYP GGA for correlation[133], with Becke's three-parameter hybrid functional B3 for exchange[19]. Common hybrid functionals, such as B3, mix a functional of Hartree-Fock exchange into the DFT exchange functional. This mixing involves a certain amount of empiricism and optimization for selected classes of molecules.

[4]Bulk modulus or incompressibility: $B = -V\left(\frac{\partial P}{\partial V}\right)_T$, where V and P denotes volume and pressure. Murnaghan assumes that the bulk modulus B has linear dependence with the pressure P: $B = B_0 + B_0^{'}P$[149]

Table 7.1: Results for bulk Pt: lattice constant (a_0), Bulk modulus (B_0), cohesive energy (E_{coh}) of bulk Pt obtained from PBE, PBE0 and HSE03 calculations. The HSE03 calculations are done with employing the reduced 12x12x12 k-point grid (downsampling), while those with PBE and PBE0 with a full 12x12x12 k-point grid. Relative errors (%) with respect to experiment are also given.

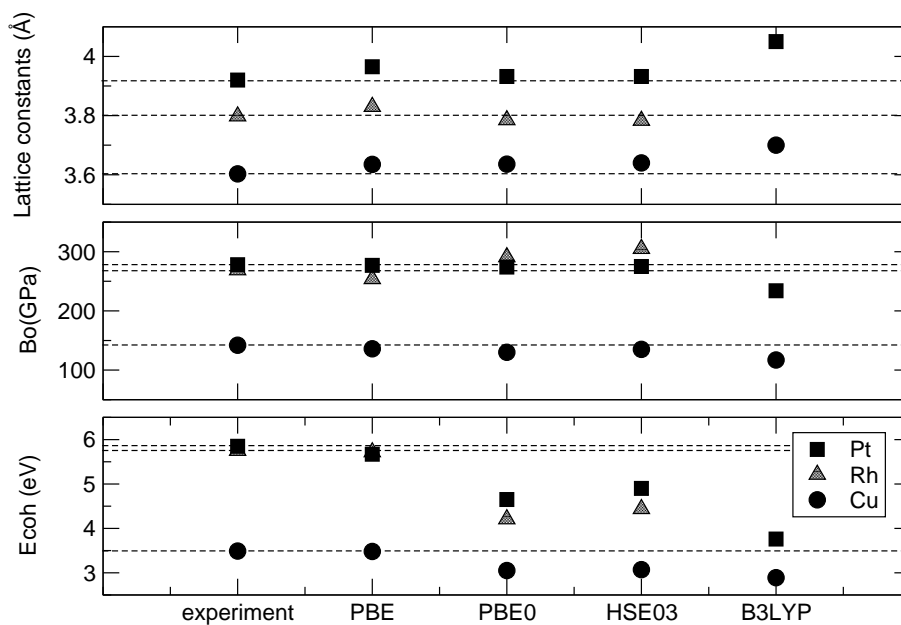| Functional	a_0(Å)	error(%)	B_0(GPa)	error(%)	E_{coh}(eV)	error(%)
PBE	3.97	1.2	277	-0.4	5.67	-3.1
PBE0	3.93	0.3	274	-1.4	4.65	-20.5
HSE03	3.93	0.3	275	-1.1	4.90	-16.2
B3LYP[152][42]	4.05	3.3	234	-15.8	3.76	-35.8
Exp[105, 232]	3.92		278		5.85	

Figure 7.1: The experimental and the calculated with different functionals lattice constant, bulk modulus and cohesive energy for Pt, Rh, and Cu.

error is only 0.3 %. For the bulk modulus (B_0) and cohesive energy (E_{coh}) the PBE functional gives a better description compared with the PBE0 and HSE03. Among the hybrid functionals HSE03 gives the closest results to experiment and both PBE0 and HSE03 do exhibit better description for the bulk properties of Pt compared to B3LYP. In the paper of Stroppa et al[213] except Pt, there is the investigation of adsorption of CO on Rh and Cu. For Cu the most successful functional, which gives the least error for the three quantities is the PBE functional. For Rh, PBE0 and HSE03 give better description for the lattice constant, but worst for bulk moduli and cohesive energy. Generally when there is overestimation of the lattice constants, there is an underestimation of the bulk moduli and vice versa. The trends from the comparison of the three functionals, for the three quantities are:

- For the lattice constant the hybrid functionals give a slightly better description compared to PBE, on the other hand PBE gives a maximum error of 1.2% and this is for the case of Pt.

- For bulk modulus the best description is given by PBE, with maximum error 5% for Cu, while for Pt the calculated value is in almost absolute accordance with the experimental value.

- For the cohesive energy PBE gives again the values closest to experiment, with 0.2 and 0.4 % underestimation for Cu and Rh respectively, and 3.1 % overestimation for the Pt.

- Pt is the metal compared to Cu and Rh that is described the best for its bulk properties with all the three functionals PBE, PBE0 and HSE03.

The underbinding of hybrid functionals (underestimation of the cohesive energies) might be due to the admixture of Fock exchange and to the fact that Hartree-Fock usually underbinds for metals. On the other hand the PBE0 and HSE03 give better results compared with the third hybrid functional, the B3LYP[152] for all of these three metals.

7.3.2 Clean Pt(111) surfaces

Table 7.2 summarizes the calculated properties for the clean Pt(111) surface: d_{12} is the distance of the first and the second surface layer, Δd_{12} is the % variation compared to the distance of two layers in the bulk of the material,

Table 7.2: Results for the clean Pt(111) surface: interlayer distance d_{12} of the first and the second topmost layers, relative change Δd_{12} to the theoretical interlayer bulk distance $(\alpha/\sqrt{3})$ and E_{surf} the average surface energy of the relaxed and unrelaxed side of the slab. To extract these results, the slab consisted by 4 layers and 6x6x1 for structural and 8x8x1 for energetics k-point mesh used.

Functional	d_{12}(Å)	Δd_{12}(%)	E_{surf}(eV/unit cell)
PBE	2.30	+0.7	0.618
PBE0	2.30	+1.3	0.644
HSE03	2.30	+1.3	0.672
B3LYP[42]	2.39	+2.1	0.517
Exp		+1.1±0.4[143]	

and the surface energies, E_{surf}. While Cu and Rh relax inwards for all the functional[213], for Pt(111) the top layer relaxes outwards, in accordance with other calculated results[143].

The convergence of the total energy for Pt(111) clean surface has been checked extensively for PBE functional. 2,3,4,6 layers have been used and several k-points meshes (2x2x1, 4x4x1, 6x6x1, 8x8x1, and 12x12x1). The results are displayed in Fig. 7.2.

7.3.3   Free CO molecule

The calculated bond length d_{CO} is 1.14 Å for PBE, 1.13 Å for PBE0 and 1.14 Å for HSE03. This is in a good agreement with the values reported by Neef[152](1.15 for PW91 and 1.14 for B3LYP). The experimental bond length of CO is 1.13 Å. The HOMO-LUMO gap is 7 eV for PBE, 8.9 eV for HSE03 and 10 eV for PBE0 calculations, while the experimental value is 6.9 eV[23]. As the HOMO-LUMO gap is increased ($PBE \rightarrow HSE03 \rightarrow PBE0$), the interaction of $2\pi^*$ orbitals with d states of metal is decreased.
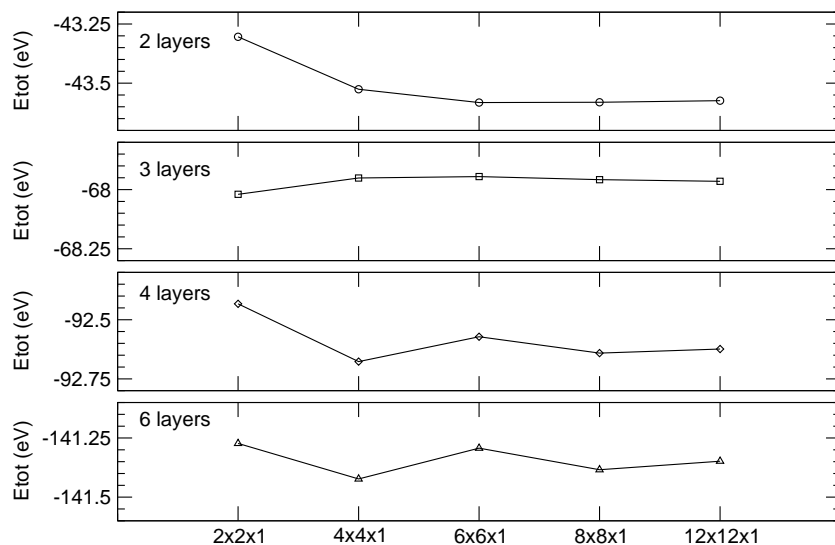
Figure 7.2: Dependence of the total energy for the clean Pt(111) surface on the sampling of the Brillouin zone and on the number of layers using PBE functional. The convergence has been checked for the 2x2x1, 4x4x1, 6x6x1, 8x8x1 and 12x12x1 k-mesh, and for 2, 3, 4, and 6 layers of Pt.

7.4 Adsorption of CO-molecule on Pt(111)

7.4.1 Energetics and Structural properties

With the standard PBE functional, the wrong site is preferred, fcc for Pt (fcc for Cu, and hcp for Rh[213]) in agreement with previous studies[42, 109, 152]. The order of the sites with respect to the energy is fcc, hcp and top for Pt (fcc, hcp, top for Cu and hcp, fcc, top for Rh[213]).

The convergence of PBE calculations has been studied extensively also for the adsorption of CO molecule on Pt(111), with respect to the number of layers and the k-point sampling (Fig. 7.3). For all number of layers, except for the case of the 3 layers where the hcp hollow site is slightly favored, the fcc hollow site is the most favorable energetically for all k-grids, while the top site is the least favorable for all of them. For the 2-layer slab the bridge and the hcp sites are energetically degenerate, for a 3-layer slab fcc and hcp are degenerated, while for 4 and 6-layers the degeneracy of fcc and hcp is less pronounced. Finally the energy difference between fcc and top is about 120
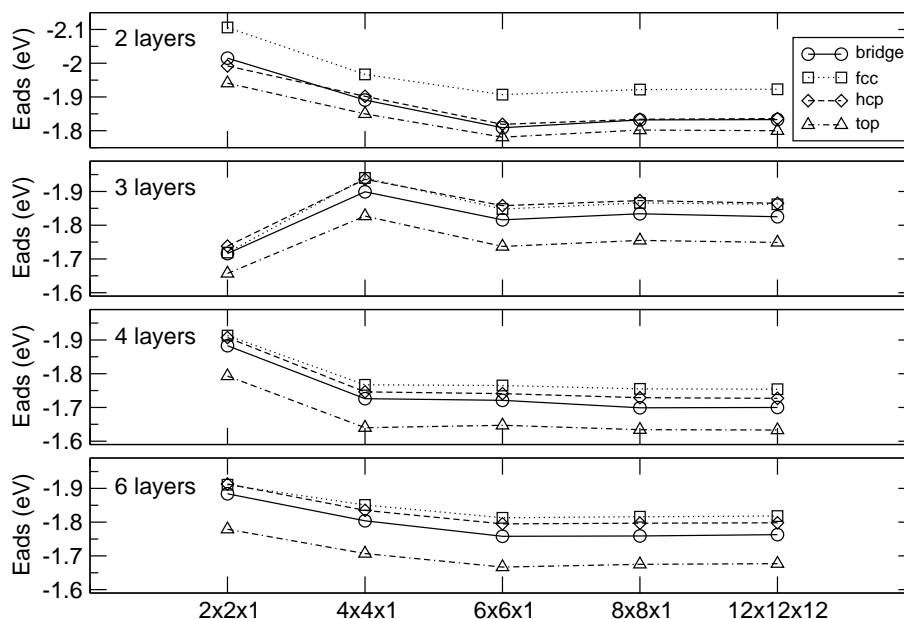
Figure 7.3: Dependence of the adsorption energy for the all the high symmetry adsorption sites for CO on Pt(111) surface on the sampling of the Brillouin zone and on the number of layers using the PBE functional. It has been checked the 2x2x1, 4x4x1, 6x6x1, 8x8x1 and 12x12x1 k-mesh, for 2, 3, 4, and 6 layers of Pt.

meV for all tested slabs with all k-points samplings.

For the PBE calculations with a 4x4x1 k-point grid the error relative to full convergence is 30 meV and with 6x6x1 15 meV (Table 7.3). Calculations using PBE0 functional converge extremely slow and it is impossible to increase the k-point mesh further than 8x8x1. HSE03 on the other hand is superior in terms of computational requirements. To exclude possible errors due to the k-point mesh, additional calculations were performed for the HSE03 case and CO on Pt using even 12x12x1 k-point grid, and downsampling the HF exchange part to 6x6x1 k-points[5]. The relative stability of the top-fcc sites changes by only 20 meV.

For PBE the C-O bond length is more elongated compared to the hybrid

---

[5]This has been done to investigate the effect of the downsampling of the reciprocal space representation of the Fock exchange operator. The downsampling is done by a factor of 2: $\frac{n}{2} \times \frac{n}{2} \times 1$ grid, for details see Ref.[166]

Table 7.3: Dependence of the site order on the sampling of the surface Brillouin zone using hybrid functionals and the PBE functional for CO on Pt(111). Energies are referenced to the top site. PBE0 results are evaluated using the "full" k-point grid, while HSE03 results are evaluated using the "reduced" as well as the "full" grid, for 4x4x1, 6x6x1 and 8x8x1 k-mesh.

Functional	sites	4x4x1	6x6x1	8x8x1
PBE	fcc	-0.127	-0.118	-0.121
	hcp	-0.106	-0.094	-0.095
PBE0	fcc	0.047	-0.073	-0.056
	hcp	-0.027	0.067	-0.003
HSE03 "reduced"	fcc	-0.091	-0.062	-0.069
"full"	fcc	-0.112	-0.070	-0.069
"reduced"	hcp	-0.045	-0.011	-0.015
"full"	hcp	-0.062	-0.014	-0.015

functionals, while the height of the CO molecule above the surface is greater compared to hybrid functionals (Table 7.4). It can been seen in the same table that there is a tendency to increase the adsorption energy with HSE03 and even more pronounced with PBE0. This increase is in opposite direction to what was expected. PBE gives the closest to the experiment values for the adsorption energies. The difference between fcc and top site adsorption energies is reduced for calculations done with hybrid functionals.

Unfortunately, the PBE0 and HSE03 functionals don't correct the site preference for Pt (Table 7.4, Fig. 7.4), as the top site remains unfavored with respect to the fcc site (PBE0 and HSE03 give the correct top site for the Cu and Rh in accordance with experiment, but the relative differences are comparable to the numerical uncertainty[213]). On the other hand the energy difference between top and fcc is reduced compared to the PBE results (120 meV for PBE, 55 meV for PBE0 and 70 meV for HSE03). Therefore, hybrid functionals reduce the tendency of GGA functionals to disfavor the low coordination site with respect to the hollow sites for Pt, while for Cu and Rh, they give the correct adsorption sites.

While for Pt, the fcc hollow site is the most preferable energetically and is

Table 7.4: Structure and energetics of the adsorption of a CO-molecule on the Pt(111) surface for the top, hcp and fcc sites, using PBE, PBE0 and HSE03 functionals: E_{ads} is the adsorption energy, d_{CO} is the bond length of C-O and Δd_{CO} is the difference of the bond length in respect to the theoretical value of the free CO molecule in percentage, d_{Pt-C} is the height difference of the C atom from the Pt surace atom that binds CO molecule, b is the buckling of the surface layer (distance between the outermost and the innermost Pt atom of the surface layer), while the Δd_{12} is again the change of the distance between the first and the second surface layer with respect to the bulk value. The preferred site is written in boldface

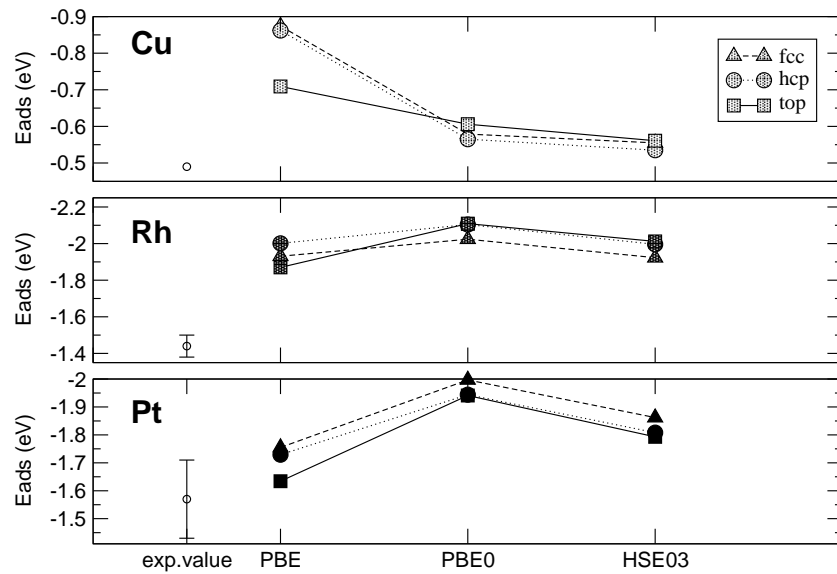| Functional	Site	E_{ads}(eV)	d_{CO}(Å)	Δd_{CO}(%)	d_{Pt-C}(Å)	b(Å)	Δd_{12}(Å)
PBE	top	-1.634	1.158	1.3	1.839	0.227	0.5
	fcc	**-1.755**	1.194	4.4	1.329	0.132	2.3
	hcp	-1.729	1.194	4.4	1.324	0.149	2.4
PBE0	top	-1.941	1.142	1.1	1.818	0.237	0.8
	fcc	**-1.997**	1.177	4.2	1.304	0.215	3.2
	hcp	-1.944	1.180	4.4	1.291	0.226	2.6
HSE03	top	-1.793	1.143	1.1	1.821	0.200	0.5
	fcc	**-1.862**	1.177	4.2	1.320	0.177	3.3
	hcp	-1.808	1.177	4.2	1.330	0.177	2.2

Figure 7.4: Dependance of Adsorption energy of CO for adsorption on top and fcc, hcp hollow sites on the functionals (PBE, PBE0, and HSE03) for Cu, Rh, Pt. The experimental values for the adsorption energies are -0.49 for Cu[125], -1.38 to -1.5 for Rh[200], while for Pt there are several results ranging from -1.43 eV till -1.71 eV[50, 234], with most popular values: -1.48 to -1.50 eV[37, 209]

followed by the hcp and top site with all the three functionals, the sequence for Cu and Rh doesn't remain the same. For Cu, PBE gives fcc hollow site to be the most preferable, but it becomes the least favorable for the hybrid functionals, for which the top becomes the most preferable, followed by the hcp and last the fcc. For Rh, while hcp is the most preferable site energetically with PBE functionals, for the hybrid functionals again the top is the most preferable followed by the hcp. Unfortunately even if the hybrid functionals correct the site preference, they yield almost degenerate adsorption energies for top and hcp hollow site.

Concerning the geometry relaxations (Table 7.4), the trends for the three functionals are: i) The CO bond length is slightly elongated with respect to the theoretical value for an isolated molecule ($d_{CO}^{theor.}$=1.14 Å) for the top and the hollow sites (this holds for all the three metals[213]). ii) There is a reverse correlation between the d_{CO} and d_{Pt-C}. iii) The buckling induced by the adsorption is increased for the top sites compared to the hollow sites. iv) There is an outward relaxation for Pt (also for Rh[213])(Table 7.4).

7.4.2 Electronic properties

The CO adsorption on metal surfaces is described very well by the Blyholder model[28] with donation from the 5σ (HOMO) orbital of the CO molecule to the metal and back donation from the metal to the $5\pi^*$ (LUMO) orbital of CO. In order to gain understanding of the effect of hybrid functionals on the electronic properties the electronic density of states for Pt is shown in Fig. 7.5. Displayed are the DOS for a clean Pt(111) surface atom and Pt(111) with CO molecule adsorbed on top and hcp and also the DOS for the CO molecule adsorbed on these sites from calculations using PBE and HSE03 functionals (PBE0 and HSE03 exhibit no differences in DOS).

The metal d-bands broaden and shift down to lower energies due to the interaction with the CO molecule (compare (b) and (c) with (a)). For the top site the major orbital interaction is between the 5σ of CO and the d_{z^2} state of Pt, which gives rise to a bonding contribution below the Fermi level (about -7.5 eV) and anti-bonding contributions partly even above the Fermi level.

For the hcp site, the 1π and $2\pi^*$ CO molecular orbitals are more important: they interact with the d_{xz} and d_{yz} respectively and in plane ($d_{x^2-y^2}$, d_{xy}) metal
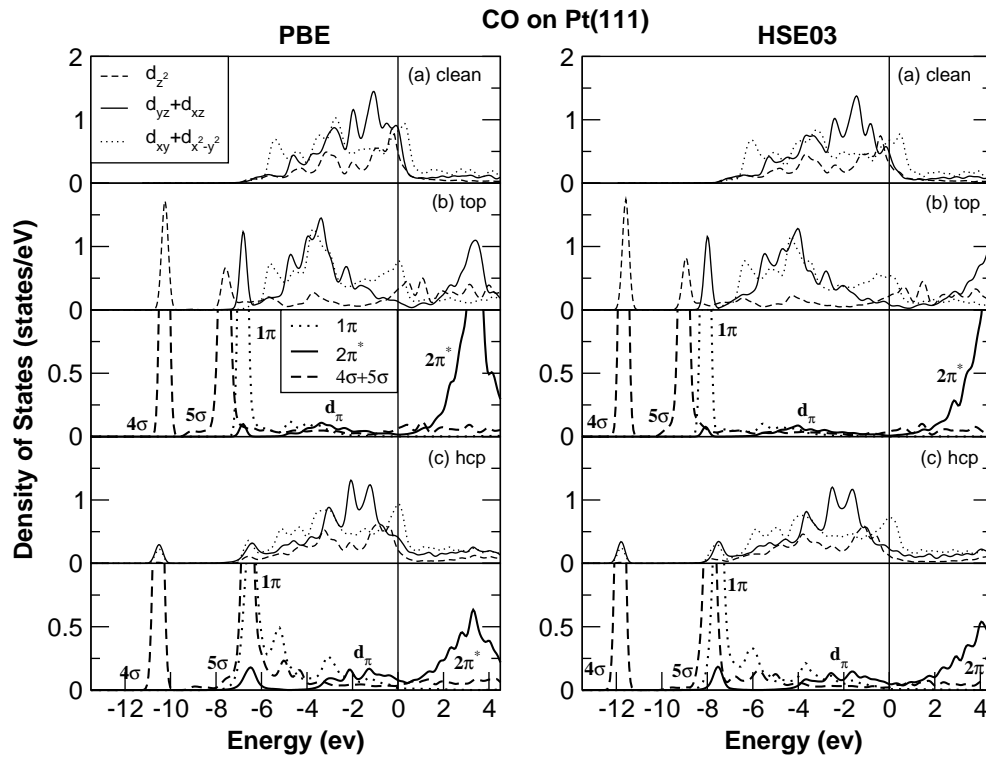
Figure 7.5: Density of States for the topmost Pt(111) surface atoms for (a) a clean surface, and for the adsorption of CO molecule at (b) top and (c) hcp hollow site. The DOS for CO is shown by thick lines below panels (b) and (c) for top and hollow site respectively. The vertical line corresponds to the Fermi energy (0 eV).

states. In panel (b) of Fig. 7.5 the d_{z^2} orbital is broadened and shifted more than the other metal d states, while in panel (c) the broadening and the shifts are larger for the d_{xz} and d_{yz} states.

The picture of the $\sigma - d$ and $\pi - d$ interactions holds both for top and hcp hollow sites with some differences. For the hollow site, simple geometrical and symmetry considerations suggest that the 5σ orbital interacts mainly with the d_{xy} and $d_{x^2-y^2}$ states. The direct interaction with d_{z^2} is weaker compared with the top adsorption site. The donation from the 5σ orbital to the substrate tends to favor the top site (bassically due to the $5\sigma - d_{z^2}$) interaction, where the back-donation from the $2\pi^*$ orbital tends to favor the hollow sites (due to the $2\pi - d$).[124]

The adsorption energy is controlled by the balance between donating (HOMO) and backdonating (LUMO) interaction terms. The effect is that there is a stronger 5σ and 2π bonding interaction at the HSE03 level.

The back donation is larger for hollow sites than for the top sites and it tends to favor the hollow sites, because the smaller the gap and the closer the LUMO is to the Fermi energy, the stronger the back donation is through the $2\pi - d$. Consequently the HSE03 functional reduces the tendency to favor the hollow sites compared to the top. For both the top and hcp case (b,c panels), the d_π peak is less intense and broadened at the HSE03 level than at the PBE level, suggesting less charge back-donation (less charge is back-donated).

The above analysis can be better rationalized in terms of the position of the center if gravity of the d-band (both occupied and unoccupied states) for the clean, top and hcp cases for PBE and HSE03 functionals (Table 7.5).

7.5 Conclusions

Periodic slab calculations using hybrid Hartree-Fock density functionals are perfectly practicable for metallic systems using a plane wave basis set. The HSE03 functional yields practically identical results as the more conventional PBE0 functionals, with the advantage that the computational cost is reduced by a factor of 10. This is achieved by replacing the long range part of the Fock exchange by its density functional approximation, leading to a rapid k-point convergence of the non-local exchange and total energies. Thus, the HSE03

Table 7.5: Calculated binding energies of d-band centers (for occupied and unoccupied states) for PBE and HSE03 functionals for the clean Pt(111), and also for the adsorption of CO on-top and hcp site of Pt(111). The values are in eV.

Functional	d-band centers	clean-Pt(111)	CO on top	CO on hcp
PBE	$\epsilon_{d_{z^2}}$	2.87	1.32	2.33
	$\epsilon_{d_{yz}+d_{xz}}$	2.96	0.81	2.21
	$\epsilon_{d_{xy}+d_{x^2+y^2}}$	2.96	1.94	1.91
HSE03	$\epsilon_{d_{z^2}}$	3.23	1.32	2.37
	$\epsilon_{d_{yz}+d_{xz}}$	3.08	0.73	2.37
	$\epsilon_{d_{xy}+d_{x^2+y^2}}$	3.27	1.75	1.87

functional presents a promising functional for large scale studies of molecules on surfaces.

The PBE gives the wrong site preference for Cu(111), Rh(111), and Pt(111). In contrast the PBE0 and HSE03 functionals predict the correct site order for CO on Cu(111) and Rh(111). For Cu and Rh the fcc and the hcp are destabilized by 150meV compared to top sites[213]. Unfortunately the hybrid functionals do not work so well for Pt(111), were the destabilization is only 50 meV for the fcc and 80 meV for the hcp site, which is not sufficient to yield the correct site order.

It is well accepted that gradient corrected functionals have a tendency to overestimate adsorption energies on metal surfaces. One would hope that admixing a certain fraction of the exact non-local exchange will overcome this deficiency, but this is not the case at least for PBE0 and HSE03 functionals. Cu is the only case where the hybrid functional improves the overall energetic description. This is related to the upshift of the empty CO $2\pi^*$ orbital and a simultaneous downshift of the filled Cu $3d$ states. Both effects reduce the $2\pi^* - d$ interaction, thats why the top site becomes preferred.

For Rh and Pt the d-band is restrained to stay at the Fermi-level, and for the transition metals the main effect of the inclusion of non-local exchange is an increase of the d-band width. This increase opposes the reduced interaction caused by the upshift of the CO $2\pi^*$ orbital. One general rule is that the

interaction energies increase from PBE, over HSE03 to PBE0, with the last one yielding the largest d-band width and the largest CO-metal interaction energies.

The main origin of problems is the increased d-band width caused by the non-local exchange: it partially restores the CO $2\pi^* - d$ interaction, which we wanted to reduce using the hybrid functionals. In metals the proper description involves only a very weak screened-exchange interaction and the LDA describe this well.

Although hybrid functional calculations for metal and metal surfaces are feasible, the results are not satisfactory. Agreement with experiment is improved for CO adsorption on Cu(111)[213], while the results for CO on Rh(111) and CO on Pt(111) are partially improved. For Rh(111) one gets the right site order, but much too large adsorption energies[213], while for Pt(111) we get the wrong site order and too large adsorption energies. It is argued that this failure is related to the inclusion of non-local exchange in the metal slab, which results in an incorrect description of the exchange interaction.

Bibliography

[1] Adam S.F. and Krasheninnikov A.V., 1996 Lecture notes: **Introduction to electronic structure simulation**.

[2] Adamo C. and Barone V., 1997, *Chem. Phys.Lett.* **274**, 242.

[3] Adamo C., and Barone V., 1999, *J. Chem. Phys.* **110**, 5029.

[4] Adamo C. and Barone V., 1999, *J. Chem. Phys.* **110**, 6158.

[5] Adamo C. Ernzerhof M., and Scuseria G.E., 2000, *J. Chem. Phys.* **112**, 2643.

[6] Aldén M., Abrikosov I., Johansson B., Rosengaard N., and Skriver H., 1994, *Phys. Rev. B* **50**, 5131.

[7] Aldén M., Skriver H., and Johansson B., 1994, *Phys. Rev. B* **50**, 12118.

[8] Argaman N. and Makov G., 2000, *Amer. J. Phys.* **68**, 69.

[9] Bagus P., Nelin C., and Bauschlicher C., 1983, *Phys. Rev. B* **28**, 5423.

[10] Bagus P., Hermann K., Müller W., Nelin C., 1986, *Phys. Rev. Lett.* **57**, 1496.

[11] Balázs N., 1967, *Phys. Rev.* **156**, 42.

[12] Balbuena B. and Seminario J.M. 1999 **Molecular Dynamics, From classical to Quantum Methods, Theoretical and Computational Chemistry Vol 7, Elsevier**.

[13] Baro A., and Ibach H., 1979, *J. Chem. Phys.* **71**, 4812.

[14] Barone V, Heyd J, and Scuseria G., 2004, *J. Chem. Phys.* **120**, 7169.

[15] Bartlett R.J. and Stanton J.F., 1995, *Rev. Comput. Chem.* **5**, 65.

[16] Becke A.D., 1986, *J. Chem. Phys.* **84**, 4524.

[17] Becke A.D. and Roussel M.R., 1989, *Phys. Rev. A* **39**, 3761.

[18] Becke A.D., 1992, *J. Chem. Phys.* **98**, 1372.

[19] Becke A.D., 1993, *J. Chem. Phys.* **98**, 5648.

[20] Becke A.D., 2000, *J. Chem. Phys.* **112**, 4020.

[21] Bertolini J., Tardy B., Abon M., Billy J., Delichère P. and Massardieret J., 1983, *Surf. Sci.* **135**, 117.

[22] Besenbacher F., Chorkendorff I., Clausen B.S., Hammer B., Molenbroek A., Nørskov J.K. and Stensgaard I., 1998, *Science* **279**, 1913.

[23] Bickelhaupt M., Radius U., Ehlers A., Hoffmann R., Baerends E., 1998, *New J. Chem.* **18**, 1.

[24] Blackman G., Xu H., Ogletree D., van Hove M., and Somorjai G., 1988, *Phys. Rev. Lett.* **61**, 2352.

[25] Bligaard T., 2003, in **Understanding Materials Properties on the Basis of Density Functional Theory Calculations.**, PhD thesis, Technical University of Denmark.

[26] Blöchl P., 1994, *Phys.Rev.B* **50**, 17953.

[27] Blöchl P., Först C., Schimpl J., 1994, *Bull. Mater. Sci.* **26**, 33.

[28] Blyholder G., 1964, *J. Phys. Chem.* **68**, 2772.

[29] Blyholder G., 1975, *J. Vac. Scie. Technol.* **11**, 865.

[30] Born M. and Oppenheimer R., 1927, *Ann. Phys.* **84**, 457.

[31] M. Boudart, 1997, in **Handbook of Heterogeneous Catalysis**, Ertl G, Krözinger H., Weitkamp J.

[32] Brivio G. and Trioni M., 1999, *Rev. Mod. Phys.* **711**, 231.

[33] Buatier de Mongeot F., Scherer M., Gleich B., Kopatzki E., Behm R., 1998, *Surf. Sci.* **411**, 249.

[34] Campuzano J., 1990, in: **The Chemical Physics of Solid Surfaces and Heterogeneous Catalysis**, Vol 31.

[35] Capelle K., 2003, *arXiv:cond-mat/0211443v5*.

[36] http://www-ledss.ujf-grenoble.fr/PERSONNEL/LEDSS7/casida-/CompChem/DFT.html#B96

[37] Conrad H., Ertl G., Koch J., and Latta E., 1974, *Surf. Sci.* **43**, 462.

[38] Copel M., Fenter P., and Gustafsson T., 1987, *J. Vac. Sci. and Techn. A* **5**, 742.

[39] Daruka I., and Hamilton J., 2003, *J.Phys.: Condens. Matter* **15**, 1827.

[40] Deskins A., Lauterbach J., and Thomson K., 2005, *J. Chem. Phys.*, **122**, 184709.

[41] Dodson B., 1987, *Phys. Rev. B*, **35**, 880.

[42] Doll K., 2004, *Surf. Sci.* **573**, 464.

[43] Eichler A., Kresse G., and Hafner J., 1998, *Surf. Sci.* **397**, 116.

[44] Eichler A., Hafner J., Groß A., and Scheffler M., 1999, *Phys. Rev. B* **59**, 13297.

[45] Eichler A., 2003, *Surf. Sci.* **526**, 332.

[46] Elliot J., and Ward C., 1996, *J. Chem. Phys.* **105**, 5677.

[47] Ercolessi F., Tosatti E., and Parrinello M., 1986, *Phys. Rev. Lett.*, **57**, 719.

[48] Ernzerhof M., and Scuseria G., 1999, *J. Chem. Phys.* **110**, 6158.

[49] Ernzerhof M. and Scuseria G.E., 1999, *J. Chem. Phys.* **111**, 911.

[50] Ertl G, Neumann M., and Streit K., 1977, *Surf. Sci.* **64**, 393.

[51] Eschrig H., 2004, *Lectures notes in Physics* **642**, 7.

[52] Fermi E., 1928, *Z. Phys.* **61**, 1928.

[53] Feibelman P., Hammer B., Nørskov J., Wagner F., Scheffler M., Stumpf R., Watwe R., and Dumesic J., 2000, *J. Phys. Chem.* **105**, 4018.

[54] Fetter A.L. and Walecka J.D., 1971, in **Quantum Theory of Many-Particle Systems**, McGraw-Hill, New York.

[55] Filatov M. and Thiel W., 1998, *Phys. Rev. A* **57**, 189.

[56] Filippi C., Umrigar C.J. and Taut M, 1994, *J. Chem. Phys.* **100**, 1290.

[57] Fock V., 1930, *Z. Phys.* **61**, 126.

[58] Föhlisch A., Nyberg M., Bennich P., Triguero L., Hasselström J., Karis O., Pettersson LG. and Nilsson A., 2000, *J. Chem. Phys.* **112**, 1946.

[59] Foster A.S. and Krasheninnikov A.V., **Introduction to electronic structure calculations**, Helsinki University of Technology, 2006.

[60] Gajdos M., Eichler A., and Hafner J., 2005, *J. Phys.: Cond. Mat.* **16**, 1141.

[61] Gajdos M., Hafner J., and Eichler A., 2006, *J. Phys.: Cond. Mat.* **18**, 41.

[62] Gauthier Y., Schmid M., Padovani S., Lundgren E., Bus. V., Kresse G., Redinger J., and Varga P., 2001, *Phys. Rev. Lett.* **87**, 036103.

[63] Ghosh S.K. and Parr R.G., 1986, *Phys. Rev. A* **34**, 785.

[64] Ghosh S.K., 2003, *Bull. Mater. Sci.* **26**, 3.

[65] Gil A., Clotet A., Ricart J., Kresse G., Garcia-Hernandez M., Rosh N., and Sautet P., 2003, *Surf. Sci.* **530**, 71.

[66] Greeley J., Nørskov J., and Mavrikakis M., 2002, *Annu. Rev. Phys. Chem.* **53**, 319.

[67] Golding B. and Moss S., 1967, *Acta Metall.* **15**, 1239.

[68] Gross A., 2002 **Theoretical Surface Science, A microscopic Perspevtive**, Springer.

[69] Groß A., 2003, in: **Theoretical Surface Science, A Microscopic Perspective**, Springer.

[70] Groß A., 2006, *Topics in Catalysis* **37**, 29.

[71] Gunnarsson O., and Lundqvist B., 1976, *Phys. Rev. B* **13**, 4274.

[72] Gunnarsson O., and Jones R.O., 1980, *J. Chem. Phys.* **72**, 5357.

[73] Hafner J., 2000, *Acta. Mater.* **48**, 71.

[74] Hafner J, 2005, in **Theoretical Solid State Physics**, lecture notes, University of Vienna.

[75] Hafner J., Wolverton C. and Ceder G., 2006, *MRS Bulletin* **31**, 659.

[76] Häkkinen H., Moseler M., and Landman U., 2002, *Phys. Rev. Let.* **89**, 033401.

[77] Hammer B., and Nørskov J., 1995, *Surf. Sci.* **343**, 211.

[78] Hammer B., and Nørskov J., 1995, *Nature* **376**, 238.

[79] Hammer B., Morikawa Y., and Nørskov J., 1996, *Phys. Rev. Let.* **76**, 2141.

[80] Hammer B., and Nørskov J., 1996, *Surf. Sci.* **359**, 306.

[81] Hammer B., and Nørskov J., 1997, *Phys. Rev. Lett.* **79**, 4441.

[82] Hammer B., and Nørskov J., 1997, in: **Chemisorption and Reactivity on supported clusters and thin films**, RM Lambert, G Pacchioni.

[83] Hammer B., Hansen L. B. and Nørskov J. K., 1999, *Phys. Rev. B* **59**, 7413.

[84] Hammer B., and Nørskov J., 2000, *Adv. Catal.* **45**, 71.

[85] Hartree D.R., 1928, *Proc. R. Soc. London* **A113**, 621.

[86] Heine V. and Cohen M.L., 1970 in **Solid State Physics**, Vol. 24.

[87] Heinonen O., Lubin M., and Johnson M., 1995, *Phys. Rev. Lett.* **75**, 4110.

[88] Henkelman G., Uberuaga B., and Jonsson H., 2000, *J. Chem. Phys.* **113**, 9901.

[89] Henkelman G. and Jonsson H., 2000, *J. Chem. Phys.*, **113**, 9978.

[90] Hoffmann F., 1983, *Surf. Sci. Rep.* **3**, 107.

[91] Hermann K., Bagus P., and Nelin C., 1987, *Phys. Rev. B* **35**, 9467.

[92] Heyd J., Scuseria G., and Ernzerhof M., 2003, *J. Chem. Phys.* **118**, 8207.

[93] Hoffmann R., 1988, *Rev. Mod. Phys.* **60**, 601.

[94] Hohenberg P., and Kohn W, 1964, *Phys. Rev. B* **136**, 864.

[95] Holmblad P., Hvolbaek-Larsen J., and Chorkendorffet I., 1996, *J. Chem. Phys.* **104**, 7289.

[96] Illas F., in: **Models in Computational Material Science**, Lecture notes, University of Barcelona, Spain.

[97] Inglesfield J., 1985, *Prog. Surface Sci.* **20**, 105.

[98] Jacobsen J., Nielsen L., Besenbacher F., Stensgaard I., Lægsgaard E., Rasmussen T., Jacobsen K., and Nørskov J., 1995, *Phys. Rev. Lett.* **75**, 489.

[99] Jaramillo J., Scuseria G.E. and Ernzerhof M., 2003, *J. Chem. Phys.* **118**, 1.

[100] http://newton.ex.ac.uk/research/qsystems/people/jenkins/mbody/mbody3.html

[101] Jones R.O., and Gunnarsson O., 1985, *Phys. Rev. Lett.* **55**, 107.

[102] Jones R.O., and Gunnarsson O., 1989, *Rev. Mod. Phys.* **61**, 689.

[103] Jónsson H., Mills G. and Jacobsen K., in **Classical and Quantum Dynamics in Condensed Phase Simulations**, World Scientific, page 385.

[104] Kayser H., 1881, *Wiederman's Ann. Phys. Chem.* **14**, 450.

[105] Kittel C., in **Introduction to Solid State Theory**, 6th edn, New York; Wiley, 1986.

[106] Klein A., Schmidt A., Hammer L., and Heinz K., 2004, *Europhys. Lett.*, **65**, 830.

[107] Koch R., Borbonus M., Haase O., Rieder K., 1991, *Phys. Rev. Lett.* **67**, 3416.

[108] Koch R., Borbonus M., Haase O., Rieder K., 1992, *Appl. Phys. A* **55**, 417.

[109] Köhler L., and Kresse G., 2004, *Phys. Rev. B* **70**, 165405.

[110] Kohn W., and Sham L.J., 1965, *Phys. Rev. A* **140**, 1133.

[111] Kohn W., 1995, **Density Functional Theory, Chapter 21**, *Euroconference on Computer Simulation in Condensed Matter Physics and Chemistry* **49**, Italian Physical Society.

[112] Kohn W., Becke A. and Parr R., 1996, *J. Phys. Chem.* **100**, 12974.

[113] Kohn W., 1999, *Rev. Mod. Phys.* **71**, 1253.

[114] Krasheninnikov A., 2000, in: **Computational Methods for Material Science**, lecture notes, University of Helsinki.

[115] Krasheninnikov A., in **Introduction to Electronic Structure Calculations**, lecture notes, Univ. of Helsinki and Helsinki Univ. of Technology, 2006.

[116] Kratzer P., Hammer B., and Nørskov J. K., 1996, *J. Chem. Phys.* **105**, 5595.

[117] Krawczyk M., Zommer L., Sobczak J., Jablonski A., Petit M., Robert-Goumet C., and Gruzza B., 2004, *Surf. Sci.* **566-568**, 856.

[118] Kresse G. and Hafner J., 1993, *Phys.Rev.B* **48**, 13115.

[119] Kresse G. and Hafner J., 1994, *J. Phys: Cond. Mat.* **6**, 8245.

[120] Kresse G. and Furthmüller J., 1996, *Comp. Mater. Sci.* **6**, 15.

[121] Kresse G. and Furthmüller J., 1996, *Phys. Rev. B* **54**, 11169.

[122] Kresse G. and Joubert D., 1999, *Phys. Rev. B* **59**, 1758.

[123] Kresse G., 2000, in: **"Computational Material Science"**, lecture notes, University of Vienna.

[124] Kresse G., Gil A., Sautet P., 2003, *Phys. Rev. B* **68**, 073401.

[125] Kirstein W., Kruger B., and Thieme F., 1986, *Surf. Sci.* **176**, 505.

[126] Kulkarni G., Aiyer H., Vijayakrishnan V., Arunarkavalli T., and Rao C., 1993, *J. Chem. Soc., Chem. Commun.* **1545**, 10.1039.

[127] Kurth S., Perdew J., and Blaha P., 1999, *Int. J. Quantum Chem.* **75**, 889.

[128] Labat S., Bocquet F., Gilles B., and Thomas O., 2004, *Scripta Materialia* **50**, 717.

[129] Lahr D., and Ceyer S., 2006, *J. Am. Chem. Soc.* **128**, 1800.

[130] Laidler K., 1996, *Pure and Appl. Chem.* **68**, 149.

[131] Lau K. and Kohn W., 1977, *Surf. Sci.* **65**, 607.

[132] Lauritsen J. V., Vang R. T., and Besenbacher F., 2006, *Catalysis Today* **111**, 34.

[133] Lee C., Yang W., and Parr R.G., 1988, *Phys.Rev.B* **37** 785.

[134] Leeor K., The Computational Materials Science Group, www.weizmann.ac.il/materials/Leeor

[135] Lieb E., and Simon B., 1973, *Phys. Rev. Lett.* **31**, 681.

[136] Lin B., and Shern C., 1990, *Chin. J. Phys.*, **28**, 355.

[137] Linke R., 1994,*Surf. Sci.* **307-309**, 407.

[138] Lopez N. and Nørskov J. K., 2002, *J. Am. Chem. Soc.* **124**, 11262.

[139] Masel R., 1996, in: **Principles of Adsorption and Reaction on Solid Surfaces**, Wiley Series in Chemical Engineering

[140] Mason M., 1983, *Phys. Rev. B* **27**, 748.

[141] Mason S., Grinberg I., Rappe A., 2006, *J. Phys. Chem. B* **110**, 3816.

[142] Massalski (Ed.) T., 1987, *Binary Alloy Phase Diagrams* (American Society for Metals, Metals Park, OH).

[143] Materer N., Starke U., Barbieri A., Doll R, Heinz K. van Hove M., and Somorjai G., 1995, *Surf. Sci.* **325**, 207.

[144] Mavrikakis M., Stoltze P., and Nørskov J., 2000, *Catal. Lett.* **64**, 101.

[145] Methfessel M. and Paxton A., 1988, *Phys. Rev. B* **40**, 3616.

[146] Mittendorfer F., Eichler A., and Hafner J., 1999, *Surf. Sci.* **423**, 1.

[147] Mortensen J., Morikawa Y., Hammer B. and Nørskov J., 1997, *J. Catal.* **169**, 85.

[148] Monkhorst H., and Pack J., 1976, *Phys. Rev. B* **13**, 5188.

[149] Murnaghan F., 1944, *Proceedings of the National Academy of Sciences* **30**, 244.

[150] Muscat J., Wander A., and Harrison N.M., 2001, *Chem. Phys.Lett.* **342**, 397.

[151] Mills G., Jónsson H., and Schenter G., 1994, *Surf. Sci.* **324**, 305.

[152] Neef M., and Doll K., 2006, *Surf. Sci.* **600**, 1085.

[153] Nemoshkalenco V., and Antonov V., 1998, **Computational Methods in Solid State Physics**, OPA.

[154] Nielsen L., Besenbacher F., Stensgaard I., Lægsgaard E., Engdahl C., Stoltze P., Jacobsen K., and Nørskov J., 1993 *Phys. Rev. Lett.* **71**, 754.

[155] Nielsen L., Besenbacher F., Stensgaard I., Lægsgaard E., Engdahl C., Stoltze P., and Nørskov J., 1995 *Phys. Rev. Lett.* **74**, 1159.

[156] Nieuwenhuys B., 1996,*Surf. Rev. Lett.* **3**, 1869.

[157] Nørskov J., 1990, *Rep. Prog. Phys.* **53**, 1253.

[158] Nørskov J., Bligaard T., Logadottir A., Bahn S., Hansen L., Bollinger M., Bengaard H., Hammer B., Sljivancanin Z., Mavrikakis M., Xu Y., Dahl S., and Jacobsen C., 2002, *J. Catal.* **209**, 275.

[159] Ogletree D., Van Hove M., and Somorjai G., 1986, *Surf. Sci.* **173**, 351.

[160] Olsen R., Philipsen P., and Baerends E., 2003, *J. Chem. Phys.* **119**, 4522.

[161] Orita H., Itoh N., and Inada Y., 2004, *Chem. Phys. Lett.* **384**, 271.

[162] Over H., 1998, *Prog. Surf. Sci.* **58**, 249.

[163] Over H., 2001, *Prog. Surf. Sci.* **58**, 249.

[164] Ozolins V., Wolverton C., and Zunger A., 1998, *Phys. Rev. B* **57**, 6427.

[165] Paier J., Hirschl R., Marsman M., and Kresse G., 2005, *J. Chem. Phys.* **122**, 234102.

[166] Paier J., Marsman M., Kresse G., Gerber I. and Angyan J., 2006, *J. Chem. Phys.* **124**, 154709.

[167] Parr R.G. and Yang W., 1989, in: **Density-Functional Theory of Atoms and Molecules**, Oxford University Press.

[168] Payne M., Teter M., Allan D., Arias T. and Joannopoulos J., 1992, *Rev. Mod. Phys.* **64**, 1045.

[169] Perdew J., Burke K., and Ernzerhof M., 1996, *Phys. Rev. Lett.* **77**, 3865.

[170] Perdew J., and Zunger A., 1981, *Phys. Rev. B* **23**, 5048.

[171] Perdew J., Parr R., Levy M., Balduz J., 1982, *Phys. Rev. Lett.* **49**, 1691.

[172] Perdew J., 1985, *Phys. Rev. Lett.* **55**, 1665.

[173] Perdew J., and Wang Y., 1986, *Phys. Rev. B* **33**, 8800.

[174] Perdew J., 1986, *Phys. Rev. B* **33**, 8822 and **34**, 7406(E).

[175] Perdew J., Chevary J., Vosko S., Jackson K., Pederson M., Singh D., and Fiolhais C., 1992, *Phys. Rev. B* **46**, 6671.

[176] Perdew J., Burke K., and Ernzerhof M., 1996, *Phys. Rev. Lett.* **77**, 3865.

[177] Perdew J., Burke K., and Wang Y., 1996, *Phys. Rev. B* **54**, 16533.

[178] Perdew J., Ernzerhof M., and Burke K., 1996, *J. Chem. Phys.* **105**, 9982.

[179] Perdew J., Burke K., and Ernzerhof M., 1997, *Phys. Rev. Lett.* **78**, 1396.

[180] Perdiew J., Kurth S., Zupan A., and Blaha P., 1999, *Phys. Rev. Lett.* **82**, 2544.

[181] Phillips J.C., 1958, *Phys.Rev.* **112**, 685.

[182] Pines D., 1951, *Solid State Physics* **1**, 367.

[183] Pleth-Nielsen L., Besenbacher F., Stensgaard I., Lægsgaard E., Engdahl C., Stoltze P., Jacobsen K., and Nørskov J., 1993, *Phys. Rev. Lett.* **71**, 754.

[184] Pleth-Nielsen L., Besenbacher F., Stensgaard I., Lægsgaard E., Engdahl C., Stoltze P., and Nørskov J., 1995, *Phys. Rev. Lett.* **74**, 1159.

[185] Ponec V., 1983, *Adv.Catal.***31**, 149.

[186] Pople J., 1999, *Rev. Mod. Phys* **71**, 1267.

[187] Proynov E., Vela A., and Salahub D., 1995, *Chem. Phys. Lett.* **230**, 419.

[188] Prutton M., 1994, in: **Introduction to Surface Physics**, Oxford Science Publications.

[189] http://www.chem.qmul.ac.uk/surfaces/scc/

[190] Reichert H., Schöps A., Ramsteiner I., Bugaev V., Shchyglo O., Udyansky A., Dosch H., Asta M., Drautz R., and Honkimäki V., 2005, *Phys. Rev. Lett.* **95**, 235703.

[191] Rostrup-Nielsen J., 1984, *J.Catal.* **85**, 31.

[192] Ruban A., Hammer B., Stolze P., Skriver H. and Nørskov J., 2002, *J. Mol. Catal. A: Chem.* **115**, 421.

[193] Ruban A., Skriver H. and Nørskov J., 1999, *Phys. Rev. B* **59**, 15990.

[194] Rushton P., 2002, in: **Towards a Non-Local Density Functional, Description of Exchange and Correlation**, Dissertation Departments of Chemistry and Physics University of Durham.

[195] Sabatier P., 1911, *Ber. Deutsch. Chem. Gesellshaft* **44**, 1984.

[196] Scheffler M., and Stampfl C., **Theory of Adsorption on Metal Substrates**, 2000, Handbook of Surface Science, Vol 2, edited by K.Horn and M.Scheffler.

[197] Schrödinger E., 1926, *Ann. Physik* **79**, 361.

[198] Sinfelt J., 1983, *Bimetallic Catalysts: Discoveries, Concepts,and Applications* (Wiley, New York).

[199] Slater J., 1951, *Phys. Rev.* **81**, 385.

[200] Smedh H., Borg M., Nyholm R., and Andersen J., 2001, *Surf. Sci.* **491**, 115.

[201] Smoluchowski R., 1941, *Phys. Rev.* **60**, 661.

[202] Somorjai G., 1994, in: **Introduction to Surface Chemistry and Catalysis**, Wiley.

[203] Spisak D., and Hafner J., 2002, *Phys. Rev. B*, **65**, 235405.

[204] Spisak D., and Hafner J., 2003, *J. Surf. Sci.*, **546**, 27.

[205] Spisak D., and Hafner J., 2004, *Phys. Rev. B*, **70**, 195426.

[206] Stampfl C., and Scheffler M., 1999, *Surf. Sci.* **433-435**, 119.

[207] Staroverov V., Scuseria G., Tao J., and Perdew J., 2003, *J. Phys. Chem.* **119**, 12129.

[208] Staroverov V., Scuseria G., Tao J., and Perdiew J., 2004, *Phys. Rev. B* **69**, 075102.

[209] Steininger H., Lehwald S., Ibach H., 1982, *Surf. Sci.* **123**, 264.

[210] Steirgerwald D., Miller S., and Wynblatt P., 1985 *Surf. Sci.* **155**, 79.

[211] Stevens P.J., Devlin J.F., Chabolowski C.F and Frisch M.J., 1994 *J. Phys. Chem.*, **98**, 11623.

[212] Stibor A., Kresse G., Eichler A., Hafner J., 2002, *Surf. Sci.* **99**, 507.

[213] Stroppa A., Termentzidis K., Paier J., Kresse G., and Hafner J., 2007, **CO adsorption on metal surfaces: a hybrid functional study with plane wave basis set.** under preparation.

[214] Sung S., and Hoffmann R., 1985, *J. Am. Chem. Soc.* **107**, 578.

[215] Tao J., Perdew P., Staroverov V., and Scuseria E., 2003, *Phys. Rev. Lett.* **91**, 146401.

[216] Tao J., Perdew P., Staroverov V., and Scuseria E., 2003, *J. Chem. Phys.* **119**, 12129.

[217] Teller E., 1962, *Rev. Mod. Phys.* **34**, 627.

[218] Termentzidis K., Hafner J., and Mittendorfer F., 2006, *J. Phys.: Condens. Matter* **18**, 10825.

[219] Thijssen J., **Computational Physics**, Cambridge University Press, 1999.

[220] Thomas L., 1927, *Proc. Cambridge Philos. Soc.* **23**, 542.

[221] Umezawa K., Nakanishi S., and Gibson S., 1998, *Phys. Rev. B* **57**, 8842.

[222] http://cms.mpi.univie.ac.at/CMSPage/main/

[223] Vanderbilt D., 1990, *Phys. Rev. B* **41**, 7892.

[224] Vestergaard E., Vang R., Knudsen J., Pedersen T., An T., Lægsgaard E., Stensgaard I., Hammer B., and Besenbacherat F., 2005, *Phys. Rev. Let.* **95**, 126101.

[225] Vogtenhuber D., 2001, in: **Surface Theory**, lecture notes.

[226] Voorhis T., and Scuseria G., 1998, *J. Chem. Phys.* **109**, 400.

[227] Vosko S., Wilk L., and Nusair M., 1980, *Can. J. Phys.* **58**, 1200.

[228] Detailed information on VASP may be found on the web-site: www.cms.mpi.univie.ac.at/vasp

[229] Wimmer E., Fu C., and Freeman A., 1985, *Comput. Phys. Commun.* **55**, 230.

[230] Wolverton C., Ozolins V., and Zunger A., 1998, *Phys. Rev. B* **57**, 4332.

[231] Wu T., Cohen J., and Yelon W., 1982, *Acta Metall.* **30**, 2065.

[232] Wyckoff R., in **Crystal Structures**, 2nd edn, New York, 1963.

[233] Wynblatt P. and Ku R., 1977 *Surf. Sci.* **65**, 511.

[234] Yeo Y., Vattuone L., and Kind D., 1997, *J. Chem. Phys.* **106**, 392.

[235] Zafeiratos S. and Kennou S., 2001, *Appl. Surf. Sci.* **173**, 69.

[236] Zafeiratos S. and Kennou S., 2002, *J. Phys. Chem. B* **106**, 41.

[237] Zangwill A., 1988, in: **Physics at Surfaces**, Cambridge University Press.

[238] Zhdanov V., Vang R., Knudsen J., Vestergaard E., Besenbacher F., 2006, *Surf. Sci. Let.* **600**, L260.

[239] Ziesche P., Kurth S. and Perdew J., 1998, *Comp. Mat. Sci.* **11**, 122.

Curriculum Vitae

Mag. Konstantinos Termentzidis

Institut für Materialphysik, University of Vienna

A-1090 Wien, Sensengasse 8/12

Tel.: +43 1 4277 51402, Fax: +43 1 4277 9514

E-Mail: kostas.termentzidis@univie.ac.at, konstantinos.termentzidis@hotmail.com

Personal data

Nationality:	Greek
Date of Birth:	November 3rd, 1974
Place of Birth:	Serres, Greece

Education

2004–2007	**Studies for a doctorate in Physics**
	University of Vienna
	Topic: "Adsorption of small molecules on metal surfaces"
1998–2001	**Master: "Physic of Materials"**
	Faculty of Physics,
	Aristotle University of Thessaloniki, Thessaloniki, Greece
	Degree: Master of Science
	Topic: "Forth Shell Model, Application to cubic diamond"
1993–1998	**Diploma: "Physic"**
	Faculty of Physics,
	Aristotle University of Thessaloniki, Thessaloniki, Greece
	Degree: Diploma of Science
	Topic: "Callibration of a system for CV measurement"
1986–1992	5th Gymnasium and Lyceum of Serres, Greece